nature communications

Article

https://doi.org/10.1038/s41467-024-49002-9

An axonemal intron splicing program sustains *Plasmodium* male development

Received: 14 December 2023

Accepted: 15 May 2024

Published online: 01 June 2024

Check for updates

Jiepeng Guan[1,4], Peijia Wu[1,4], Xiaoli Mo[1,4], Xiaolong Zhang[2,4], Wenqi Liang[1], Xiaoming Zhang[1], Lubin Jiang[2] ✉, Jian Li[1] ✉, Huiting Cui[1] ✉ & Jing Yuan[1,3] ✉

Differentiation of male gametocytes into flagellated fertile male gametes relies on the assembly of axoneme, a major component of male development for mosquito transmission of the malaria parasite. RNA-binding protein (RBP)-mediated post-transcriptional regulation of mRNA plays important roles in eukaryotic sexual development, including the development of female *Plasmodium*. However, the role of RBP in defining the *Plasmodium* male transcriptome and its function in male gametogenesis remains incompletely understood. Here, we performed genome-wide screening for gender-specific RBPs and identified an undescribed male-specific RBP gene *Rbpm1* in the *Plasmodium*. RBPm1 is localized in the nucleus of male gametocytes. RBPm1-deficient parasites fail to assemble the axoneme for male gametogenesis and thus mosquito transmission. RBPm1 interacts with the spliceosome E complex and regulates the splicing initiation of certain introns in a group of 26 axonemal genes. RBPm1 deficiency results in intron retention and protein loss of these axonemal genes. Intron deletion restores axonemal protein expression and partially rectifies axonemal defects in RBPm1-null gametocytes. Further splicing assays in both reporter and endogenous genes exhibit stringent recognition of the axonemal introns by RBPm1. The splicing activator RBPm1 and its target introns constitute an axonemal intron splicing program in the post-transcriptional regulation essential for *Plasmodium* male development.

Malaria is a worldwide infectious disease caused by the protozoan parasite *Plasmodium*[1]. The spread of *Plasmodium* depends on the transition between the mammal host and the *Anopheles* mosquito. In mammal hosts, a small proportion of intraerythrocytic asexual parasites undergo sexual development, irreversibly differentiating into the sexual precursor gametocytes, which are transmission-competent for the mosquito vector[2]. Within 10 min after being ingested into the mosquito midgut, the gametocytes escape from host erythrocytes and develop into fertile gametes, a process known as gametogenesis[3]. A flagellated motile male gamete fertilizes with a female gamete to form a zygote. After the zygote-ookinete-oocyst-sporozoite development in mosquitoes, the parasites are finally injected from the salivary gland into a mammal host, completing the transmission of the malaria parasite[4].

Sexual development plays a central role in malaria transmission[5,6]. When activated by two joint environmental stimuli (a temperature drop[7] and a metabolite xanthurenic acid[8]) in the mosquito midgut, a female gametocyte produces a haploid gamete, while a male gametocyte gives rise to 8 haploid gametes[3]. Female gametogenesis undergoes minor morphological changes, while male gametogenesis involves fast and spectacular changes[9,10]. During the male gametogenesis, two spatially distinct components are coordinated. One is the

[1]State Key Laboratory of Cellular Stress Biology, School of Life Sciences, Faculty of Medicine and Life Sciences, Xiamen University, Xiamen, China. [2]Shanghai Institute of Immunity and Infection, Chinese Academy of Sciences, Shanghai, China. [3]Department of Infectious Disease, Xiang'an Hospital of Xiamen University, School of Medicine, Faculty of Medicine and Life Sciences, Xiamen University, Xiamen, China. [4]These authors contributed equally: Jiepeng Guan, Peijia Wu, Xiaoli Mo, Xiaolong Zhang. ✉e-mail: lbjiang@siii.cas.cn; jianli_204@xmu.edu.cn; cuihuiting@xmu.edu.cn; yuanjing@xmu.edu.cn

cytoplasmic assembly of 8 basal bodies and axonemes, and the other is the 3 successive rounds of genome replication without nuclear division, resulting in an octoploid nucleus. Subsequently, 8 axonemes with chromosomes attached are released from the cell body of male gametocytes, resulting in 8 flagellated daughter gametes, which is the process termed "exflagellation".

Parasite stage transition during the *Plasmodium* life cycle requires a fine-tuned multilayer regulation of gene expression[11–13]. Previous studies have identified transcriptional and epigenetic programs critical for the sexual commitment and development of the gametocytes[14–23]. However, how the *Plasmodium* establishes distinct repertoires of transcripts between male and female gametocytes remains incompletely illustrated. RNA-binding proteins (RBPs) can interact with transcripts in all manner of RNA-driven processes[24]. RBPs regulate all aspects of the life cycle of mRNA, including mRNA transcription, splicing, modification, trafficking, translation, and decay[25,26]. RBP-containing ribonucleoprotein complexes, such as the DOZI (development of zygote inhibited) complex and CITH (CARI/Trailer Hitch homolog) complex, had been shown to repress the translation of multiple mRNAs in female gametocytes[27–29]. So far, our understanding of post-transcription control is still limited in the male gametogenesis. Recent transcriptome studies in both human malaria parasite *P. falciparum* and mouse malaria parasite *P. berghei* revealed that certain RBPs are specifically or preferentially expressed in male gametocytes[30,31], implying gender-specific roles of RBPs in the post-transcriptional regulation for male development. However, systematic identification of male RBPs for male gametogenesis and their precise roles in defining the gender distinct transcriptome via the post-transcription regulation have not been reported.

In this work, we perform comparative transcriptome analysis on male and female gametocytes and obtain a list of gender-specific RBPs in the rodent malaria parasite *P. yoelii*. From this list, we identify a functionally unknown gene (PY17X_0716700, named as *Rbpm1* in this study), which is specifically transcribed in male gametocytes. We demonstrate that RBPm1 is a nuclear RBP essential for male gametogenesis and mosquito transmission of parasite. RBPm1 interacts with the spliceosome E complex and initiates the splicing of certain introns in a group of axonemal genes. RBPm1-deficient parasites cannot express these axonemal proteins and fail to assemble the axoneme. These findings reveal an RBPm1-mediated intron splicing program of the axonemal genes essential for *Plasmodium* male development.

Results

RNA-binding protein RBPm1 is expressed in the nucleus of male gametocytes

Approximately 180 putative *Plasmodium* RBPs had been predicted in silico[32]. To identify the key RBPs for male gametogenesis, we searched the male gametocyte-specific RBPs in the rodent malaria parasite *P. yoelii*. Using the fluorescence-activated cell sorting, highly purified male and female gametocytes were collected from a *P. yoelii* reporter line *DFsc7* (Fig. 1A and Supplementary Fig. 1A), in which fluorescent proteins GFP and mCherry are expressed in male and female gametocytes, respectively[33]. We performed RNA-seq and obtained gender-specific gametocyte transcriptome (Supplementary Fig. 1B and Supplementary Data 1). Among the 179 *P. yoelii* RBPs, an unstudied gene (PY17X_0716700) was identified with the greatest enrichment in male compared to female gametocytes (Fig. 1B, left panel). This gene was named as *Rbpm1* for RBP in male gametocyte. Notably, the *Rbpm1* orthologs PBANKA_0716500 and PF3D7_0414500 are also among the top male RBP genes of *P. berghei* and *P. falciparum*, respectively, (Fig. 1B, middle and right panels) based on the gender gametocyte transcriptomes[30,31].

To investigate RBPm1 expression during the parasite life cycle, we tagged endogenous RBPm1 with a sextuple HA (6HA) at the carboxyl (C)-terminus in the *P. yoelii* 17XNL strain (wild type or WT) using CRISPR-Cas9[34,35]. The tagged parasite *Rbpm1::6HA* developed normally in mice and mosquitoes, indicating no detectable detrimental effect of tagging on protein function. Immunofluorescent assay (IFA) showed that RBPm1 was expressed only in gametocytes, but not in asexual blood stages, ookinetes, oocysts, or sporozoites (Fig. 1C, upper panel). Immunoblot also confirmed the gametocyte-restricted expression of RBPm1 (Fig. 1D). Gametocyte-specific expression of RBPm1 was observed in another parasite line *Rbpm1::gfp*, in which RBPm1 was tagged with GFP from the 17XNL (Fig. 1C, lower panel). To dissect whether RBPm1 expression is male-specific, the *Rbpm1::6HA* gametocytes were co-stained with antibodies against HA and α-Tubulin II (a highly expressed protein in male gametocytes[36]. RBPm1 was only detectable in the male gametocytes (Fig. 1E). Additionally, we tagged RBPm1 with 6HA in the reporter line *DFsc7* and observed the male-specific expression of RBPm1 (Fig. 1F). We noticed the nuclear localization of RBPm1 in all the male gametocytes tested (Fig. 1C, E, F), which was further confirmed by immunoblot of nuclear and cytoplasmic fractions from the *Rbpm1::6HA* gametocytes (Fig. 1G). Last, we analyzed the localization dynamics of RBPm1 throughout the process of gametogenesis (0, 2, 8, and 15 min post activation, mpa) in the *Rbpm1::6HA* parasites. Both IFA and immunoblot revealed consistent protein expression profile and nuclear localization of RBPm1 during gametogenesis (Fig. 1H, I). Together, these results demonstrated that RBPm1 was a nuclear protein specifically expressed in the male gametocytes.

RBPm1 is essential for male gametogenesis and mosquito transmission of parasite

P. yoelii Rbpm1 gene encodes a protein of 361 amino acid (aa) residues, with two RNA recognition motifs (RRM1 and RRM2). To investigate its function, we generated a mutant line, *ΔRbpm1*, by deleting the entire genomic sequence (1904 bp) of *Rbpm1* gene in *P. yoelii* 17XNL strain using CRISPR-Cas9 (Fig. 2A). *ΔRbpm1* produced normal level of male and female gametocytes in mice (Fig. 2B), indicating that RBPm1 is not essential for asexual blood stage proliferation and gametocyte formation. We next measured the male gametogenesis by counting exflagellation centers (ECs) in vitro after stimulation with 50 μM xanthurenic acid (XA) at 22 °C. *ΔRbpm1* showed a striking deficiency in the EC formation (Fig. 2C, D) and male gamete release (Fig. 2E). In contrast, RBPm1 disruption had no impact on female gamete formation in vitro (Fig. 2F), which corresponded with no RBPm1 expression in female. *ΔRbpm1* produced no ookinetes in vitro (Fig. 2G) or midgut oocysts and salivary gland sporozoites in the infected mosquitoes (Fig. 2H, I), indicating transmission failure in mosquito. Additionally, we deleted each of the RNA recognition motifs RRM1 (119–190 aa) and RRM2 (203-274 aa) of endogenous RBPm1 in the 17XNL (Fig. 2A). Both mutants, *Δrrm1* and *Δrrm2*, displayed similar defects as those observed in *ΔRbpm1* (Fig. 2B, D), suggesting essential role of both two RNA recognition motifs in RBPm1 function.

To further confirm that the *ΔRbpm1* phenotype was caused by *Rbpm1* deficiency, we introduced a sequence consisting of the coding region of *Rbpm1* and a N-terminal quadruple Myc epitope (4Myc) back to the *Rbpm1* locus in the *ΔRbpm1* line, generating the complemented line, referred to as *rescue* (Fig. 2A). The 4Myc-tagged RBPm1 was detected in the *rescue* gametocytes (Fig. 2J) and localized in the nucleus of male gametocytes (Fig. 2K). The *rescue* parasites restored the formation of ECs (Fig. 2C, D), male gametes (Fig. 2E), ookinetes (Fig. 2G), midgut oocysts (Fig. 2H), and salivary gland sporozoites (Fig. 2I).

Lastly, we performed genetic crosses between *ΔRbpm1* mutant and the male-deficient line Δ*map2* or the female-deficient line Δ*nek4*. As expected, the cross between Δ*map2* and Δ*nek4* produced the ookinetes in vitro (Fig. 2L). The ookinete formation was restored in the Δ*Rbpm1* parasites that were crossed with Δ*nek4* but not Δ*map2*, further confirming the defective male gamete formation in the *ΔRbpm1*. Together, these results demonstrated that RBPm1 is essential for male gametogenesis and mosquito transmission of parasites.

https://doi.org/10.1038/s41467-024-49002-9

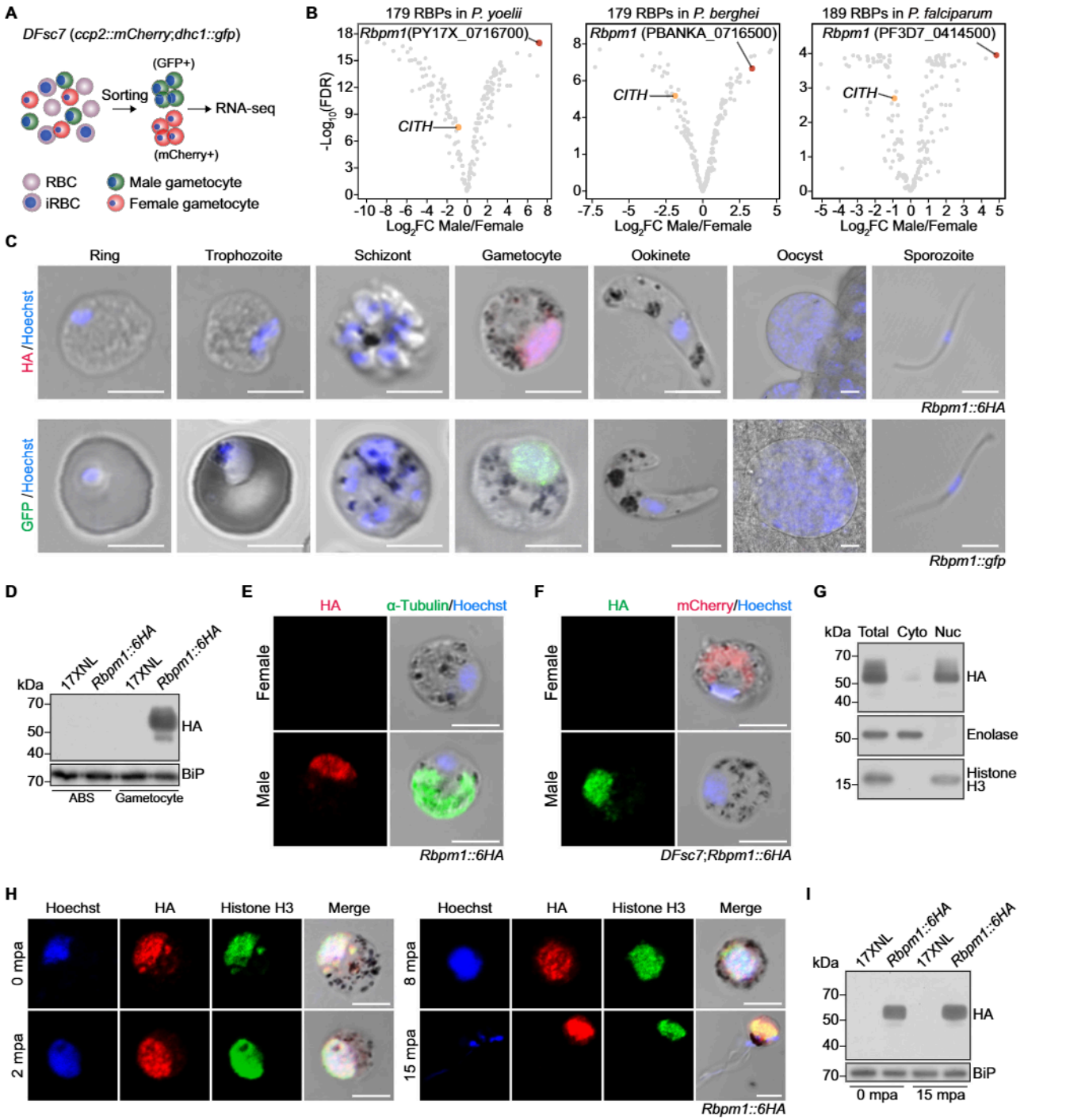

Fig. 1 | RNA-binding protein RBPm1 is expressed in the nucleus of male gametocytes. A Flowchart showing the purification and transcriptome analysis of male (green, GFP+) and female (red, mCherry+) gametocytes from a *P. yoelii* parasite reporter line *DFsc7*. **B** Gender analysis of gene transcription for the *Plasmodium* genome-wide putative RBPs between male and female gametocytes. The top male gene PY17X_0716700, *RBPm1*, is marked in red. CITH (orange dot) is a known female RBP. The results of *P. berghei* (middle panel) and *P. falciparum* (right panel) were based on the published gametocyte transcriptomes contributed by Yeoh, L.M. 2017 and Lasonder, E. 2016. The *p*-values were calculated by quasi-likelihood F-test and adjusted by false discovery rate (FDR). **C** Stage expression of RBPm1 during the *P. yoelii* life cycle. Immunofluorescence assay (IFA) of RBPm1 expression in the *Rbpm1::6HA* parasites stained with anti-HA antibody (top panel). Live cell imaging of the RBPm1::GFP protein in the *Rbpm1::gfp* parasites (bottom panel). Nuclei were stained with Hoechst 33342. Three independent experiments with similar results. Scale bars: 5 μm. **D** Immunoblot of RBPm1 in the asexual blood stage (ABS) and gametocyte of the *Rbpm1::6HA* parasites. BiP as a loading control. Three independent experiments with similar results. **E** IFA of HA-tagged RBPm1 and α-Tubulin (male gametocyte marker protein) in *Rbpm1::6HA* gametocytes. Three independent experiments with similar results. Scale bars: 5 μm. **F** IFA of HA-tagged RBPm1 and mCherry (expressed in female gametocytes) in the *DFsc7;Rbpm1::6HA* gametocytes. Three independent experiments with similar results. Scale bars: 5 μm. **G** Immunoblot of RBPm1 in cytosolic and nuclear fractions of *Rbpm1::6HA* gametocytes. Enolase (cytoplasmic/Cyto) and histone H3 (nuclear/Nuc) proteins used as controls respectively. Two independent experiments with similar results. **H** IFA of HA-tagged RBPm1 and histone H3 during male gametogenesis of the *Rbpm1::6HA* parasites. mpa: minute post activation. Three independent experiments with similar results. Scale bars: 5 μm. **I** Immunoblot of RBPm1 expression in the *Rbpm1::6HA* parasites during male gametogenesis. Two independent experiments with similar results.

https://doi.org/10.1038/s41467-024-49002-9

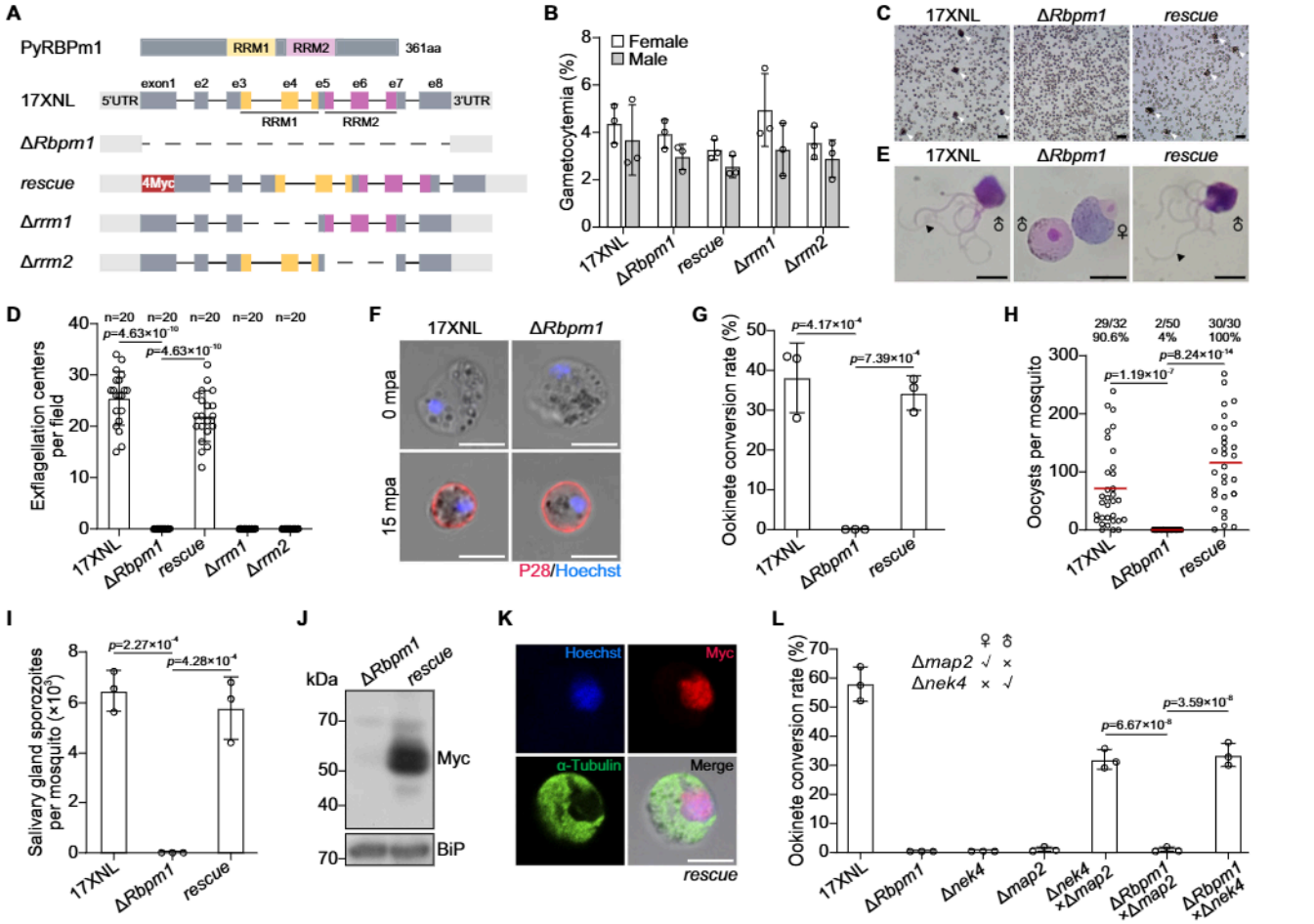

Fig. 2 | RBPm1 is essential for male gametogenesis and mosquito transmission of parasite. A A schematic showing genetic modification at the *Rbpm1* locus in the *P. yoelii* parasite. The top panel depicts the protein structure of RBPm1 with two RNA recognition motifs RRM1 (residues 119-190, yellow) and RRM2 (residues 203-274, purple). Δ*Rbpm1*, deletion of the whole coding sequence from the 17XNL (wild type) strain; *rescue*, the Δ*Rbpm1* line complemented with *Rbpm1* fused with a 4Myc tag; Δ*rrm1* and Δ*rrm2*, deletion each of RRM1 and RRM2 from the 17XNL. **B** Female and male gametocyte formation in mice for the modified parasite. Data are means ± SEM of three independent experiments. **C** Exflagellation center (EC) formation of activated male gametocytes at 10 mpa. Cell clusters representing the EC are marked with white arrows. Four independent experiments with similar results. Scale bars: 20 μm. **D** Quantification of EC formation. The ECs were counted within a 1 × 1-mm square area in the hemocytometer under a light microscope. n represents the number of fields counted. Means ± SEM, one-way ANOVA with Tukey multiple pairwise-comparisons. Three independent experiments. **E** Light microscope images of the exflagellated male gametes (black arrow) after Giemsa staining. Four independent experiments with similar results. Scale bars: 5 μm. **F** Female gamete formation assayed by P28 staining. P28 is a female gamete plasma membrane protein. *n* = 32 and 35 female gametocytes in 17XNL and Δ*Rbpm1* respectively. Scale bars: 5 μm. **G** Ookinete formation in vitro. Data are means ± SEM from three independent experiments, one-way ANOVA with Tukey multiple pairwise-comparisons. **H** Midgut oocyst formation in mosquitoes at 7 days after blood feeding. x/y at the top represents the number of mosquitoes containing oocysts/the number of dissected mosquitoes, and the percentage represents the infection prevalence of mosquitoes. Red lines show the mean value of oocyst numbers, one-way ANOVA with Tukey multiple pairwise-comparisons. Three independent experiments with similar results. **I** Salivary gland sporozoite formation in mosquitoes at 14 days after blood feeding. At least 20 infected mosquitoes were counted in each group. Data are means ± SEM of three independent experiments, one-way ANOVA with Tukey multiple pairwise-comparisons. **J** Immunoblot analysis of RBPm1 expression in gametocytes of the complemented line *rescue*. BiP as a loading control. Two independent experiments with similar results. **K** IFA of Myc-tagged RBPm1 and α-Tubulin in gametocytes of the *rescue* parasite. Three independent experiments with similar results. Scale bars: 5 μm. **L** Gender gamete fertility assay of the Δ*Rbpm1* by parasite genetic cross. Fertility was determined by ookinete development of Δ*Rbpm1* gametes after cross-fertilization with mutant lines that are defective in either female (Δ*nek4*) or male (Δ*map2*) gametes. Data are means ± SEM of three independent experiments, one-way ANOVA with Tukey multiple pairwise-comparisons.

Defective axoneme assembly in RBPm1-deficient male gametogenesis

Next, we delineated more detailed defects of Δ*Rbpm1*. During male gametogenesis, the parasites undergo axoneme assembly, genome replication, rupture of the parasitophorous vacuole membrane (PVM) and erythrocyte membrane (EM), and finally releasing eight uniflagellated male gametes. We first assessed the axoneme assembly. At 0 mpa, both α- and β-Tubulin were evenly distributed in the cytosol of male gametocytes of WT and Δ*Rbpm1* (Fig. 3A, upper panel). Immunoblot also detected comparable level for both Tubulins in gametocytes between WT and Δ*Rbpm1* (Fig. 3B). At 8 mpa, the axonemal microtubules (MTs) were observed to be coiled around the enlarged nucleus in the WT gametocytes. However, aberrant axonemes were formed in Δ*Rbpm1* (Fig. 3A, middle panel). At 15 mpa, Δ*Rbpm1* failed to produce flagellated male gametes (Fig. 3A, lower panel). Under ultrastructure expansion microscopy (U-ExM)[37], the axonemes lost bundled structures at 8 mpa in Δ*Rbpm1* compared to the organized axonemes in WT (Fig. 3C). We used electron microscope to dissect the ultrastructural defects of axoneme in Δ*Rbpm1* male gametocytes at 8 mpa. The majority of axonemes (93%, 150 axonemes from 43 section images) displayed 9 + 2 arrangement of MTs in WT (Figs. 3D). In contrast, no intact axonemes (from 69 section images) were detected in either

https://doi.org/10.1038/s41467-024-49002-9

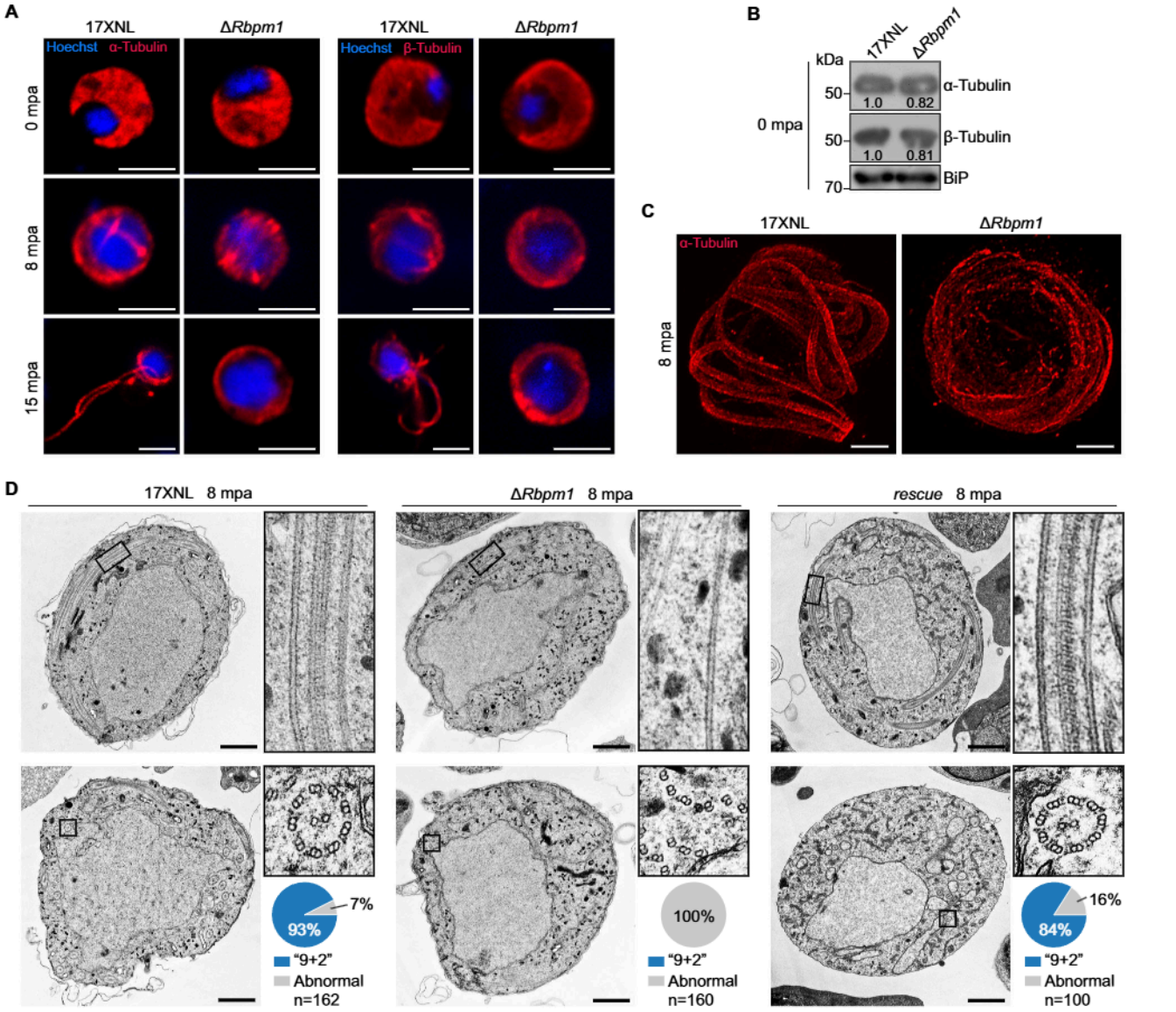

Fig. 3 | Defective axonemal assembly in RBPm1-null male gametogenesis. **A** Detection of formation and exflagellation of axonemes during male gametogenesis (0, 8, and 15 mpa) by staining α-Tubulin (left panels) and β-Tubulin (right panels). Nuclei were stained with Hoechst 33342. Four independent experiments with similar results. Scale bars: 5 μm. **B** Immunoblot of α- and β-Tubulins in gametocytes. The numbers indicate the relative intensities of the bands in the immunoblots. BiP as a loading control. Two independent experiments with similar results. **C** Ultrastructure expansion microscopy (U-ExM) of the axonemes in male gametocytes stained with α-Tubulin antibody at 8 mpa. Three independent experiments with similar results. Scale bars: 5 μm. **D** Transmission electron microscopy of axoneme architecture in male gametocytes at 8 mpa. Inset panels show longitudinal sections (top panels) and cross sections (bottom panels) of axonemes. The enclosed area (black box) was zoomed in. Pie charts show the quantification of axoneme ("9 + 2" microtubules) in the mutant parasites. n is the total number of intact and defective axoneme structures observed in each group. Three independent experiments with similar results. Scale bars: 1 μm.

longitudinal or cross sections of Δ*Rbpm1* (Figs. 3D). All the axonemes in Δ*Rbpm1* showed severe defects with loss of either central singlet MTs or peripheral doublet MTs (Fig. 3D), consistent with the observation of Tubulin staining in Fig. 3C. In the complemented line *rescue*, the axoneme assembly restored to normal as in WT (Figs. 3D). These results demonstrated that RBPm1 is required for axoneme assembly during male gametogenesis.

We additionally analyzed genome replication and erythrocyte rupture during male gametogenesis. Flow cytometry analysis of male gametocytes at 8 mpa detected a comparable increase in DNA content in both parental *DFsc7* and its derivative mutant *DFsc7*;Δ*Rbpm1* parasites (Supplementary Fig. 2A). These results indicated normal genome replication in the absence of RBPm1, consistent with the enlarged nucleus observed in the activated Δ*Rbpm1* male gametocytes from both the fluorescence and electron microscope images (see Fig. 3A, D). In addition, immunostaining of SEP1 (parasite PVM protein) and TER119 (mouse EM protein) showed that RBPm1 deficiency had no notable effect on parasite rupture from the gametocyte-residing erythrocytes (Supplementary Fig. 2B, C).

RBPm1 deficiency causes defective intron splicing of axonemal genes

To investigate the mechanism of RBPm1 in regulating the axoneme assembly, we performed RNA-seq to examine the changes in male transcriptome due to the loss of RBPm1 (Fig. 4A). To purify the RBPm1-null male gametocytes for comparison, we deleted *Rbpm1* in the *DFsc7* line. The mutant line *DFsc7*;Δ*Rbpm1* displayed the same phenotypes as Δ*Rbpm1* (Supplementary Fig. 3A–D). Purified male gametocytes of the *DFsc7*;Δ*Rbpm1* were collected by fluorescence-activated cell sorting for RNA-seq (Supplementary Fig. 3E, F). We analyzed the differentially

https://doi.org/10.1038/s41467-024-49002-9

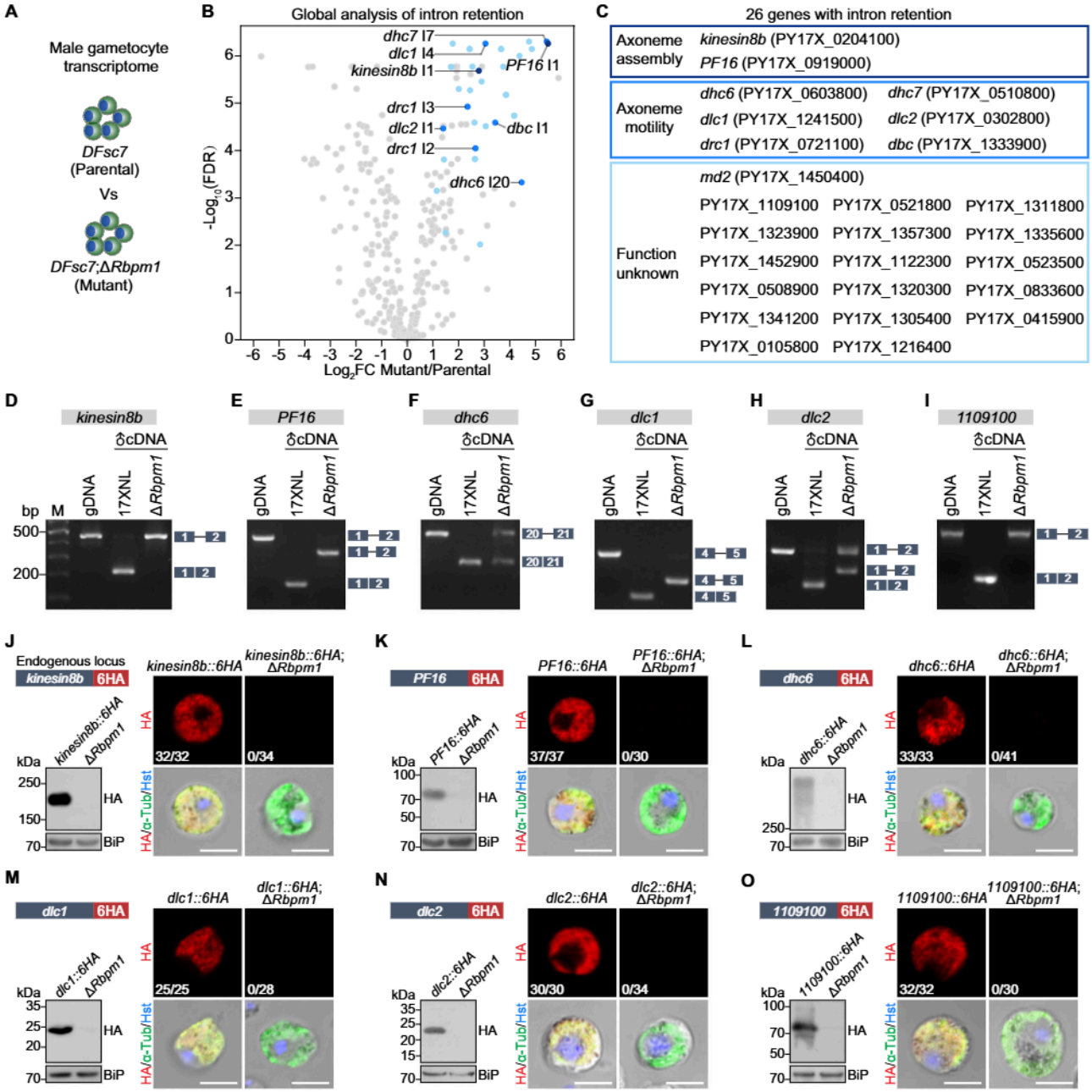

Fig. 4 | RBPm1 deficiency causes intron retention and protein loss of axonemal genes. A A schematic showing the transcriptome analysis of RBPm1-null male gametocytes. *DFsc7*;Δ*Rbpm1* is a *DFsc7*-derived RBPm1 mutant line. *DFsc7* (parental) and *DFsc7*;Δ*Rbpm1* (mutant) male gametocytes were sorted by FACS for RNA-seq. **B** Global analysis of differential intron retention identified 30 retained introns (blue dots) in the mutant versus the parental line. Retained introns with $\log_2FC \geq 1$ and $p \leq 0.05$ were further verified manually by visualization in IGV. The *p*-values were calculated by quasi-likelihood F-test and adjusted by FDR. These introns were originated from 26 genes. Detailed information of these genes and introns is provided in Supplementary Fig. 4A. **C** List of the 26 genes with intron retention from (**B**), categorized by protein function. **D**–**I**. RT-PCR confirmation of intron retention in 6 selected genes *kinesin8b*, *PF16*, *dhc6*, *dlc1*, *dlc2*, and *PY17X_1109100*. Genomic DNA (gDNA) from 17XNL parasite, complementary DNA (cDNA) from male gametocytes of parental and mutant parasites were analyzed. Exons are indicated by boxes and introns by lines. Three independent experiments with similar results. RT-PCR analysis for all 26 genes is presented in Supplementary Fig. 5A. **J**–**O**. Protein expression analysis of the 6 genes shown in (**D**–**I**) in male gametocytes after loss of RBPm1. Each endogenous gene was tagged with a 6HA at the C-terminus in both 17XNL and Δ*Rbpm1* parasites (the schematic in the top left panel), generating two tagged lines. Immunoblot of the 6HA-tagged protein in gametocytes with and without RBPm1 (bottom left panel). IFA of the 6HA-tagged protein in male gametocytes with and without RBPm1 (right panel). x/y at bottom-left represents the number of HA-positive male gametocytes/the total number of male gametocytes tested. Three independent experiments with similar results. Scale bars: 5 μm.

expressed genes between *DFsc7* and *DFsc7*;Δ*Rbpm1* (Supplementary Data 2). As expected, the *Rbpm1* transcripts were undetectable in the *DFsc7*;Δ*Rbpm1* (Supplementary Fig. 3G, H). RBPm1 deficiency led to changed expression of several genes (Supplementary Fig. 3G), but none of the differentially expressed genes was known to be implicated in axoneme assembly during male gametogenesis.

We found 30 intron retention (IR) events in transcripts of 26 genes after loss of RBPm1 (Fig. 4B, C) by bioinformatic analysis of global intron retention and manual examination on Integrative Genomics Viewer[38]. These genes were specifically or preferentially transcribed in the male gametocytes (Supplementary Fig. 4A). Among them (Fig. 4C), the orthologs of *kinesin8b* and *PF16* had been reported essential for

axoneme assembly of male gametogenesis in *P. berghei*[39–41]. Six putative dynein motor-associated genes, *dhc6* (dynein heavy chain, PY17X_0603800), *dhc7* (dynein heavy chain, PY17X_0510800), *dlc1* (dynein light chain, PY17X_1241500), *dlc2* (dynein light chain, PY17X_0302800), *drc1* (dynein regulatory complex protein, PY17X_0721100), and *dbc* (dynein beta chain, PY17X_1333900), were included. The *md2* (male development protein 2, PY17X_1450400), a male gene recently identified[42], was also included. The rest 17 IR genes had not been previously described in the *Plasmodium*. Gene Ontology (GO) enrichment analysis of these IR genes found significant GO terms that are associated with MT or cytoskeleton (Supplementary Fig. 4B). RT-PCR using the primers anchored in the flank exons of each of 26 introns further confirmed that these introns were retained in the transcripts in the absence of RBPm1, while their neighboring introns were correctly removed (Fig. 4D–I and Supplementary Fig. 5A). Using RT-qPCR, we further confirmed the IR of *kinesin8b* intron1 and *PF16* intron1 in the RBPm1-null male gametocytes (Supplementary Fig. 5B). Interestingly, the whole part of intron was retained in the transcripts for most IR genes, while only a N-terminal part of intron was retained for three IR genes, including *PF16* intron1, *dlc1* intron4, and PY17X_1311800 intron5 (Fig. 4D–I and Supplementary Fig. 5A). Therefore, RBPm1 is required for the splicing of selective introns in certain male genes, especially MT or cytoskeleton-related genes.

We speculated that the RBPm1-regulated IR genes are axonemal given the following facts: (1) RBPm1 depletion causes defective axoneme assembly; (2) All IR genes are male-specific; (3) 8 IR genes are axoneme-related. To test it, we selected 12 out of the 26 genes, including 6 annotated (*kinesin8b*, *PF16*, *dhc6*, *dhc7*, *dlc1*, *dlc2*) and 6 unannotated (PY17X_1109100, PY17X_0521800, PY17X_1311800, PY17X_1323900, PY17X_1357300, PY17X_1335600). Each gene was endogenously tagged at the N- or C-terminus with a 6HA in the 17XNL. All 12 proteins were specifically expressed in male gametocytes during parasite life cycle (Supplementary Fig. 6A), in agreement with their transcript profile. In the inactivated gametocytes, these proteins were distributed in the cytoplasm, while after activation, 11 of 12 proteins displayed axoneme localization in the flagellating male gametes (Supplementary Fig. 6B–M). These results suggested that RBPm1 controls intron splicing for a group of the axonemal genes.

Intron retention leads to loss of axonemal protein in RBPm1-null male gametocytes

Nucleotide sequence analysis revealed that IR would result in premature translation and thus cause loss of protein expression for the axonemal genes (Supplementary Fig. 7). To analyze the effect of IR on the axonemal proteins after RBPm1 loss, we deleted *Rbpm1* gene in each of two tagged lines *kinesin8B::6HA* and *PF16::6HA* (Fig. 4J, K). In the absence of RBPm1, 6HA-tagged Kinesin8B, and PF16 were not detected or under detectable thresholds in male gametocytes compared to the parental counterparts in both IFA and immunoblot (Fig. 4J, K). To further confirm the protein loss, we analyzed 4 other IR genes *dhc6*, *dlc1*, *dlc2*, and PY17X_1109100. Endogenous *Rbpm1* gene was deleted in all the 4 tagged lines (*dhc6::6HA*, *dlc1::6HA*, *dlc2::6HA*, and *1109100::6HA*) (Fig. 4L–O). These 6HA-tagged proteins lost expression in the RBPm1-null male gametocytes (Fig. 4L–O), similarly as Kinesin8B and PF16 did. These results demonstrated that RBPm1 deficiency causes expression loss of target axonemal proteins.

To confirm the essential roles of *P. yoelii* Kinesin8B and PF16 in axoneme assembly as reported in *P. berghei*[39–41], we disrupted *kinesin8b* and *PF16* genes in the 17XNL, obtaining mutant lines *Δkinesin8b* and *ΔPF16* (Supplementary Fig. 8A). As expected, depletion of *kinesin8b* or *PF16* either blocked or severely impaired male gamete formation, respectively (Supplementary Fig. 8B). Neither mutant produced any midgut oocysts in the infected mosquitoes (Supplementary Fig. 8C). Ultrastructure analysis of male gametocytes at 8 mpa revealed that the *Δkinesin8b* mutant failed to develop "9 + 2" axoneme, with loss of both central and peripheral MTs, while most of the axonemes lost central MTs (shown as "9 + 0" or "9 + 1") in the *ΔPF16* (Supplementary Fig. 8D, E), in line with gene disruption phenotypes in *P. berghei*[39–41]. Therefore, depletion of Kinesin8B or PF16 phenocopies RBPm1 deficiency in axoneme assembly.

Intron deletion restores axonemal proteins and partially rectifies axoneme assembly defects in RBPm1-null gametocytes

Since IR disrupted the axonemal proteins expression, we tested whether enforced genomic deletion of the retained intron could restore protein expression by bypassing intron splicing at the transcripts in RBPm1-null male gametocytes. The endogenous *kinesin8b* intron1 (239 bp) was removed in the *kinesin8b::6HA*;*ΔRbpm1* parasite by CRISPR-Cas9 (Fig. 5A), generating the intron-null mutant *kinesin8bΔintron1* (*kinesin8bΔI1*). Both IFA and immunoblot revealed that the deletion of intron1 restored Kinesin8B::6HA expression to WT level in the RBPm1-null gametocytes (Fig. 5B, C). To further confirm the restoration effect, we tested 3 other retained introns (*PF16* intron1, *dlc1* intron4, and *PY17X_1109100* intron1). Compared to the parental RBPm1-null parasites, the expression of PF16::6HA and 1109100::6HA in male gametocytes were fully restored (Fig. 5D–F, J–L), while the Dlc1::6HA was partially restored after removal of the corresponding intron (Fig. 5G–I). Expression restoration of these axonemal proteins (Kinesin8b, PF16, Dlc1, and PY17X_1109100) via intron deletion strongly confirmed the causative effect of IR on axonemal protein loss in the absence of RBPm1.

We next tested whether genomic deletion of the retained introns could rescue or rectify the defective axoneme assembly in the Δ*Rbpm1* mutant. We deleted the *kinesin8b* intron1 in the Δ*Rbpm1* line, but this deletion of single intron failed to restore any EC formation in the Δ*Rbpm1*;*kinesin8bΔintron1* parasites. However, compared to complete lack of axonemes showing "9 + 2", "9 + 1", or "9 + 0" MTs in the parental Δ*Rbpm1*, some axoneme-like structures ("9 + 2": 1%, "9 + 1": 3%, and "9 + 0": 15%) were detected in the Δ*Rbpm1*;*kinesin8bΔintron1* (Fig. 5M, N), indicating that deletion of *kinesin8b* intron1 could partially rescue the defective axoneme assembly caused by RBPm1 deficiency. Notably, additional deletion of the *PF16* intron1 in the Δ*Rbpm1*;*kinesin8bΔintron1* parasite further mitigated axoneme defects in the resulted Δ*Rbpm1*;*kinesin8b*Δintron1;*PF16*Δintron1 parasite line ("9 + 2": 1%, "9 + 1": 11%, and "9 + 0": 32%) (Fig. 5M, N). These results demonstrated that RBPm1 regulates axoneme assembly by controlling intron splicing of a group of axonemal genes. Without RBPm1, deletion of 2 introns (*kinesin8b* intron1 and *PF16* intron1) was insufficient to restore axoneme assembly to the WT level ("9 + 2": 93%) (Fig. 5M, N). Therefore, in addition to *kinesin8b* and *PF16*, other axonemal genes targeted by RBPm1 may also play important roles in axoneme assembly during male gametogenesis.

RBPm1 interacts with spliceosome E complex and introns of axonemal genes

To investigate whether RBPm1 associates with the spliceosome responsible for intron splicing, we used the biotin ligase TurboID-based proximity labeling to identify RBPm1-interacting proteins in the gametocytes. The endogenous RBPm1 was tagged with a HA::TurboID motif in the 17XNL, generating the line *Rbpm1::TurboID* (Fig. 6A). A control parasite *Rbpm1::T2A::TurboID* was generated by fusing endogenous RBPm1 with a "ribosome skip" T2A peptide, a NLS (nuclear localization signal), and a HA::TurboID (Fig. 6A), permitting separated expression of RBPm1 and biotin ligase. Gametocytes expressing the ligase were incubated with 50 μM biotin for 20 min at 37 °C. Staining with fluorescent-conjugated streptavidin and anti-HA antibody detected a nuclear distribution of biotinylated proteins in both TurboID-modified gametocytes (Supplementary Fig. 9A), indicating biotinylation of the potential RBPm1-interacting proteins in the nucleus. Mass spectrometry of the streptavidin affinity purified proteins from the

https://doi.org/10.1038/s41467-024-49002-9

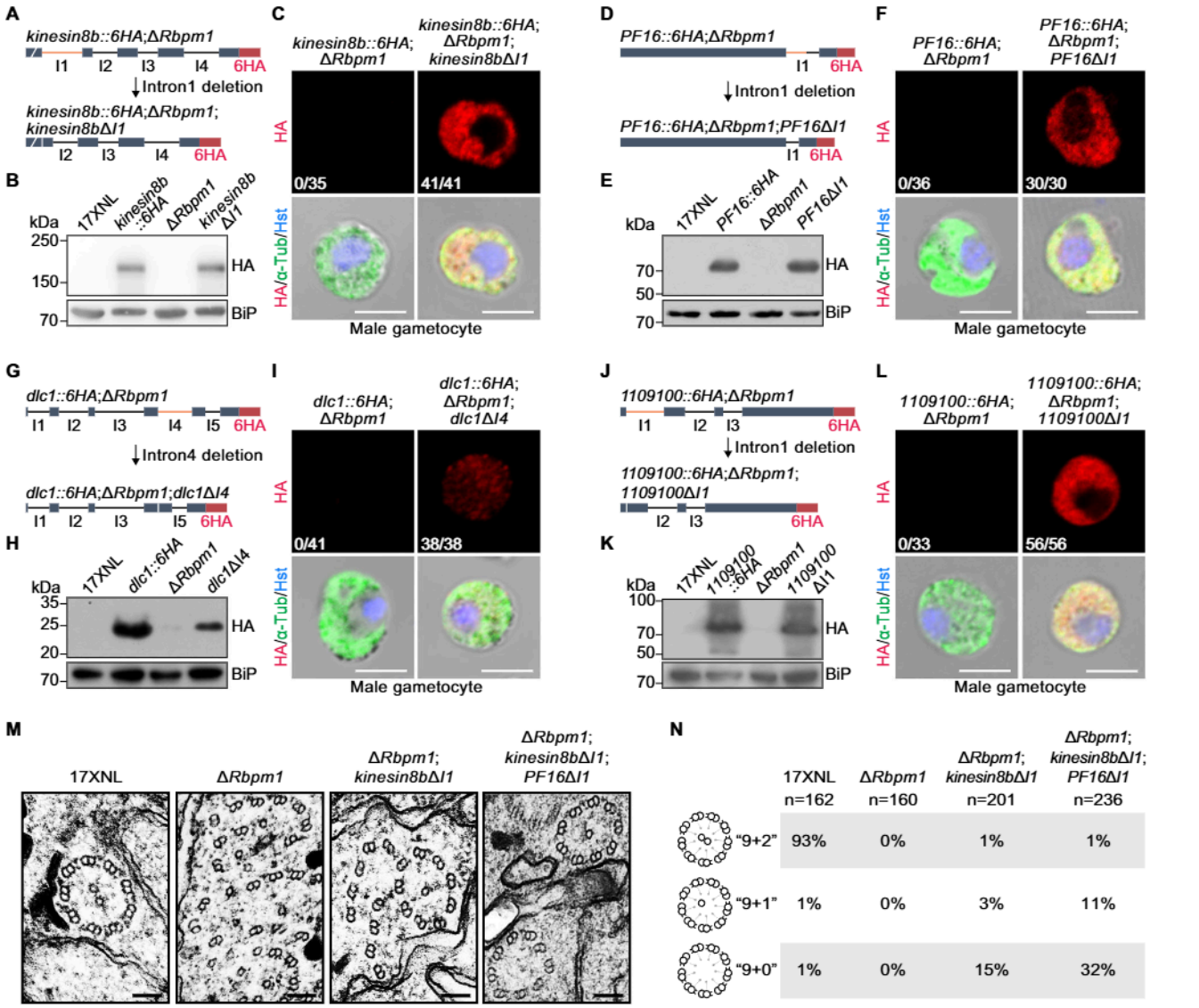

Fig. 5 | Intron deletion restores axonemal protein expression and partially rectifies axoneme assembly defects in RBPm1-null male gametocytes. A A schematic showing the genomic deletion of retained intron (*kinesin8b* intron1, orange) in the *kinesin8b::6HA;ΔRbpm1* parasite (abbreviated as *ΔRbpm1*), generating the mutant *kinesin8b::6HA;ΔRbpm1;kinesin8bΔintron1* (abbreviated as *kinesin8bΔI1*). **B** Immunoblot of 6HA-tagged Kinesin8B protein in gametocytes. Three independent experiments with similar results. **C** IFA of 6HA-tagged Kinesin8B in male gametocytes. x/y represents the number of HA-positive male gametocytes/the total number of male gametocytes tested. Three independent experiments with similar results. Scale bars: 5 μm. **D**, **E**, **F** Effect of intron deletion (*PF16* intron1) on the restoration of PF16 protein in RBPm1-null male gametocytes. Similar analysis as in (**A**, **B**, **C**). **G**, **H**, **I** Effect of intron deletion (*dlc1* intron4) on the restoration of Dlc1 protein in RBPm1-null male gametocytes. **J**, **K**, **L** Effect of intron deletion (*PY17X_1109100* intron1) on the restoration of PY17X_1109100 protein in RBPm1-null male gametocytes. **M** Transmission electron microscopy of axoneme architecture in male gametocytes at 8 mpa. *ΔRbpm1;kinesin8bΔI1* is a *ΔRbpm1*-derived modified line with deletion of *kinesin8b* intron1. *ΔRbpm1;kinesin8bΔI1;PF16ΔI1* is a *ΔRbpm1* derived modified line with deletion of both *kinesin8b* intron1 and *PF16* intron1. Scale bars: 100 nm. **N** Quantification of axoneme formation from parasites in (**M**). n is the total number of the intact and defective axoneme structures observed in each group. Three independent experiments with similar results.

Rbpm1::TurboID resulted in a list of 113 proteins enriched with high confidence compared to the control (Fig. 6B and Supplementary Data 3). RBPm1 was the top hit, confirming cis-biotinylation of RBPm1 (Fig. 6B). Among the significantly enriched proteins, we found the components of the spliceosome earliest assembling E complex[43–45], including the U1 small nuclear ribonucleoproteins (snRNP) U1-70K, U1-A, U1-C, Sm-B, Sm-D1, Sm-D2, Sm-D3, Sm-E, Sm-F and Sm-G (Fig. 6B, C), and three E complex key factors SF1, U2AF1, and U2AF2 (Fig. 6B, C). Tagging the endogenous U1-70K, U1-A, and U1-C proteins with 4Myc in the *Rbpm1::6HA* parasite showed that these three U1 snRNPs co-localized with RBPm1 in the nucleus (Fig. 6D). Co-immunoprecipitation also confirmed the interaction between RBPm1 and these U1 snRNPs (Fig. 6E–G). Spliceosome A, B, and C complex are formed after the assembly of splicing initiating E complex[46,47]. However, the components of A, B, and C complex were not detected (Supplementary Fig. 9B, C). Therefore, RBPm1 interacted only with spliceosome E complex, possibly helping to initiate splicing for certain introns in the axonemal genes (Fig. 6H).

Nuclear localization and interaction with spliceosome E complex imply that RBPm1 may bind to the target introns in the pre-mRNA of axonemal genes. We performed UV crosslinking RNA immunoprecipitation (UV-RIP) followed by RT-qPCR with primers recognizing the target pre-mRNAs. In the *Rbpm1::6HA* gametocytes, RBPm1 bound to the intron1 of the *kinesin8b* transcripts using anti-HA nanobody (Fig. 6I). As a control, RIP using anti-GFP nanobody detected no binding (Fig. 6I). Additionally, we analyzed the interaction between

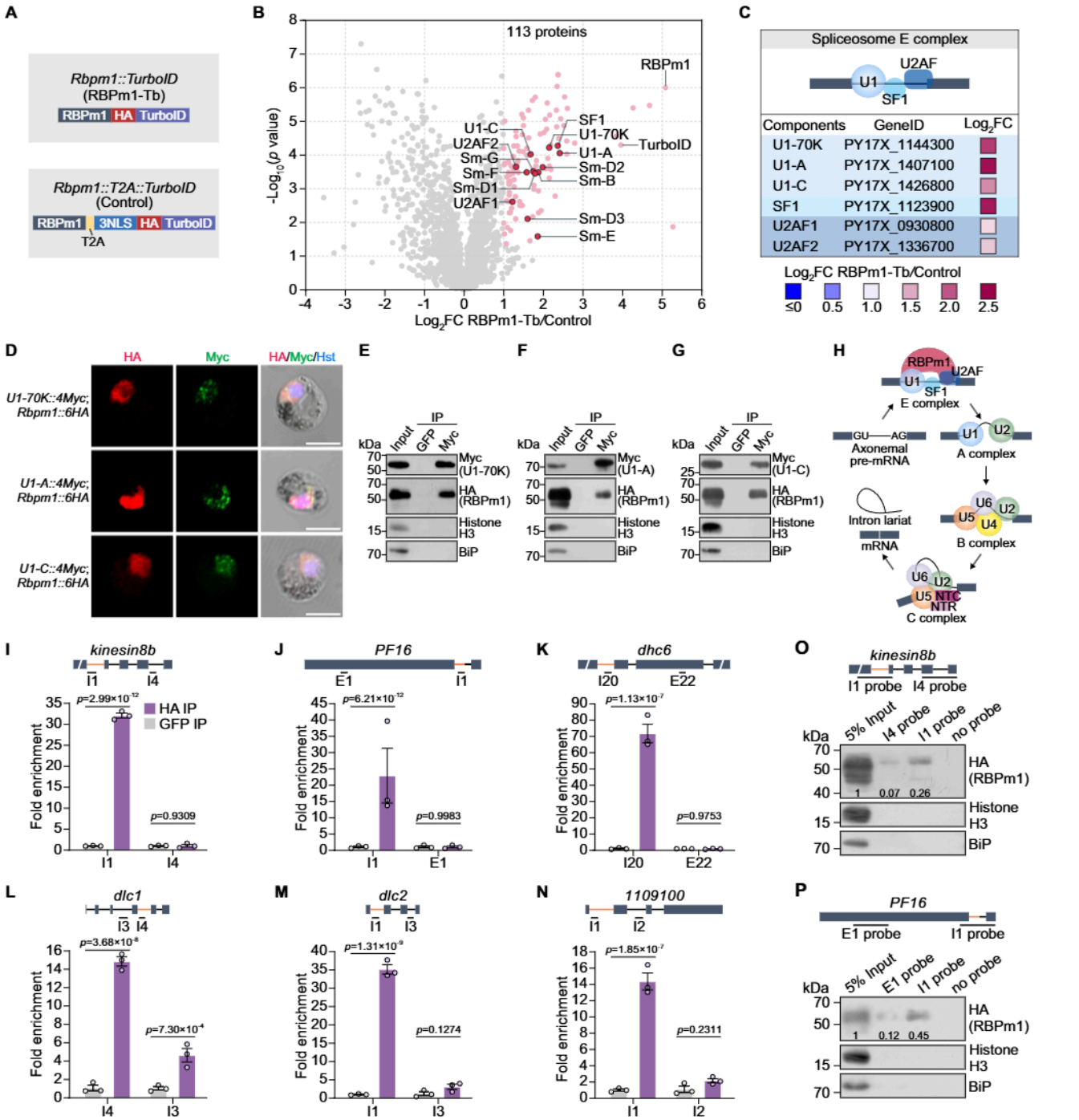

RBPm1 and five other target introns (*PF16* intron1, *dhc6* intron20, *dlc1* intron4, *dlc2* intron1, and *PY17X_1109100* intron1). As expected, RBPm1 bound these target introns. As expected, RBPm1 bound these target introns but not the neighboring introns or exons since each intron is individually excised as a lariat RNA during the splicing (Fig. 6J–N).

Furthermore, we used RNA pull-down to validate the interaction of RBPm1 with the *kinesin8b* intron1 and *PF16* intron1. A biotinylated 500nt RNA probe *kinesin8b* I1 and a control probe *kinesin8b* I4 were synthesized (Fig. 6O, upper panel) and incubated with the *Rbpm1::6HA* gametocyte lysate. The potential RNA-interacted proteins were precipitated using the streptavidin beads and detected by immunoblot. The *kinesin8b* I1 probe retrieved more RBPm1 protein than the *kinesin8b* I4 probe (Fig. 6O). Similarly, the *PF16* I1 probe captured more RBPm1 protein than the probe *PF16* E1 (Fig. 6P). Both RIP and RNA pull-down experiments supported that RBPm1 binds the *kinesin8b* intron1 and *PF16* intron1.

RBPm1 directs splicing of axonemal introns inserted in a reporter gene

To further investigate the interaction between RBPm1 and the axonemal introns, we test whether RBPm1 could direct splicing of target introns when inserted into a reporter gene. We developed a blue fluorescence protein (BFP) reporter assay that allows an easy splicing readout in male and female gametocytes of the *DFsc7* parasite. The intact *bfp* transcript driven by the *hsp70* 5′-UTR and the *dhfr* 3′-UTR was integrated into the *p230p* locus of *DFsc7* using CRISPR-Cas9, generating the control line *BFP* (Fig. 7A). The *kinesin8b* intron1 (*Kin8b*I1, 239 bp) was inserted to the *bfp* gene at the nucleotides

Fig. 6 | RBPm1 interacts with spliceosome E complex and introns of axonemal genes. A A schematic showing two modified parasite lines generated for searching RBPm1-interacting proteins by TurboID-based proximity labeling and mass spectrometry. The motif of HA::TurboID and T2A::3NLS::HA::TurboID, respectively, was inserted at the C-terminus of the endogenous RBPm1, generating the line *Rbpm1::TurboID* and the control line *Rbpm1::T2A::TurboID*. **B** Volcano plot displaying 113 significantly enriched proteins (pink dot, cutoffs $\log_2$FC ≥ 1 and $p \le 0.05$) in the *Rbpm1::TurboID* versus *Rbpm1::T2A::TurboID*. Among them, 13 subunits (red dot) of the early spliceosome E complex were included. The *p*-values were calculated by two-sided *t*-test and adjusted by FDR. **C** Protein interaction analysis between RBPm1 and six spliceosome E complex subunit proteins (U1-70K, U1-A, U1-C, SF1, U2AF1, and U2AF2) from (**B**). **D** IFA of 6HA-tagged RBPm1 and 4Myc-tagged U1 snRNP proteins (U1-70K, U1-A, and U1-C) in male gametocytes of three double-tagged parasites. Three independent experiments with similar results. Scale bars: 5 μm. **E** Co-immunoprecipitation of RBPm1 and U1-70K in gametocytes of the double-tagged parasite *U1-70K::4Myc;Rbpm1::6HA*. Anti-Myc nanobody was used. Bip as a loading control. Three independent experiments with similar results. **F** Co-immunoprecipitation of RBPm1 and U1-A in gametocytes of the double-tagged parasite *U1-A::4Myc;Rbpm1::6HA*. Three independent experiments with similar results. **G** Co-immunoprecipitation of RBPm1 and U1-C in gametocytes of the double-tagged parasite *U1-C::4Myc;Rbpm1::6HA*. Three independent experiments with similar results. **H** Proposed model showing the interaction between RBPm1 and early spliceosome E complex for intron splicing of axonemal genes. **I**–**N**. UV-RIP detection of RBPm1 interaction with the retained introns of 6 axonemal genes (*kinesin8b*, *PF16*, *dhc6*, *dlc1*, *dlc2*, and *PY17X_1109100*). A top schematic shows the exon-intron structure of the RBPm1 target axonemal genes. The retained introns are indicated with orange lines, and the genomic regions for qPCR amplicon are shown. UV-RIP was performed in *Rbpm1::6HA* lines using anti-HA nanobody. Anti-GFP nanobody was used as a control. Bound RNA was analyzed by RT-qPCR. Means ± SEM from three independent experiments, two-sided *t*-test. **O** RNA pull-down assay detecting RBPm1 interaction with *kinesin8b* intron1. A top schematic shows the exon-intron structure of the *kinesin8b* gene. The retained introns are indicated in orange lines. A biotinylated 500 nt RNA probe I1 (comprising intron1 and its flanking sequences) and a control probe I4 (comprising intron4 and its flanking sequences) were used. Proteins via RNA pull-down were immunoblot with anti-HA antibody. The numbers are the relative intensities of bands in the blot. Histone H3 and Bip were used as negative controls. Two independent experiments with similar results. **P** RNA pull-down assay detecting RBPm1 interaction with *PF16* intron1. A top schematic shows the exon-intron structure of the *PF16* gene. The retained introns are indicated in orange lines. A biotinylated 500 nt RNA probe I1 (comprising intron1 and its flanking sequences) and a control probe E1 in exon1 were used. Two independent experiments with similar results.

396–397, generating the line *BFP-Kin8b*I1 (Fig. 7B). The inserted *kinesin8b* intron1 would result in premature translation of the *bfp* transcript if it is not spliced. In the control *BFP* line, BFP was expectedly detected in both male (GFP+) and female (mCherry+) gametocytes (Fig. 7A). However, in the *BFP-Kin8b*I1 line, BFP was detected only in male gametocytes (Fig. 7B), indicating that splicing of *kinesin8b* intron1 in the *bfp* transcripts occurred only in male gametocytes. To prove that splicing of *kinesin8b* intron1 in male was RBPm1-dependent, we deleted *Rbpm1* in the *BFP-Kin8b*I1 line and obtained the mutant line *BFP-Kin8b*I1;Δ*Rbpm1* (Fig. 7C). RBPm1 deletion disrupted BFP expression in the *BFP-Kin8b*I1;Δ*Rbpm1* male gametocytes (Fig. 7C). We parallelly analyzed the *kinesin8b* intron2 (*Kin8b*I2, 148 bp), whose splicing from the native gene transcript required no RBPm1 (Supplementary Fig. 5A). In both transgenic line *BFP-Kin8b*I2 (Fig. 7D) and its derivative mutant line *BFP-Kin8b*I2;Δ*Rbpm1* (Fig. 7E), BFP was detected in both male and female gametocytes, confirming RBPm1-independent splicing of *kinesin8b* intron2 from the *bfp* transcript.

Using the reporter assay, we tested 3 other target introns, including *PF16* intron1 (Fig. 7F, G), *dlc1* intron4 (Supplementary Fig. 10A, B), and *PY17X_1109100* intron1 (Supplementary Fig. 10C, D). The *PF16* intron1 (276 bp) was inserted to the *bfp* at the nucleotides 500-501 (Fig. 7F), the *dlc1* intron4 (193 bp) at the nucleotides 455–456 (Supplementary Fig. 10A), while the *PY17X_1109100* intron1 (353 bp) at the nucleotides 390-391 (Supplementary Fig. 10C). As expected, these introns were spliced from the *bfp* transcript only in male gametocytes (Fig. 7F, Supplementary Fig. 10A, C). Similarly, these introns were not spliced at male gametocytes in the RBPm1-null parasites compared to their parental parasites (Fig. 7G, Supplementary Fig. 10B, D). Additionally, we analyzed the *PY17X_1109100* intron2 (272 bp), which could be spliced in the RBPm1-null parasites (Supplementary Fig. 5A), and found that RBPm1 was not required for splicing of this intron from *bfp* transcript in both male and female gametocytes (Supplementary Fig. 10E, F).

Furthermore, we analyzed the RBPm1 interaction with the *kinesin8b* intron1 and *PF16* intron1 in the *bfp* transcript by RNA pull-down. A biotinylated RNA probe *bfp-Kin8b*I1, corresponding to the *kinesin8b* intron1-inserted *bfp* transcript (Fig. 7H, upper panel), retrieved significantly more RBPm1 from the *Rbpm1::6HA* gametocyte lysate compared to the control probe *bfp* (Fig. 7H, middle panel). Similarly, the probe *bfp-PF16*I1, corresponding to the *PF16* intron1-inserted *bfp* transcript, captured more RBPm1 than the control probe *bfp* (Fig. 7H, lower panel). Therefore, RBPm1 could recognize the axonemal introns in the reporter transcript for splicing (Fig. 7I).

RBPm1 directs splicing of axonemal introns inserted in an endogenous gene

In addition to the reporter gene, we also tested whether RBPm1 could direct splicing of target introns when inserted into an endogenous gene which does not require RBPm1 for intron splicing. We chose the *gep1*, a 4-exon gene expressed in both gender gametocytes and essential for initiating both genders' gametogenesis[48]. We analyzed male and female gametogenesis by measuring EM rupture (TER119 staining), genome replication (DNA staining), and axoneme assembly (α-Tubulin staining). Compared to 17XNL, the *gep1*-deleted parasite line *Δgep1* expectedly lost ability in EM rupture, genome replication, and axoneme assembly in activated male gametocytes, as well as EM rupture in activated female gametocytes (Fig. 8A, B, E, F, G, and H). Using CRISPR-Cas9, the *kinesin8b* intron1 was inserted into the exon3 of *gep1* locus at the nucleotides 273-274 in the 17XNL (Fig. 8C), while the *PF16* intron1 inserted into the exon1 at the nucleotides 885-886 (Fig. 8D). In both intron-inserted lines *gep1-Kin8b*I1 and *gep1-PF16*I1, normal male gametogenesis and defective female gametogenesis was speculated because GEP1 is not expressed in female due to no RBPm1-mediated intron splicing from the *gep1* transcript. Notably, both the *gep1-Kin8b* I1 and *gep1-PF16* I1 parasites underwent EM rupture only in male (Fig. 8C–F). These results supported that both *kinesin8b* intron1 and *PF16* intron1 were spliced from the *gep1* transcript only in male gametocytes with RBPm1 expression. Consistent with GEP1 expression in male gametocytes, normal genome replication and axoneme assembly were detected during male gametogenesis in both *gep1-Kin8b* I1 and *gep1-PF16* I1 parasites (Fig. 8C, D, G, H). Collectively, the results from the reporter and the endogenous gene assays (Fig. 8I) indicated that the tested axonemal introns themselves could be specifically recognized by RBPm1 for splicing.

Intron retention prevents expression of axonemal proteins in female gametocytes

Despite the male-biased transcription, the axonemal genes still displayed low-level transcripts in female gametocytes (Supplementary Fig. 11A, C, E). However, no axonemal proteins are expressed in female gametocytes (Supplementary Fig. 11B, D, F). The facts of no protein product of low-level transcripts for the axonemal genes observed in this study are consistent with results from previous transcriptomic and proteomic studies[30,31,49,50], suggesting a post-transcription regulation for the axonemal genes in female gametocytes. Enforced genomic deletion of the retained intron could restore expression of the axonemal proteins Kinesin8b, PF16, Dlc1,

https://doi.org/10.1038/s41467-024-49002-9

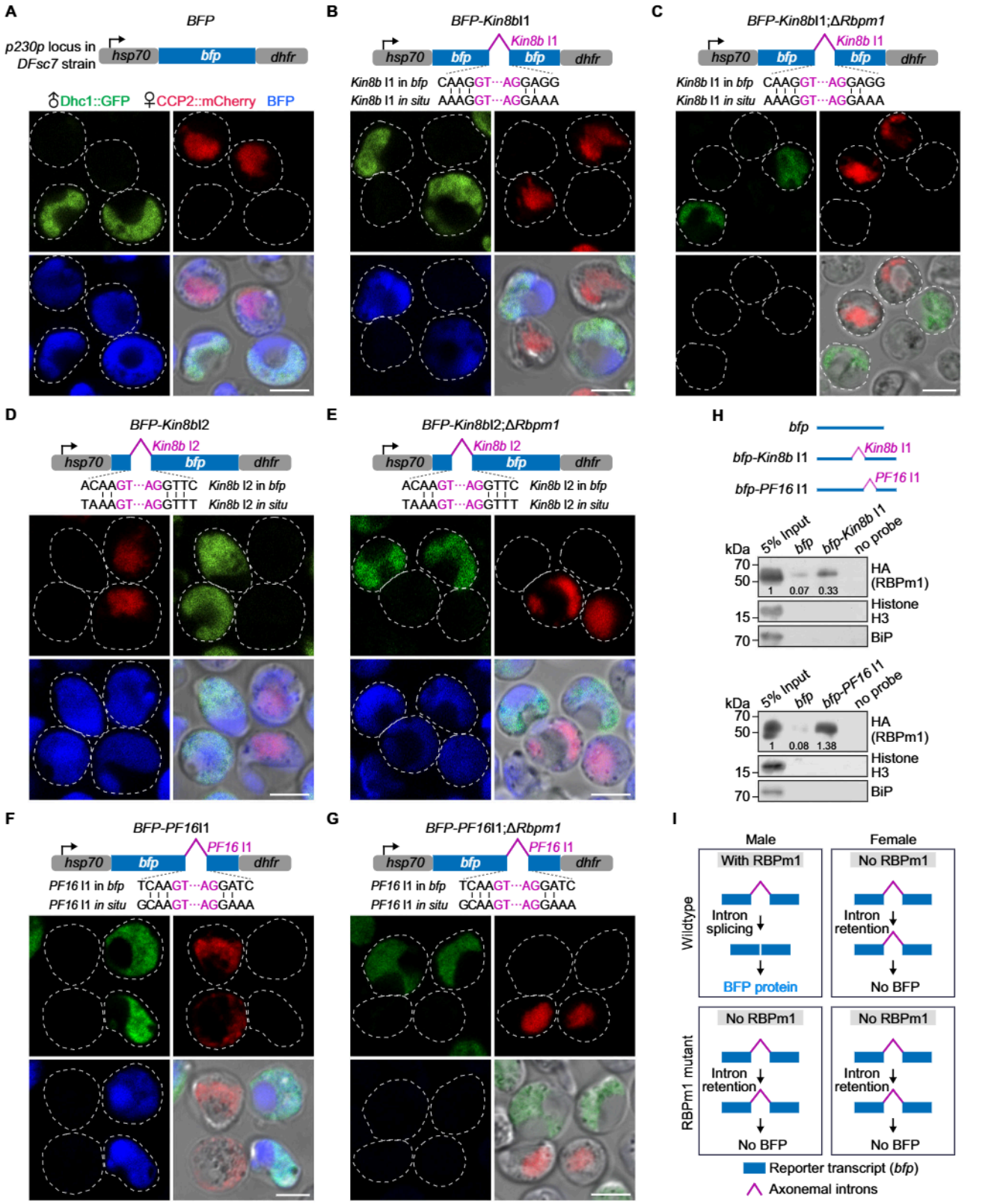

and PY17X_1109100 in the RBPm1-null male gametocytes (Fig. 5A–L). Strikingly, we found that deletion of these introns (*PF16* intron1, *dlc1* intron4, and *PY17X_1109100* intron1) unexpectedly resulted in low-level expression of PF16, Dlc1, and PY17X_1109100 in the counterpart female gametocytes (Supplementary Fig. 11B, D, F). Kinesin8B was not detected in female gametocytes after deletion of *kinesin8b intron1* (Supplementary Fig. 11H), fitting with the extremely low transcription of *kinesin8b* in female gametocytes (Supplementary Fig. 11G). Furthermore, RT-PCR not only detected the transcripts of these axonemal genes (*PF16*, *dlc1*, and *PY17X_1109100*), but also IR in these transcripts from the purified female gametocytes (Supplementary Fig. 11I–L). These results indicated a role of the RBPm1-target introns in preventing the expression of axonemal proteins in female gametocytes.

Fig. 7 | RBPm1 directs splicing of axonemal introns inserted in a reporter gene. **A** A top schematic shows a transgenic line *BFP* with a *bfp* reporter expression cassette integrated at the *p230p* locus of the *DFsc7* reporter line. The intact *bfp* is driven by the 5′UTR of *hsp70* and the 3′UTR of *dhfr*, allowing expression of BFP in both male (GFP+) and female (mCherry+) gametocytes. Live cell imaging was shown. Three independent experiments with similar results. Scale bars: 5 μm. **B.** A transgenic line *BFP-Kin8b*I1 with a *kinesin8b* intron 1 (*Kin8b* I1, purple line)-inserted *bfp* cassette integrated at the *p230p* locus of the *DFsc7* line. *Kin8b* I1 (purple) was inserted into the *bfp* gene at the nucleotides 396-397 to mimic the splice site (vertical lines) of in situ *Kin8b* I1. BFP expression was detected specifically in male gametocytes of the *BFP-Kin8b*I1 parasites. Three independent experiments with similar results. Scale bars: 5 μm. **C** A *BFP-Kin8b*I1 derived RBPm1 mutant line *BFP-Kin8b*I1;Δ*Rbpm1*. No BFP expression was detected in male gametocytes of the *BFP-Kin8b*I1;Δ*Rbpm1* parasites. Three independent experiments. Scale bars: 5 μm. **D** Effect of the *kinesin8b* intron 2 (*Kin8b* I2) insertion on the gametocyte expression of BFP. Similar analysis as in (**B**). BFP expression was detected in both male and female gametocytes of the *BFP-Kin8b*I2 parasites. **E** A *BFP-Kin8b*I2 derived RBPm1 mutant line *BFP-Kin8b*I2;Δ*Rbpm1*. Similar analysis as in (**C**). BFP expression was detected in both male and female gametocytes of the *BFP-Kin8b*I2;Δ*Rbpm1* parasites. **F** Effect of the *PF16* intron1 (*PF16* I1) insertion on the gametocyte expression of BFP. Similar analysis as in (**B**). BFP expression was detected specifically in male gametocytes of the *BFP-PF16*I1 parasites. **G** A *BFP-PF16*I1 derived RBPm1 mutant line *BFP-PF16*I1;Δ*Rbpm1*. Similar analysis as in (**C**). No BFP expression was detected in male gametocytes of the *BFP-PF16*I1;Δ*Rbpm1* parasites. **H** RNA pull-down assay detecting RBPm1 interaction with the *Kin8b* I1 and *PF16* I1 -inserted *bfp* transcripts from *BFP-Kin8b*I1 and *BFP-PF16*I1 gametocytes, respectively. Three biotinylated RNA probes *bfp*, *bfp-Kin8b*I1 (corresponding to the *Kin8b* I1-inserted *bfp* transcript), *bfp-PF16*I1 (corresponding to the *PF16* I1-inserted *bfp* transcript) were used. Proteins via RNA pull-down were immunoblotted with anti-HA antibody. The numbers are the relative intensities of bands in the blot. Histone H3 and Bip were used as negative controls. Two independent experiments with similar results. **I** A schematic of RBPm1-dependent splicing of axonemal introns inserted in the reporter transcript.

Discussion

For efficient transmission, the malaria parasites in the vertebrate host differentiate into sexual precursor gametocytes that are poised to rapidly activate to fertile gametes upon entering into the mosquito midgut for fertilization and further development. So far, a limited number of transcription and epigenetic factors have been identified during gametocyte and gamete development[51,52]. Among ~180 putative *Plasmodium* RBPs, about one-third of RBP genes exhibit stage specific or elevated expression in the gametocyte[32]. From this list of RBPs, we identified a previously undescribed male-specific nuclear RBP, RBPm1, which is essential for male gametogenesis and mosquito transmission of the *Plasmodium*. RBPm1 operates as a stage- and gender-specific splicing factor for spliceosome assembly initiation and regulates the protein expression of a group of 26 male genes, most of which are axoneme-related.

Recent studies had discovered several RBPs playing roles in the developmental programs of gametocyte and gametes. During gametocytes development, UIS12 contributes to the development of gametocytes of both genders[53]. Disrupting *Puf1* led to a reduction in gametocytes, especially female gametocytes[54], while *ccr4-1* gene deletion obstructs male gametocyte development[55]. *Puf2* knockout, on the other hand, promotes male gametocyte development[56]. The CCCH zinc finger protein MD3 regulates the gametocyte maturation and male gametocytogenesis[57]. In female gametocytes, the DOZI/CITH/ALBA translation repressor complex and PUF2 hold the stored mRNAs for translation repression until their proteins were needed during the development of post fertilization[28,58]. Additionally, the CAF1/CCR4/NOT complex also plays a role in safeguarding the stored mRNAs from degradation. In male gametocytes, two functional RBPs have been identified. The alternative splicing factor SR-MG promotes the establishment of sex-specific splicing patterns and knocking it out reduces the formation of male gamete[59]; the *ZNF4*'s knockout results in deregulation of 473 genes, including axonemal dynein-related genes[60]. These documented RBPs and RBPm1 identified in this study may function together at the post-transcriptional regulation to shape the male transcriptome for gametocyte and gamete development.

During the manuscript preparation of this study, another work by ref. 42 demonstrated that deletion of the *Rbpm1* ortholog of *P. berghei* (PBANKA_0716500, named as *md5*) had no effect on female and male gametocyte formation, but resulted in male-specific infertility. These findings are consistent with the defective male gamete formation phenotype of the *ΔRbpm1* in *P. yoelii* in this study, indicating conserved function of RBPm1 in the rodent malaria parasites. As *P. falciparum* is the most lethal human malaria parasite, future studies are worthy to investigate whether the RBPm1 ortholog in the *P. falciparum* functions similarly in male gametogenesis.

The RBPm1-deficient parasites showed specific defects in axoneme assembly during male gametogenesis (Fig. 3). Axoneme is a MT cytoskeleton essential for the eukaryotic flagellar motility, consisting of a central pair of singlet MTs encircled by 9 outer doublet MTs. This 9 + 2 organization of axonemes is highly conserved in the eukaryotes, including *Plasmodium*[61]. However, the axoneme in *Plasmodium* differs from that in other model organisms in several aspects[10,62,63]. First, the biogenesis of axoneme in *Plasmodium* male gametogenesis is extremely fast, taking only 6-8 min to assemble 8 axonemes[9,10]. Second, location of basal body. In the canonical cilium, the basal body is localized under the plasma membrane. In *Plasmodium* male gametocytes, the basal bodies are residing at the nuclear membrane[63]. Third, location for axoneme assembly. The canonical axoneme protrudes distally from the cell simultaneously when growing from the basal body. The *Plasmodium* assemblies the axoneme within the cytoplasm, independent of intraflagellar transport required for cilium formation[10,62]. Last, each assembled axoneme associates with a haploid nuclei to progressively protrude from the parasite plasma membrane, resulting in a free motile flagellum[10]. Mechanisms underlying the cytoplasmic assembly and exflagellation of axonemes in *Plasmodium* remain largely unknown, although the involvement of some conserved basal body and axonemal proteins has been described, including armadillo repeat protein PF16[41], motor protein Kinesin8B[39,40,64], basal body proteins SAS4 and SAS6[63,65–67], and radial spoke protein RSP9[68]. It is possible that the *Plasmodium* had evolved novel mechanisms to fulfill the requirement for the axoneme. In this study, we identified a group of 26 male genes targeted by RBPm1. Several known or putative axoneme-associated genes were included. Importantly, analysis of endogenous protein localization showed that most of the tested proteins encoded by RBPm1-target genes co-localizing with axoneme (Supplementary Fig. 6B–M), suggesting their roles in biogenesis, structure, regulation, or function of axoneme. For future studies, it will be intriguing to understand the roles of these 26 RBPm1-regulated genes, especially 17 previously undescribed ones, during male gametogenesis in the *Plasmodium*.

In the RBPm1 deficient male gametocytes, 30 IR events were detected in 26 male genes. One intron was retained in each of 22 genes while two introns were retained in each of 4 other genes, respectively (Fig. 4B and Supplementary Fig. 4A). Mechanistically, RBPm1 not only bound to the intron-retained transcripts, but also interacted with spliceosome E complex. U1 snRNPs recognize and pair with the 5′ splice site of intron. SF1, U2AF1 and U2AF2 form a complex and bind to branch point, 3′ splice site, and polypyrimidine tract respectively[69,70]. These above factors assemble the E complex as a spliceosome earliest stage. After that, the spliceosome dynamically releases and recruits different snRNPs to establish the assembly for further stages, including spliceosome A, B, and C complex. RBPm1 was detected to interact

https://doi.org/10.1038/s41467-024-49002-9

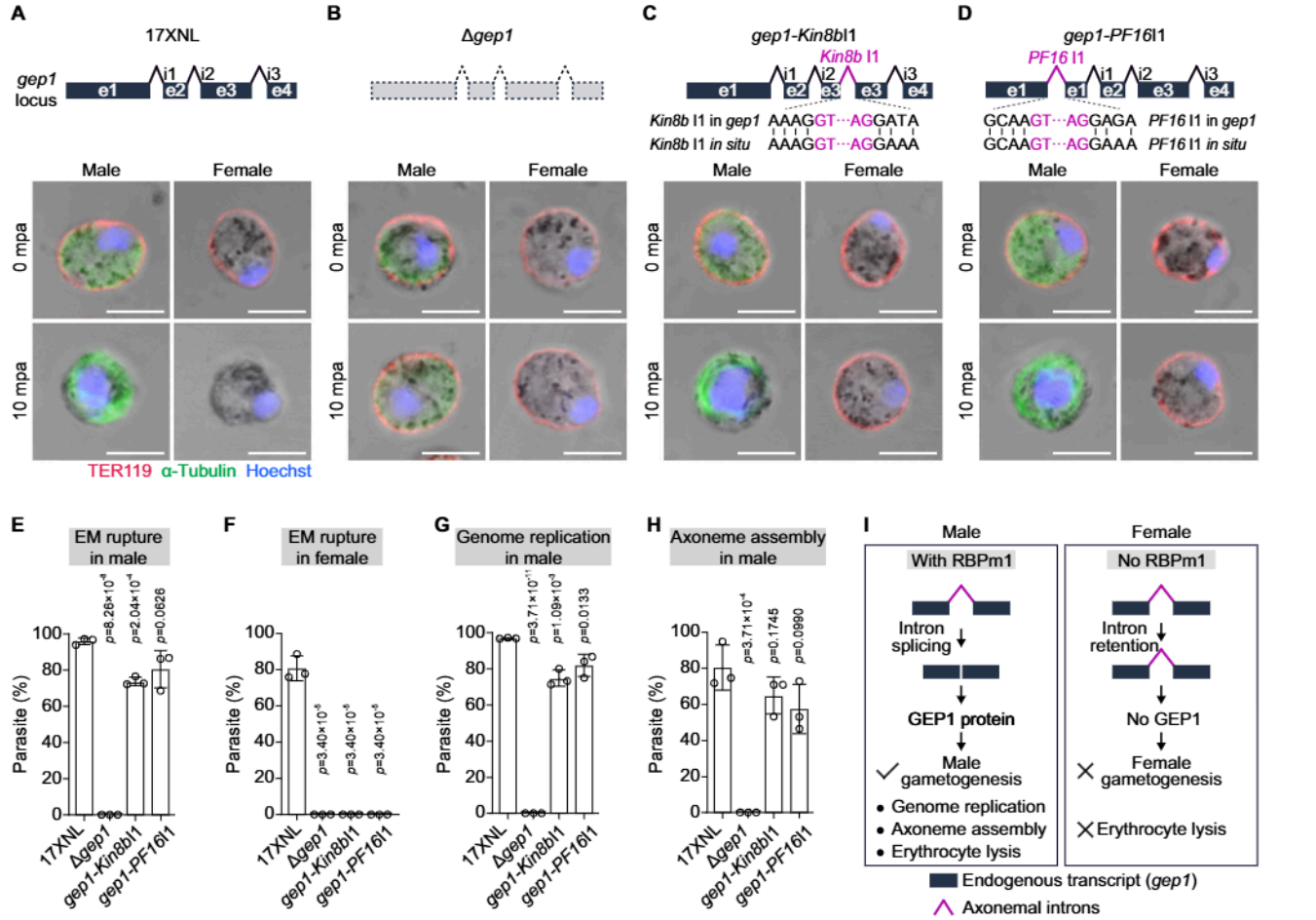

Fig. 8 | RBPm1 directs splicing of axonemal introns inserted in the endogenous gene. A A top schematic shows the genomic locus of a 4-exon gene *gep1*, which is expressed in both gender gametocytes and essential for both genders' gametogenesis. Erythrocyte plasma membrane (EM) rupture, genome replication, and cytoplasmic assembly of the axoneme were analyzed in gametocytes of the 17XNL parasites at 10 mpa. The parasites were co-stained with anti-TER-119 and anti-α-Tubulin antibodies and Hoechst 33342. TER-119 (red) negative gametocytes were recognized as EM rupture. Enlarged nuclei represent the genome replication in male gametocytes. Enhanced α-Tubulin (green) signal represents cytoplasmic assembly of the axoneme in male gametocytes. Three independent experiments with similar results. Scale bars: 5 μm. **B.** A top schematic shows a modified line Δ*gep1*, in which the endogenous *gep1* gene was deleted in the 17XNL. Similar analysis for the Δ*gep1* parasites as in (**A**). **C** A top schematic shows a modified line *gep1-Kin8b*I1, in which the *kinesin8b* intron1 (*Kin8b*I1) was inserted into the exon3 of *gep1* locus at the nucleotides 273-274 in the 17XNL. Similar analysis for the *gep1-Kin8b*I1 parasites as in (**A**). **D** A top schematic shows a modified line *gep1-PF16*I1, in which the *PF16* intron1 (*PF16*I1) was inserted into the exon1 of *gep1* locus at the nucleotides 885-886 in the 17XNL. Similar analysis for the *gep1-PF16*I1 parasites as in (**A**). **E** Quantification of EM rupture in male gametocytes of the four parasites tested. Data are means ± SEM from three independent experiments, two-sided *t*-test. **F** Quantification of EM rupture in female gametocytes of the four parasites tested. Data are means ± SEM from three independent experiments, two-sided *t*-test. **G** Quantification of genome replication in male gametocytes of the four parasites tested. Data are means ± SEM from three independent experiments, two-sided *t*-test. **H** Quantification of axoneme assembly in male gametocytes of the four parasites tested. Data are means ± SEM from three independent experiments, two-sided *t*-test. **I** Schematic of RBPm1-dependent splicing of axonemal introns inserted in the endogenous gene *gep1*. Male-specific RBPm1 could recognize and splice the axonemal introns (*kinesin8b* intron1 or *PF16* intron1) inserted in the *gep1* transcript, allowing male-specific GEP expression and thus male gametogenesis.

exclusively with the components of spliceosome E complex, but not those of the A, B, and C complex (Supplementary Fig. 9C). Therefore, RBPm1 likely function as a splicing activator, linking spliceosome E complex with the selective introns of axonemal genes for splice site recognition. In mammals and plants, a RBP of Dek played a similar role and promoted the splicing of certain introns by bridging the intron with the U1/U2 snRNPs[71,72]. At this stage, the data support an association of RBPm1 and spliceosome E complex, but it is not yet clear if it is a direct association.

Both RIP and RNA pull-down assays demonstrated that RBPm1 interacts with the target introns in transcripts of the axonemal genes, suggesting the presence of signals recognized by RBPm1 in these introns. To investigate if the signals for RBPm1 recognition are imparted by the introns themselves but not the adjoining exons, we analyzed the splicing capability of these introns when they were inserted in either a reporter gene (*bfp*) or an irrelevant endogenous gene (*gep1*). The results from both intron splicing assays establish stringent dependencies of splicing on RBPm1 for these axonemal introns, suggesting intrinsic signals within the introns for RBPm1 recognition. In addition, the adjoining exons may play less modulatory role in the RBPm1 recognition of the axonemal introns. We attempted to search for the common features, such as length, GC content, splice sites, and motif enrichment, but unfortunately observed seemingly no shared features among these 30 RBPm1 target introns. The molecular basis for the axonemal intron recognition by RBPm1 is still unknown. One possibility is that RBPm1 target introns may possess the sequence-independent features, such as RNA structures or epigenetic modifications, for RBPm1 recognition. The structure of RBPm1 is not available yet. To understand the recognition or interaction between RBPm1 and its target introns, future studies into an atomic resolution structure of the protein (RBPm1)-RNA (intron) complex will be required.

Axoneme is an essential cellular structure specifically required for male gametogenesis during the life cycle of *Plasmodium*. Consistent with this physiological requirement of male gametocytes, the axonemal genes display significant male-biased transcription[30,31,49]. Interestingly, these axonemal genes also showed low-level transcripts in female gametocytes in many others and our studies[30,31,49], likely due to the transcription leaking. However, no axonemal proteins are detected in female gametocytes[50], suggesting a post-transcription regulation for the expression turn off of axonemal genes in female gametocytes. We found that genomic deletion of the retained intron (*kinesin8b* intron1, *PF16* intron1, *dlc1* intron4, and *PY17X_1109100* intron1) could bypass the intron splicing and thus restore expression of the axonemal proteins (Kinesin8b, PF16, Dlc1, and PY17X_1109100) in the RBPm1-null male gametocytes. Notably, these introns deletion unexpectedly resulted in low-level expression of PF16, Dlc1, and PY17X_1109100 in female gametocytes (Supplementary Fig. 11B, D, F). The level of proteins restored was correlated with the level of transcripts for these axonemal genes in female gametocytes. These results confirmed the low-level transcripts of these axonemal genes in female gametocytes. In addition, no protein products of these low-level transcripts could be explained by IR and translation failure in female gametocytes. Based on these results, we proposed a dual role of RBPm1-target introns in axonemal gene expression in male and female gametocytes respectively (Supplementary Fig. 11M). In male gametocytes, RBPm1 (as a key)-directed splicing of axonemal intron (as a lock) allows protein expression of axonemal genes for axoneme assembly. In female gametocytes, dual blockage via weak transcription and IR shuts the protein expression of the axonemal genes. The splicing activator RBPm1 and its target introns constitute an intron splicing program, safeguarding the expression of axonemal proteins in male gametocytes while preventing the expression of these proteins in female gametocytes, to fulfill the sexually dimorphic protein profiles during sexual development of the *Plasmodium*.

Methods

Animals and ethics statement

The animal experiments conducted in this study were approved by the Committee for Care and Use of Laboratory Animals of Xiamen University (XMULAC20190001). Female ICR mice aged 5–6 weeks were acquired from the Animal Care Center of Xiamen University. The mice were housed in a controlled environment at 22–24 °C, relative humidity of 45–65%, and a 12-h light/dark cycle. They were used for parasite propagation, drug selection, parasite cloning, and mosquito feeding. The larvae of *Anopheles stephensi* mosquitoes (Hor strain) were maintained in an insect facility under controlled conditions of 28 °C, 80% relative humidity, and a 12-h light/12-h dark cycle. Adult mosquitoes were fed with a 10% (w/v) sucrose solution containing 0.05% 4-aminobenzoic acid and kept at 23 °C.

Plasmid construction

All genetically modified parasites in this study are listed in Supplementary Table 1. The CRISPR/Cas9 plasmid pYCm was used for gene editing[34,73]. To construct plasmids for gene tagging, the 5′- and 3′-flanking sequences (300–700 bp) at the designed insertion site of target genes were amplified as homologous templates. DNA fragments encoding 6HA, GFP, or 4Myc were placed between them and in-frame with the target gene. To construct the plasmids for gene knockout, the left and right homologous arms consisted of 400–700 bp sequences upstream and downstream of the coding sequences of the target gene. To construct the plasmids for domain or intron deletion, the left and right homologous arms consisted of 200–700 bp sequences upstream and downstream of the domain or intron were PCR-amplified and inserted into specific restriction sites in pYCm. To construct the plasmids for intron insertion, the left and right homologous arms were composed of gene genomic sequences ranging from 300–600 bp upstream and downstream of the insertion site, respectively. The left homologous arm, intron, and right homologous arm were connected by overlap PCR, and the fused fragment was inserted into specific restriction sites in pYCm. In each modification, at least two small guide RNAs (sgRNAs) were designed. To construct the plasmids for the *bfp* reporter assay, the intact *bfp* reporter (717 bp) driven by the 5′-UTR (1755 bp) of the *hsp70* gene and the 3′-UTR (561 bp) of the *dhfr* gene were inserted into specific restriction sites between the left and right homologous arms for transgenic integration in the *p230p* locus of *P. yoelii*[74]. The *kinesin8b* intron1 (239 bp), *kinesin8b* intron2 (148 bp), *PF16* intron1 (276 bp), *dlc1* intron4 (193 bp), PY17X_1109100 intron1 (353 bp), and PY17X_1109100 intron2 (272 bp) were inserted into the *bfp* reporter by overlap PCR. All primers and oligonucleotides used in the plasmid construction are listed in Supplementary Table 2.

Parasite transfection and genotyping

The procedures for parasite transfection and genotyping were carried out as previously described[34,73]. Briefly, the schizonts were isolated from infected mice using a 60% Nycodenz density gradient centrifugation. The parasites were then electroporated with 5 μg plasmid using a Nucleofector 2b Device (Lonza, Germany). The transfected schizonts were immediately intravenously injected into a naïve mouse, and pyrimethamine (Pyr) selection (6 mg/ml in drinking water) was applied the day following transfection. Pyr-resistant parasites were typically observed about 7 days after drug selection. Single clone of parasite was obtained by limiting dilution in mice, and genomic DNA was extracted from infected mouse blood for PCR genotyping using specific primers listed in Supplementary Table 2. PCR confirmation of correct 5′ and 3′ homologous recombination in each gene modification are presented in Supplementary Fig. 12.

Negative selection with 5-fluorocytosine

To remove the pYCm plasmids, we employed negative selection using 5-fluorocytosine. A mouse infected with the modified parasite clone was given drinking water containing 2 mg/ml of 5-fluorocytosine (Sigma-Aldrich, cat#F6627) in a dark bottle. After ~3 days, most of the surviving parasites no longer carried pYCm plasmids and underwent limiting dilution cloning by injecting into mice via the tail vein. Seven days later, blood smears were used to identify the mice that were infected with parasites, and these parasites were genotyped again and used as the single cloned parasite.

Gametocyte induction in mice

The ICR mice were treated with phenylhydrazine (80 μg/g body weight; Sangon Biotech, China, cat#A600705-0025) to induce hyperreticulocytosis. Three days post-treatment, the mice were infected with 4×10^6 asexual stage parasites via tail vein injection. The peak of gametocytaemia usually occurred on day three post-infection. Male and female gametocytes were counted using Giemsa-stained thin blood films, and gametocytaemia was calculated as a percentage of the number of male or female gametocytes over the number of parasitized erythrocytes.

Gametocyte purification

The procedures for gametocyte purification were carried out according to previously described methods[48]. Briefly, ICR mice were intraperitoneally treated with phenylhydrazine 3 days prior to parasite infection. Starting from 2 days post-infection, the mice were orally administered 0.12 mg/d of sulfadiazine (Sigma, cat#S8626) for 2 days to eliminate asexual stage parasites. Approximately 1 ml of mouse blood containing gametocytes was collected from the orbital sinus and then suspended in 6 ml of gametocyte maintenance buffer (GMB). GMB comprises 137 mM NaCl, 4 mM KCl, 1 mM $CaCl_2$, 20 mM glucose, 20 mM HEPES, 4 mM $NaHCO_3$, 0.1% BSA, and has a pH of 7.2. The 7 ml

parasite sample was layered on top of a 2 ml 48% Nycodenz/GMB cushion in a 15 ml centrifugation tube. The cushion consisted of 27.6% w/v Nycodenz in 5 mM Tris-HCl (pH 7.2), 3 mM KCl, and 0.3 mM EDTA. After centrifugation at 1900 *g* for 20 min, the gametocytes were collected from the interphase and washed twice with GMB for further use.

Exflagellation assay of male gametocytes

2.5 μl of mouse tail blood with gametocytes was mixed with 100 μl of exflagellation medium. The exflagellation medium was composed of RPMI 1640 supplemented with 100 μM xanthurenic acid (XA, Sigma, cat#D120804), 2 unit/ml heparin, and pH 7.4. The mixture was incubated at 22 °C for 10 min. The number of parasite exflagellation centers (ECs) and total red blood cells were counted within a 1 × 1-mm square area of a hemocytometer under a light microscope. The exflagellation rate was calculated as the number of ECs per 100 male gametocytes.

In vitro ookinete culture

Mouse blood with the gametocytes was collected in the heparin-containing tubes and immediately mixed with the ookinete culture medium. This medium consisted of RPMI 1640 supplemented with 25 mM HEPES, 10% fetal calf serum, 100 μM XA, and had a pH of 8.0. The blood/medium volume ratio was 1:10. The parasite samples were incubated at 22 °C for 16 h and analyzed using Giemsa-stained thin blood films. The number of ookinetes (including normal and abnormal ookinete in morphology) per 100 female gametocytes was calculated as the ookinete conversion rate.

Parasite genetic cross

ICR mice were treated intraperitoneally with phenylhydrazine for gametocyte induction. Three days post-treatment, an equal number (3×10^6) of asexual stage parasites from two different gene knockout lines were mixed and injected via the tail vein into the phenylhydrazine pre-treated mice. After 3 days, mouse blood with mixed gametocytes from two different parasite lines was collected from the mice and subjected for the in vitro gametocyte-gamete-zygote-ookinete development analysis using the in vitro ookinete culture described above.

Mosquito transmission of the parasite

Approximately 100 female *Anopheles stephensi* mosquitoes were allowed to feed on an anesthetized mouse with 4–6% gametocytaemia for 30 min. To evaluate midgut infection of parasite, mosquito guts ($n \sim 30$) were dissected and stained with 0.1% mercurochrome 7 days post-feeding, and oocysts were tallied under a microscope. For quantifying salivary gland sporozoites, mosquito salivary glands ($n \sim 30$) were dissected 14 days after feeding, with the sporozoites counted using a hemocytometer. Transmission efficacy was assessed by allowing ~30 infected mosquitoes to feed on a naïve mouse for 30 min at day 14 post-feeding. Parasite transmission from mosquito to mouse was monitored 5 days later via Giemsa-stained thin blood films. These procedures were performed in triplicate.

Flow cytometry analysis and sorting of male and female gametocytes

To analyze DNA content of male gametocytes, parasites containing gametocytes from the *DFsc7* or *DFsc7*;Δ*Rbpm1* lines were divided into two equal parts. One part was promptly fixed with 4% paraformaldehyde in PBS, while the other was exposed to exflagellation medium at 22 °C for 8 min to initiate gametogenesis before fixation. After staining with 4 μM Hoechst 33342 (Thermo Fisher Scientific, cat# 62249) for 10 min at room temperature and subsequent PBS washes, the samples were analyzed via flow cytometry on a BD LSRFortessa device (BD Biosciences, San Jose, CA, USA). Based on cell size and granularity, forward and side scatter signals were used to distinguish red blood cells from debris, doublets and white blood cells. Male gametocytes were identified by GFP fluorescence and analyzed for Hoechst 33342 fluorescence. For sorting gametocytes, parasites containing gametocytes were kept in GMB at 4 °C and sorted on a BD FACS AriaIII based on GFP and mCherry fluorescence for male and female gametocytes, respectively. Sorted gametocyte purity was verified by re-analysis of a sample fraction.

Bulk RNA sequencing (RNA-seq)

Total RNA from 2×10^7 purified gametocytes was isolated using TRIzol (Thermo Fisher Scientific, cat#15596026) according to the manufacturer's instructions. RNA integrity was confirmed with an Agilent 2100 Bioanalyzer (Agilent Technologies, Palo Alto, CA, USA). mRNA was isolated with Oligo (dT) beads, fragmented, and reverse-transcribed to cDNA using random primers. Using DNA polymerase I, RNase H, dNTPs, and buffer, a second cDNA strand was synthesized. The resulting cDNA fragments were purified with the QIAQuick PCR Purification Kit (Qiagen, cat#28104), end-repaired, A-tailed, and ligated to Illumina sequencing adapters. The ligation products were size-selected using agarose gel electrophoresis, PCR amplified, and sequenced using the Illumina NovaSeq 6000 by Genedenovo Biotechnology Co., Ltd (Guangzhou, China).

Differential expression analysis of RNA-seq data

Illumina-generated paired-end FASTQ files were trimmed using Trim Galore (v0.6.10)[75] (trim_galore --illumina -q 20 --paired --stringency 3 --length 25 -e 0.1 --fastqc --gzip) to remove the sequencing adapters and low quality reads. To refine the dataset, rRNA and tRNA were removed via a genome alignment program HISAT2 (v2.2.1)[76] (hisat2 -p 12 -q --un-conc-gz). The cleaned reads, around 40 million per sample, were aligned to the *Plasmodium yoelii* 17X reference genome (PlasmoDB-62 release) using HISAT2 (hisat2 -p 12 -q). The resulting BAM files were sorted by position and indexed with SAMtools (v1.16.1)[77] (samtools -sort | samtools index). Mapped reads were summarized using featureCounts (v2.0.3)[78]. Gene expression analysis were performed in R (v4.2.1). Gene expression levels were normalized using transcripts per million (TPM) with the R package t-arae/ngscmdr (v0.1.0.181203)[79]. Differential expressed genes (DEGs, fold change > 2, and false discovery rate < 0.05) were assessed by the R package edgeR (v3.40.2)[80]. The volcano plot of DEGs were generated by the ggplot2 (v3.4.2)[81].

Bioinformatic analysis of global intron retention

A GFF file containing genomic intron information was crafted using a perl script from agat package[82] and an in-house bash script, then converted into a BED file with BEDOPS convert2bed (v2.4.41)[83]. DeepTools bamCoverage (v3.5.1)[84] was used to generate the bigWig files for peak visualization in Integrative Genomics Viewer (IGV, v2.16.1)[38], and calculate the peak score of each exon and intron regions. Low expressed genes (TPM below 30) were excluded. To exclude potential false hits, introns with peak scores exceeding 50% of adjacent exons were discarded in parental parasites. In mutant parasites, introns with peak scores under 50% of neighboring exons were also omitted. Before differential intron retention analysis, the introns were normalized based on the gene expression level:

$$\text{Normalized intron counts} = \frac{\text{Intron region counts} \times 1000}{\text{Corresponding gene counts}}$$

Differentially retained introns (fold change > 2 and false discovery rate <0.05) were assessed with the R package edgeR (v3.40.2)[80]. These introns were further validated by IGV visualization and RT-PCR.

Bioinformatic analysis of RBP in the *P. falciparum* and *P. berghei*

189 putative RBPs had been predicted in silico in the *P. falciparum*[32]. Among them, 179 RBPs have homologous proteins in *P. yoelii* and *P. berghei*. Differential expression analysis of the 179 RBPs between male and female gametocytes of *P. berghei* was based on the public dataset

by Yeoh, L.M., 2017[31]. The RNA-seq FASTQ files from NCBI SRA database (Accession: PRJNA374918) were processed using Trim Galore (v0.6.10) and HISAT2 (v2.2.1) for quality trimming and rRNA/tRNA removal, respectively. The cleaned reads were mapped to the *P. berghei* ANKA strain genome (PlasmoDB-62 release) using HISAT2 (v2.2.1), and the resulting BAM files were sorted and indexed with SAMtools (v1.16.1). Mapped reads were summarized using featureCounts (v2.0.3), and the differential expression analysis of RBPs was performed by the R package edgeR (v3.40.2). Differential expression analysis of the 189 RBPs between male and female gametocytes of *P. falciparum* is based on the public dataset from Lasonder E. 2016[30]. The RNA-seq FASTQ files from NCBI SRA (Accession: PRJNA305391) were processed similarly as above. The cleaned reads were mapped to the *Plasmodium falciparum* 3D7 reference genome. Given the absence of biological replicates in this dataset, differential expression analysis was performed by Cufflinks (v2.2.1)[85] (cuffdiff -p 8 --dispersion-method blind --library-norm-method geometric --library-type ff-firststrand). RBPs with fold change > 2 and false discovery rate <0.05 were considered differentially expressed. The volcano plot of differentially expressed RBPs were generated by the ggplot2 (v3.4.2).

Antibodies and antiserum

The following primary antibodies were utilized: rabbit anti-HA (Cell Signaling Technology, cat#3724 S; IFA, 1:1000 dilution; IB, 1:1000 dilution), rabbit anti-mCherry (Abcam, cat# ab167453; IFA, 1:1000 dilution), rabbit anti-histone H3 antibody (Abcam, cat#ab1791; IFA, 1:1000 dilution), rabbit anti-Myc (Cell Signaling Technology, cat#2272 S; IFA, 1:1000 dilution; IB, 1:1000 dilution), mouse anti-α-Tubulin (Sigma-Aldrich, cat#T6199; IFA, 1:1000 dilution; IB, 1:1000 dilution; U-ExM, 1:500 dilution), mouse anti-β-Tubulin (Sigma-Aldrich, cat#T5201; IB, 1:1000 dilution) and mouse anti-HA (Santa Cruz Biotechnology, cat#sc-57592; IFA, 1:200 dilution). The secondary antibodies included: Alexa Fluor 555 goat anti-rabbit IgG (Thermo Fisher Scientific, cat#A-21428; IFA, 1:1000 dilution), Alexa Fluor 488 goat anti-rabbit IgG (Thermo Fisher Scientific, cat#A-31566; IFA, 1:1000 dilution), Alexa Fluor 555 goat anti-mouse IgG (Thermo Fisher Scientific, cat# A-21422; IFA, 1:1000 dilution; U-ExM, 1:500 dilution), Alexa Fluor 488 goat anti-mouse IgG (Thermo Fisher Scientific, cat#A-11001; IFA, 1:1000 dilution), Alexa Fluor 488 goat anti-mouse TER-119 (BioLegend, cat#116215; IFA, 1:500 dilution), Alexa Fluor 488 conjugated streptavidin (Invitrogen, cat# S32354; IFA, 1:1000 dilution), HRP-conjugated goat anti-rabbit IgG (Abcam, cat#ab6721; IB, 1:5000 dilution) and HRP-conjugated goat anti-mouse IgG (Abcam, cat#ab6789; IB, 1:5000 dilution). The antiserum, including rabbit anti-BiP (IB, 1:1000 dilution) and rabbit anti-P28 (IFA, 1:1000), were previously in-house prepared in the laboratory[86].

Immunofluorescence assay

Parasites fixed in 4% paraformaldehyde in PBS were placed on poly-L-lysine-coated coverslips in a 24-well plate and centrifuged at 550 *g* for 5 min. They were then permeabilized with 0.1% Triton X-100 in PBS for 10 min at room temperature, blocked with 5% BSA/PBS at 4 °C overnight, and incubated with primary antibodies in 5% BSA/PBS for 1 h at room temperature. After three PBS washes, the samples were incubated with fluorescently labeled secondary antibodies in 5% BSA/PBS for 1 h at room temperature. Hoechst 33342 at a 1:5000 dilution in PBS was applied for 15 min at room temperature. Finally, the coverslips were washed, mounted in 90% glycerol, and sealed with nail varnish. Imaging was performed with a Zeiss LSM 780 confocal microscope at 100 × magnification.

Ultrastructure expansion microscopy (U-ExM)

According to the method described in[87], gametocytes were fixed in 4% paraformaldehyde in PBS, then transferred to poly-D-lysine-coated coverslips in a 24-well plate and centrifuged. They were incubated in a 1.4% formaldehyde (Sigma-Aldrich, cat#F8775) and 2% acrylamide (Sigma-Aldrich, cat# A4058) mixture in PBS overnight at 37 °C. Afterward, the coverslips were gelled in a monomer solution containing 23% sodium acrylate (Sigma-Aldrich, cat#408220), 10% acrylamide, and 0.1% N,N′-methylenbisacrylamide (Sigma-Aldrich, cat#M1533) in PBS with tetramethylethylenediamine (TEMED) and ammonium persulfate (APS) at 37 °C for 1 h of polymerization. After polymerization, the coverslips were moved to a 6-well plate with denaturation buffer (200 mM SDS, 200 mM NaCl, 50 mM Tris-HCl, and pH 8.8) for 15 min at room temperature to detach the gels. The gels were denatured in 1.5 ml Eppendorf tubes with denaturation buffer at 95 °C for 30 min, incubated with ddH_2O at room temperature overnight in a 10 cm dish for the first round of expansion. The expanded gels were incubated with mouse anti-α-Tubulin antibody diluted in 2% BSA/PBS at room temperature for 3 h, washed 3 times with PBS, and incubated with anti-mouse Alexa 555 diluted in 2% BSA/PBS at room temperature for 3 h. After 3 washes in PBS, the gels were transferred into 10 cm dishes and incubated with ddH_2O at room temperature for the second round of expansion. Subsequently, gel blocks of ~5 mm × 5 mm were excised from the expanded gels and placed in the cavity well of cavity well microscope slides, covered with a coverslip, and imaged using a Zeiss LSM 980 confocal microscope.

Protein extraction and immunoblot

Asexual blood parasites, gametocytes or ookinetes were lysed in RIPA buffer (Solaribio, cat#R0010) containing a protease inhibitor cocktail (MedChemExpress, cat#HY-K0010). After ultrasonication, the lysate was centrifuged at 14,000 *g* at 4 °C for 10 min. The resulting supernatant was mixed with SDS-PAGE loading buffer and heated at 95 °C for 5 min. Following SDS-PAGE separation, samples were transferred to a PVDF membrane (Millipore, cat#IPVH00010) and blocked with 5% milk in 1 × TBST (20 mM Tris-HCl pH 7.5, 150 mM NaCl, 0.1% Tween20) at 4 °C overnight. PVDF membranes were then incubated with primary antibodies at room temperature for 1 h. After washing with 1 × TBST, the membranes were incubated with an HRP-conjugated secondary antibody and then washed again with 1 × TBST. Finally, the membranes were visualized using a high-sensitivity ECL chemiluminescence detection kit (Vazyme, cat#E412-01), and the light emission was recorded either by X-ray film or by Azure Biosystems C280 (Azure Biosystems, USA).

Isolation of nuclear and cytoplasmic fractions

The procedures were performed with modifications according to the previous study[88]. Nycodenz-purified gametocytes were first released from red blood cells by incubating them with 0.15% saponin/PBS on ice for 5 min and then washed twice with ice-cold PBS. The parasite pellet was resuspended in ice-cold lysis buffer (20 mM HEPES pH 7.9, 10 mM KCl, 1.5 mM $MgCl_2$, 1 mM EDTA, 1 mM EGTA, 1 mM DTT, and 0.65% Nonidet P-40) supplemented with protease inhibitor cocktail. The lysate was transferred to a 1 ml Dounce tissue grinder and homogenized gently for 80 strokes on ice. Nuclei were pelleted at 9000 *g* at 4 °C for 10 min, and the resulting supernatant represented cytoplasmic fractions. The nuclear pellet was washed twice with ice-cold lysis buffer before resuspension in one pellet volume of high salt buffer (20 Mm HEPES pH 7.8, 1 M KCl, 1 mM EDTA, 1 mM EGTA, and 1 mM DTT) supplemented with a protease inhibitor cocktail. After vigorous shaking at 4 °C for 30 min, the extract was centrifuged at 14,000 *g* at 4 °C for 10 min, and the resulting supernatant represented nuclear fractions. Immunoblotting was performed to analyze the proteins in each fraction.

Protein immunoprecipitation

Nycodenz-purified gametocytes containing 3×10^7 male gametocytes were lysed in 1 ml lysis buffer (0.01% SDS, 20 mM Tris-HCl pH 8.0, 50 mM NaCl, 1 mM DTT) supplemented with protease inhibitor

cocktail. The lysate was transferred to a 1 ml Dounce tissue grinder and homogenized gently for 100 strokes on ice. The homogenate was transferred to an Eppendorf tube and incubated on ice for 10 min before centrifugation at 14,000 *g* at 4 °C for 10 min. The resulting supernatant was divided into two equal portions, with one portion mixed with 20 µl pre-balanced anti-GFP nanobody agarose beads (KT HEALTH, cat#KTSM1301) and the other portion mixed with anti-Myc nanobody agarose beads (KT HEALTH, cat#KTSM1306). Both portions were incubated at 4 °C for 2 h with rotation. The beads were then washed three times with lysis buffer before elution with SDS-PAGE loading buffer, followed by incubation at 95 °C for 5 min. Immunoblotting was performed on equal volumes of the supernatant samples.

Transmission electron microscopy

Nycodenz-purified gametocytes were fixed at 8 mpa and 15 mpa in 2.5% glutaraldehyde in 0.1 M phosphate buffer at 4 °C overnight, as previously described[89]. Then, the samples were post-fixed in 1% osmium tetroxide at 4 °C for 2 h, treated *en bloc* with uranyl acetate, dehydrated, and embedded in Spurr's resin. Thin sections were sliced, stained with uranyl acetate and lead citrate, and examined in an HT-7800 electron microscope (Hitachi, Japan).

TurboID-based proximity-labeling and biotinylated protein pull-down

Nycodenz-purified gametocytes containing 1×10^8 male gametocytes from either the *Rbpm1::TurboID* or *Rbpm1::T2A::TurboID* line were incubated with 50 µM biotin (Sigma-Aldrich, cat#B4639) at 37 °C for 20 min. After biotinylation, the parasites were pelleted, washed thrice with 1 ml ice-cold PBS to remove excess biotin, and then lysed with RIPA buffer containing a protease inhibitor cocktail via ultrasonication. The lysate was incubated on ice for 10 min before centrifugation at 14,000 *g* at 4 °C for 10 min. The supernatant was then mixed with 50 µl pre-balanced streptavidin sepharose (Thermal Scientific, cat#SA10004) at 4 °C overnight. The beads were washed five times with 1 ml ice-cold RIPA buffer and then washed five times with 1 ml ice-cold PBS. The washed beads were resuspended in 200 µl 100 mM Tris-HCl pH 8.5 followed by digestion with 1 µg trypsin at 37 °C overnight.

Peptide desalting and mass spectrometry

Trifluoroacetic acid (TFA; Sigma-Aldrich, cat#T6508) was added to the trypsin-digested sample to a final concentration of 1%, and the precipitation of sodium deoxycholate was removed by centrifugation. The resulting supernatant was desalted using in-house-made StageTips that were packed with SDB-RPS (3 M EMPORE, cat#2241) and conditioned with 50 µl of 100% acetonitrile (ACN; Sigma-Aldrich, cat# 34851). After loading the supernatant onto the StageTips, centrifugation was performed at 3000 g for 5 min. The StageTips were then washed twice with 50 µl of 1% TFA/isopropyl alcohol (Sigma-Aldrich, cat# I9030) followed by a wash with 50 µl of 0.2% TFA. The peptides were eluted in glass vials (CNW Technologies, cat# A3511040) using 80% ACN/5% NH_4OH and dried at 45 °C using a vacuum centrifuge (Eppendorf, Hamburg, Germany, cat#5305). The peptide samples were resolved in 2% ACN/0.1FA for LC-MS analysis. Liquid chromatography was performed on a high-pressure nano-flow chromatography system (Elute UHPLC, Bruker Daltonics). Peptides were separated on a reversed-phase column (40 cm × 75 µm i.d.) at 50 °C packed with 1.8 µm 120 Å C18 material (Welch, Shanghai, China) with a pulled emitter tip. A solution is 0.1% FA in H_2O, and B solution is 0.1% FA in ACN. The gradient time is 60 min and the total run time is 75 min including washes and equilibration. Peptides were separated with a linear gradient from 0 to 5% B within 5 min, followed by an increase to 30% B within 55 min and further to 35% B within 5 min, followed by a washing step at 95% B and re-equilibration. LC was coupled online to a hybrid TIMS quadrupole time-of-flight mass spectrometer (Bruker timsTOF Pro) via a CaptiveSpray nano-electrospray ion source. We performed data-dependent data acquisition in PASEF mode with 10 PASEF scans per topN acquisition cycle. Singly charged precursors were excluded by their position in the m/z-ion mobility plane and precursors that reached a 'target value' of 20,000 a.u. were dynamically excluded for 0.4 min. We used 100 ms to accumulate and elute ions in the TIMS tunnel. The MS1 m/z-range was acquired from 100 to 1700, and the ion mobility range from 1.5 to 0.7 V cm^{-2}. For data-independent acquisition, we adopted the isolation scheme of 25 Da × 32 windows to cover 400-1200 mz. DIA files (raw) files were input to DIA-NN (v1.8.1)[90] FASTA files downloaded from https://www.uniprot.org (UP000072874) were added. "FASTA digest for library-free search" and "Deep learning-based spectra, RTs, and IMs prediction" were enabled. "Generate spectral library" was also enabled. "Protein inference" was set to "gene". Other parameters were kept at their default settings. The protein groups and precursor lists were filtered at 1% FDR, using global q-values for protein groups and both global and run-specific q-values for precursors.

RNA isolation, RT-PCR and RT-qPCR

Total RNA was extracted from parasites using TRIzol reagent. cDNA was synthesized with the HiScript II 1st Strand cDNA Synthesis Kit (Vazyme, cat#R212-02), using provided random hexamers, and utilized for PCR or qPCR analysis. qPCR was performed using 2×RealStar Green Fast Mixture (GenStar, cat#A301-101) with the following cycling program: a single incubation at 95 °C for 30 s, followed by 40 cycles (95 °C for 5 s, 60 °C for 40 s) on a CFX96 Real-Time PCR System (Bio-Rad, Hercules, CA, USA). The housekeeping gene *gapdh* (PY17X_1330200) was used as a reference gene in the RT-qPCR. The relative expression was calculated using the $2^{-\Delta\Delta Ct}$ method. The primers used for RT-PCRs and RT-qPCRs are listed in Supplementary Table 2.

UV crosslinking RNA immunoprecipitation (UV-RIP)

The Nycodenz-purified gametocytes, containing 6×10^7 male gametocytes in 6 ml ice-cold PBS, were placed in 10 cm dishes. Subsequently, they were irradiated using an HL-2000 HybriLinker (UVP, Upland, CA, USA) with 254 nm UV light at intensities of 400 mJ/cm^2 and 200 mJ/cm^2. The gametocytes were then collected, centrifuged, and resuspended in 1 ml lysis buffer (1% TritonX-100, 50 mM Tris-HCl pH 7.4, 150 mM NaCl, 1 mM EDTA, 1 mM EGTA) supplemented with 400 U/ml RNaseOUT (Thermo Fisher Scientific, cat#10777019) and a protease inhibitor cocktail. The lysate was transferred to a 1 ml Dounce tissue grinder and gently homogenized for 100 strokes on ice. The homogenate was then transferred to a tube and incubated at 4 °C for 25 min with rotation, followed by treatment with 30 U TURBO DNase (Thermo Fisher Scientific, cat#AM2238) at 37 °C for 15 min. The lysates were centrifuged at 14,000 *g* and 4 °C for 10 min. The supernatant was divided into two equal parts. One part was mixed with 20 µl of anti-GFP nanobody agarose beads (KT HEALTH, cat#KTSM1301), and the other part was mixed with 20 µl of anti-HA nanobody agarose beads (KT HEALTH, cat#KTSM1305). The mixtures were incubated with rotation at 4 °C for 2 h. The beads were washed six times with 500 µl RIP wash buffer (Millipore, cat#CS203177) at 4 °C and then incubated with 117 µl RIP wash buffer, 15 µl 10% SDS and 18 µl 10 mg/ml proteinase K (Millipore, cat#CS203218) at 55 °C for 30 min. RNA was isolated using phenol-chloroform extraction, and the purified RNA was reverse transcribed with random hexamer primers and determined by RT-qPCR.

In vitro RNA transcription (IVT)

To prepare biotinylated probes for Fig. 6O, P, IVT templates with T7 RNA polymerase promoter were obtained by PCR using the *P. yoelii* genome as a template. For Fig. 7H, IVT templates with T7 RNA polymerase promoter were obtained by PCR using the plasmid used in the *bfp* reporter assay as a template. Supplementary Table 2 provides a list of primers used to obtain the IVT templates. Subsequently,

Biotinylated RNA was produced using a MEGAscript kit (Thermo Fisher Scientific, cat#AM1334) and a biotin RNA labeling mix (Roche, cat#11685597910). To create a 20 µl reaction volume, 1 µg of PCR-amplified IVT templates were incubated at 37 °C for 2 h with 2 µl of 10× reaction buffer, 2 µl of T7 RNA polymerase enzyme mix, 2 µl of biotin RNA labeling mix, and RNase-free water. The DNA templates were then removed from the RNA using TURBO DNase, and the biotinylated RNA was purified using the RNAclean Kit (TIANGEN, cat#4992728). In this process, the *kinesin8b* I4 probe, *kinesin8b* I1 probe, *PF16* E1 probe, and *PF16* I1 probe all have a length of 500 nt. Additionally, the *kinesin8b* I4 probe, *kinesin8b* I1 probe, and *PF16* I1 probe span the corresponding intron sequences.

RNA pull-down

Biotinylated RNA pull-down was performed using an RNA pull-down Kit (BersinBio, cat# Bes5102) following the manufacturer's protocol. Briefly, 1 µg of biotinylated RNA was denatured at 90 °C for 2 min and immediately cooled on ice for 2 min. The denatured RNA was then incubated with RNA structure buffer and RNase-free water at room temperature for 20 mi to facilitate RNA secondary structure formation. For cell lysate preparation, Nycodenz-purified gametocytes containing 3×10^7 male gametocytes were lysed by RIP buffer, and the resulting lysate was centrifuged at 14,000 *g* at 4 °C for 10 min. The supernatant was then incubated with DNase I and agarose beads to remove the chromosomes, followed by incubation with folded RNAs, streptavidin-coupled beads, and RNase inhibitor at room temperature for 2 h. The beads were subsequently washed five times with NT2 buffer at 4 °C, and proteins were retrieved from the beads by rinsing them with protein elution buffer. The retrieved proteins were then subjected to immunoblot assay.

bfp reporter assay

The Nycodenz-purified gametocytes from either *DFsc7* or *DFsc7*;Δ*Rbpm1* lines, which contain a *bfp* expression cassette in the *p230p* locus, were suspended in 200 µl of GMB. The samples were then transferred to a 15 mm glass bottom cell culture dish and imaged using a Zeiss LSM 780 confocal microscope at room temperature with 100× magnification. The laser illumination was set at 561 nm (mCherry), 491 nm (GFP), and 405 nm (BFP). BFP-positive parasites indicated that the intron in the *bfp* expression cassette had been spliced.

Other bioinformatic analysis and tools

The genomic sequences of target genes were downloaded from the PlasmoDB database (http://plasmodb.org/plasmo/). The sgRNAs of target gene were designed using EuPaGDT (http://grna.ctegd.uga.edu/). The analysis of flow cytometry data was performed using the FlowJo software (Tree Star, Ashland, OR, USA). The Gene Ontology (GO) enrichment analysis was performed using PlasmoDB. Statistical analysis was performed using GraphPad Prism (GraphPad Software Inc., San Diego, CA, USA) with either a two-tailed Student's *t*-test or Mann-Whitney test as appropriate. Error bars represent the standard error of the mean (SEM) for triplicate experiments. *p* values were indicated in the figures above the two groups being compared, with a value <0.05 considered significant. The protein signal on the blotting membrane was quantified using ImageJ software (NIH, Bethesda, MD, USA), and the background was subtracted from each signal. Each signal was then normalized to the Bip signal.

Reporting summary

Further information on research design is available in the Nature Portfolio Reporting Summary linked to this article.

Data availability

All relevant data in this study are submitted as supplementary source files. Source data are provided with this paper. The RNA-seq data for the *P. yoelii* male- and female gametocyte transcriptome have been deposited in the Gene Expression Omnibus database under the accession number GSE222860. The RNA-seq data for male gametocyte transcriptome of the *P. yoelii Rbpm1* knockout parasite line is available under accession number GSE223170. The mass spectrometry proteomic data have been deposited in the ProteomeXchange with identifier PXD044094 (https://www.iprox.cn//page/project.html?id=IPX0006804000). Source data are provided with this paper.

Code availability

All code and supporting files for transcriptome and intron retention analysis in this study were available in Zenodo (https://doi.org/10.5281/zenodo.10979262).

References

1. WHO. *World Malaria Report* 2019. (WHO, 2019).
2. Baker, D. A. Malaria gametocytogenesis. *Mol. Biochem. Parasitol.* **172**, 57–65 (2010).
3. Guttery, D. S. et al. Commit and transmit: molecular players in plasmodium sexual development and zygote differentiation. *Trends Parasitol.* **31**, 676–685 (2015).
4. Bennink, S., Kiesow, M. & Pradel, G. Malaria parasite development in the mosquito midgut. *Cell. Microbiol.* **18**, 905–918 (2016).
5. Guttery, D. S. et al. Division and transmission: malaria parasite development in the mosquito. *Annu Rev. Microbiol* **76**, 113–134 (2022).
6. Sinden, R. E. Sexual development of malarial parasites. *Adv. Parasitol.* **22**, 153–216 (1983).
7. Sinden, R. E. & Croll, N. A. Cytology and kinetics of microgametogenesis and fertilization in Plasmodium yoelii nigeriensis. *Parasitology* **70**, 53–65 (1975).
8. Billker, O. et al. Identification of xanthurenic acid as the putative inducer of malaria development in the mosquito. *Nature* **392**, 289–292 (1998).
9. Sinden, R. E. The biology of Plasmodium in the mosquito. *Experientia* **40**, 1330–1343 (1984).
10. Sinden, R. E., Canning, E. U. & Spain, B. Gametogenesis and fertilization in Plasmodium yoelii nigeriensis: a transmission electron microscope study. *Proc. R. Soc. Lond. B Biol. Sci.* **193**, 55–1976 (1110).
11. Briquet, S. et al. Preparing for transmission: gene regulation in Plasmodium sporozoites. *Front. Cell. Infect. Microbiol* **10**, 618430 (2020).
12. Hollin, T. & Le Roch, K. G. From genes to transcripts, a tightly regulated journey in Plasmodium. *Front Cell Infect. Microbiol* **10**, 618454 (2020).
13. Hollin, T., Chahine, Z. & Le Roch, K. G. Epigenetic regulation and chromatin remodeling in malaria parasites. *Annu. Rev. Microbiol.* **77**, 255–276 (2023).
14. Kafsack, B. F. et al. A transcriptional switch underlies commitment to sexual development in malaria parasites. *Nature* **507**, 248–252 (2014).
15. Sinha, A. et al. A cascade of DNA-binding proteins for sexual commitment and development in Plasmodium. *Nature* **507**, 253–257 (2014).
16. Josling, G. A. et al. Dissecting the role of PfAP2-G in malaria gametocytogenesis. *Nat. Commun.* **11**, 1503 (2020).
17. Yuda, M. et al. Female-specific gene regulation in malaria parasites by an AP2-family transcription factor. *Mol. Microbiol* **113**, 40–51 (2020).
18. Shang, X. et al. A cascade of transcriptional repression determines sexual commitment and development in Plasmodium falciparum. *Nucleic Acids Res* **49**, 9264–9279 (2021).
19. Li, Z. et al. Plasmodium transcription repressor AP2-O3 regulates sex-specific identity of gene expression in female gametocytes. *EMBO Rep.* **22**, e51660 (2021).

20. Kaneko, I. et al. Differentiation of Plasmodium male gametocytes is initiated by the recruitment of a chromatin remodeler to a male-specific cis-element. *Proc. Natl Acad. Sci. USA* **120**, e2303432120 (2023).
21. Filarsky, M. et al. GDV1 induces sexual commitment of malaria parasites by antagonizing HP1-dependent gene silencing. *Science* **359**, 1259–1263 (2018).
22. Usui, M. et al. Plasmodium falciparum sexual differentiation in malaria patients is associated with host factors and GDV1-dependent genes. *Nat. Commun.* **10**, 2140 (2019).
23. Brancucci, N. M. B. et al. Lysophosphatidylcholine regulates sexual stage differentiation in the human malaria parasite Plasmodium falciparum. *Cell* **171**, 1532–1544.e15 (2017).
24. Corley, M., Burns, M. C. & Yeo, G. W. How RNA-binding proteins interact with RNA: molecules and mechanisms. *Mol. Cell* **78**, 9–29 (2020).
25. Hentze, M. W. et al. A brave new world of RNA-binding proteins. *Nat. Rev. Mol. Cell Biol.* **19**, 327–341 (2018).
26. Gebauer, F. et al. RNA-binding proteins in human genetic disease. *Nat. Rev. Genet.* **22**, 185–198 (2021).
27. Mair, G. R. et al. Regulation of sexual development of Plasmodium by translational repression. *Science* **313**, 667–669 (2006).
28. Mair, G. R. et al. Universal features of post-transcriptional gene regulation are critical for Plasmodium zygote development. *PLoS Pathog.* **6**, e1000767 (2010).
29. Guerreiro, A. et al. Genome-wide RIP-Chip analysis of translational repressor-bound mRNAs in the Plasmodium gametocyte. *Genome Biol.* **15**, 493 (2014).
30. Lasonder, E. et al. Integrated transcriptomic and proteomic analyses of P. falciparum gametocytes: molecular insight into sex-specific processes and translational repression. *Nucleic Acids Res.* **44**, 6087–6101 (2016).
31. Yeoh, L., et al. Comparative transcriptomics of female and male gametocytes in Plasmodium berghei and the evolution of sex in alveolates. *BMC Genom.* **18**, 1–16 (2017).
32. Reddy, B. P. et al. A bioinformatic survey of RNA-binding proteins in Plasmodium. *BMC Genom.* **16**, 890 (2015).
33. Liu, C. et al. Generation of Plasmodium yoelii malaria parasite carrying double fluorescence reporters in gametocytes. *Mol. Biochem. Parasitol.* **224**, 37–43 (2018).
34. Zhang, C. et al. Efficient editing of malaria parasite genome using the CRISPR/Cas9 system. *MBio* **5**, e01414-14 (2014).
35. Zhang, C. et al. Systematic CRISPR-Cas9-mediated modifications of Plasmodium yoelii ApiAP2 genes reveal functional insights into parasite development. *MBio* **8**, e01986–17 (2017).
36. Rawlings, D. J. et al. Alpha-tubulin II is a male-specific protein in Plasmodium falciparum. *Mol. Biochem Parasitol.* **56**, 239–250 (1992).
37. Bertiaux, E. et al. Expansion microscopy provides new insights into the cytoskeleton of malaria parasites including the conservation of a conoid. *PLoS Biol.* **19**, e3001020 (2021).
38. Thorvaldsdóttir, H., Robinson, J. T. & Mesirov, J. P. Integrative Genomics Viewer (IGV): high-performance genomics data visualization and exploration. *Brief. Bioinform.* **14**, 178–192 (2013).
39. Depoix, D. et al. Vital role for Plasmodium berghei Kinesin8B in axoneme assembly during male gamete formation and mosquito transmission. *Cell. Microbiol.* **22**, e13121 (2020).
40. Zeeshan, M. et al. Kinesin-8B controls basal body function and flagellum formation and is key to malaria transmission. *Life Sci. Alliance* **2**, e201900488 (2019).
41. Straschil, U. et al. The Armadillo repeat protein PF16 is essential for flagellar structure and function in Plasmodium male gametes. *PLoS One* **5**, e12901 (2010).
42. Russell, A. J. C. et al. Regulators of male and female sexual development are critical for the transmission of a malaria parasite. *Cell Host Microbe* **31**, 305–319.e10 (2023).
43. Li, X. et al. A unified mechanism for intron and exon definition and back-splicing. *Nature* **573**, 375–380 (2019).
44. Kondo, Y. et al. Crystal structure of human U1 snRNP, a small nuclear ribonucleoprotein particle, reveals the mechanism of 5′ splice site recognition. *Elife* **4**, e04986 (2015).
45. Wan, R. et al. How is precursor messenger RNA spliced by the spliceosome? *Annu. Rev. Biochem.* **89**, 333–358 (2020).
46. Sorber, K., Dimon, M. T. & DeRisi, J. L. RNA-Seq analysis of splicing in Plasmodium falciparum uncovers new splice junctions, alternative splicing and splicing of antisense transcripts. *Nucleic Acids Res* **39**, 3820–3835 (2011).
47. Wilkinson, M. E., Charenton, C. & Nagai, K. RNA splicing by the spliceosome. *Annu Rev. Biochem* **89**, 359–388 (2020).
48. Jiang, Y. et al. An intracellular membrane protein GEP1 regulates xanthurenic acid induced gametogenesis of malaria parasites. *Nat. Commun.* **11**, 1764 (2020).
49. Howick, V. M. et al. The Malaria Cell Atlas: Single parasite transcriptomes across the complete Plasmodium life cycle. *Science* **365**, eaaw2619 (2019).
50. Khan, S. M. et al. Proteome analysis of separated male and female gametocytes reveals novel sex-specific Plasmodium biology. *Cell* **121**, 675–687 (2005).
51. Bunnik, E. M. et al. The mRNA-bound proteome of the human malaria parasite Plasmodium falciparum. *Genome Biol.* **17**, 147 (2016).
52. Rios, K. T. & Lindner, S. E. Protein-RNA interactions important for Plasmodium transmission. *PLoS Pathog.* **15**, e1008095 (2019).
53. Müller, K. et al. Pleiotropic roles for the Plasmodium berghei RNA Binding Protein UIS12 in transmission and oocyst maturation. *Front Cell Infect. Microbiol* **11**, 624945 (2021).
54. Shrestha, S. et al. The RNA-binding protein Puf1 functions in the maintenance of gametocytes in Plasmodium falciparum. *J. Cell Sci.* **129**, 3144–3152 (2016).
55. Hart, K. J. et al. Plasmodium male gametocyte development and transmission are critically regulated by the two putative deadenylases of the CAF1/CCR4/NOT complex. *PLoS Pathog.* **15**, e1007164 (2019).
56. Miao, J. et al. The Puf-family RNA-binding protein PfPuf2 regulates sexual development and sex differentiation in the malaria parasite Plasmodium falciparum. *J. Cell Sci.* **123**, 1039–1049 (2010).
57. Farrukh, A. et al. The Plasmodium falciparum CCCH zinc finger protein MD3 regulates male gametocytogenesis through its interaction with RNA-binding proteins. *Mol Microbiol*, **121**, 543–564 (2023).
58. Miao, J. et al. Puf mediates translation repression of transmission-blocking vaccine candidates in malaria parasites. *PLoS Pathog.* **9**, e1003268 (2013).
59. Yeoh, L. M. et al. Alternative splicing is required for stage differentiation in malaria parasites. *Genome biology* **20**, 1–13 (2019).
60. Hanhsen, B. et al. The Plasmodium falciparum CCCH zinc finger protein ZNF4 plays an important role in gametocyte exflagellation through the regulation of male enriched transcripts. *Cells* **11**, 1666 (2022).
61. Sinden, R. E. et al. The flagellum in malarial parasites. *Curr. Opin. Microbiol* **13**, 491–500 (2010).
62. Briggs, L. J. et al. More than one way to build a flagellum: comparative genomics of parasitic protozoa. *Curr. Biol.* **14**, R611–R612 (2004).
63. Rashpa, R. & Brochet, M. Expansion microscopy of Plasmodium gametocytes reveals the molecular architecture of a bipartite

microtubule organisation centre coordinating mitosis with axoneme assembly. *PLoS Pathog.* **18**, e1010223 (2022).
64. Liu, T. et al. Mechanochemical tuning of a kinesin motor essential for malaria parasite transmission. *Nat. Commun.* **13**, 6988 (2022).
65. Zeeshan, M. et al. Plasmodium SAS4: basal body component of male cell which is dispensable for parasite transmission. *Life Sci. Alliance* **5**, e202101329 (2022).
66. Francia, M. E., Dubremetz, J. F. & Morrissette, N. S. Basal body structure and composition in the apicomplexans Toxoplasma and Plasmodium. *Cilia* **5**, 3 (2015).
67. Marques, S. R. et al. An essential role of the basal body protein SAS-6 in Plasmodium male gamete development and malaria transmission. *Cell Microbiol* **17**, 191–206 (2015).
68. Ramakrishnan, C. et al. Radial spoke protein 9 is necessary for axoneme assembly in Plasmodium but not in trypanosomatid parasites. *J. Cell Sci.* **136**, jcs260655 (2023).
69. Will, C. L. & Lührmann, R. Spliceosome structure and function. *Cold Spring Harb. Perspect. Biol.* **3**, a003707 (2011).
70. Rino, J. et al. Splicing factors SF1 and U2AF associate in extra-spliceosomal complexes. *Mol. Cell Biol.* **28**, 3045–3057 (2008).
71. Yue, L. et al. Dek modulates global intron retention during muscle stem cells quiescence exit. *Dev. cell* **53**, 661–676.e6 (2020).
72. Zuo, Y. et al. Dek42 encodes an RNA-binding protein that affects alternative pre-mRNA splicing and maize kernel development. *J. Integr. Plant Biol.* **61**, 728–748 (2019).
73. Zhang, C. et al. CRISPR/Cas9 mediated sequential editing of genes critical for ookinete motility in Plasmodium yoelii. *Mol. Biochem. Parasitol.* **212**, 1–8 (2017).
74. Liu, C. et al. Generation of Plasmodium yoelii malaria parasite for conditional degradation of proteins. *Mol. Biochem. Parasitol.* **241**, 111346 (2021).
75. Krueger, F. TrimGalore: A wrapper around Cutadapt and FastQC to consistently apply adapter and quality trimming to FastQ files, with extra functionality for RRBS data.[(accessed on 27 August 2019)].
76. Kim, D. et al. Graph-based genome alignment and genotyping with HISAT2 and HISAT-genotype. *Nat. Biotechnol.* **37**, 907–915 (2019).
77. Danecek, P. et al. Twelve years of SAMtools and BCFtools. *Gigascience* **10**, giab008 (2021).
78. Liao, Y., Smyth, G. K. & Shi, W. featureCounts: an efficient general purpose program for assigning sequence reads to genomic features. *Bioinformatics* **30**, 923–930 (2014).
79. R Core Team, R. R: A language and environment for statistical computing. 2013.
80. Robinson, M. D., McCarthy, D. J. & Smyth, G. K. edgeR: a Bioconductor package for differential expression analysis of digital gene expression data. *bioinformatics* **26**, 139–140 (2010).
81. Wickham, H. ggplot2. *Wiley Interdiscip. Rev. Comput. Stat.* **3**, 180–185 (2011).
82. Dainat, J. AGAT: Another Gff Analysis Toolkit to handle annotations in any GTF/GFF format. (Version v0.7.0). Zenodo. https://doi.org/10.5281/zenodo.3552717 2020.
83. Neph, S. et al. BEDOPS: high-performance genomic feature operations. *Bioinformatics* **28**, 1919–1920 (2012).
84. Ramírez, F. et al. deepTools2: a next generation web server for deep-sequencing data analysis. *Nucleic Acids Res.* **44**, W160–W165 (2016).
85. Trapnell, C. et al. Differential gene and transcript expression analysis of RNA-seq experiments with TopHat and Cufflinks. *Nat. Protoc.* **7**, 562–578 (2012).
86. Gao, H. et al. ISP1-anchored polarization of GCbeta/CDC50A complex initiates malaria ookinete gliding motility. *Curr. Biol.* **28**, 2763–2776.e6 (2018).
87. Gambarotto, D., Hamel, V. & Guichard, P. Ultrastructure expansion microscopy (U-ExM), in *Methods in Cell Biology*. 57–81. (Elsevier, 2021)
88. Voss, T. S. et al. Plasmodium falciparum possesses a cell cycle-regulated short type replication protein A large subunit encoded by an unusual transcript. *J. Biol. Chem.* **277**, 17493–17501 (2002).
89. Ferguson, D. J. et al. Maternal inheritance and stage-specific variation of the apicoplast in Toxoplasma gondii during development in the intermediate and definitive host. *Eukaryot. Cell* **4**, 814–826 (2005).
90. Demichev, V. et al. DIA-NN: neural networks and interference correction enable deep proteome coverage in high throughput. *Nat. Methods* **17**, 41–44 (2020).

Acknowledgements

This work was supported by the National Natural Science Foundation of China (32170427 by J.Y., 32270503 by H.C.), the Natural Science Foundation of Fujian Province (2021J01028 by J.Y.), and the 111 Project sponsored by the State Bureau of Foreign Experts and Ministry of Education of China (BP2018017 by J.Y.).

Author contributions

J.G. and J.Y. designed the study. J.G., P.W., X.Z.(Xiaoming Zhang), W.L., and X.Z. (Xiaolong Zhang) generated the modified parasites. J.G. performed phenotype analysis, protein analysis, electron microscopy, RNA analysis, and reporter assays. P.W. conducted mass spectrometry and protein analysis. X.M. performed the bioinformatics analysis. L.J., J.L., H.C., and J.Y. supervised the work. J.G., X.M., and J.Y. wrote the manuscript.

Competing interests

The authors declare no competing interests.

Additional information

Supplementary information The online version contains supplementary material available at https://doi.org/10.1038/s41467-024-49002-9.

Correspondence and requests for materials should be addressed to Lubin Jiang, Jian Li, Huiting Cui or Jing Yuan.

Peer review information *Nature Communications* thanks the anonymous, reviewer(s) for their contribution to the peer review of this work. A peer review file is available.

Supplemental Information

An axonemal intron splicing program sustains *Plasmodium* male development

Jiepeng Guan[1,#], Peijia Wu[1,#], Xiaoli Mo[1,#], Xiaolong Zhang[3,#], Wenqi Liang[1], Xiaoming Zhang[1], Lubin Jiang[3,*], Jian Li[1,*], Huiting Cui[1,*] and Jing Yuan[1,2,*]

1. Supplementary Figures 1-13 and figure legends

2. Supplementary Table 1. List of genetically modified parasite strains used in this study

3. Supplementary Table 2. Oligonucleotides and primers used in this study

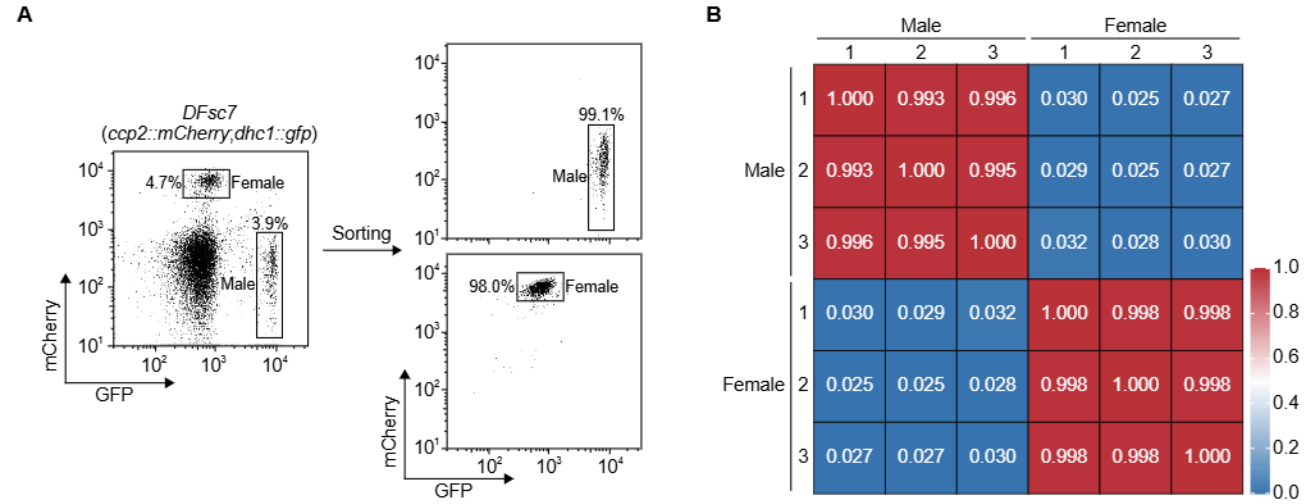
A
DFsc7
(ccp2::mCherry;dhc1::gfp)
4.7%
Female
3.9%
Male
mCherry
GFP
Sorting
99.1%
Male
98.0%
Female
mCherry
GFP
B
Male
Female
1
2
3
1
2
3
Male
Female
1.000 0.993 0.996 0.030 0.025 0.027
0.993 1.000 0.995 0.029 0.025 0.027
0.996 0.995 1.000 0.032 0.028 0.030
0.030 0.029 0.032 1.000 0.998 0.998
0.025 0.025 0.028 0.998 1.000 0.998
0.027 0.027 0.030 0.998 0.998 1.000
1.0
0.8
0.6
0.4
0.2
0.0

Supplementary Figure 1. Purification of male and female gametocytes of the *P. yoelii* parasite for transcriptome analysis

A. Purification of male (GFP+) and female (mCherry+) gametocytes from a *P. yoelii* parasite reporter line *DFsc7* using flow cytometry sorting. The purity of gametocytes was shown. Representative from three independent experiments.

B. Pearson's correlation coefficient analysis of global gene expression between male and female gametocytes based on RNA-seq data with three biological replicates.

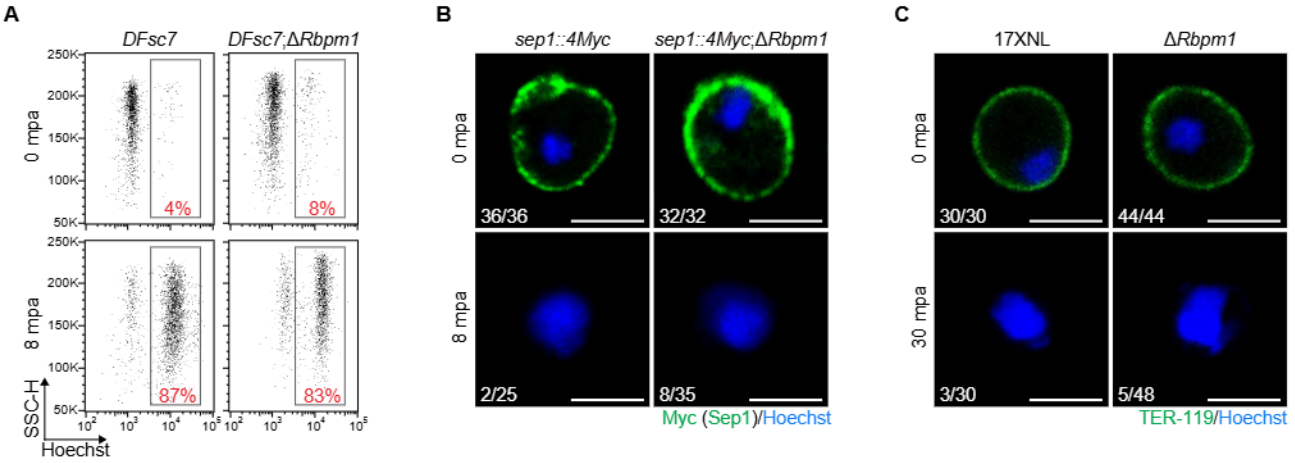
A
DFsc7
DFsc7;ΔRbpm1
0 mpa
8 mpa
4%
8%
87%
83%
SSC-H
Hoechst
B
sep1::4Myc
sep1::4Myc;ΔRbpm1
0 mpa
8 mpa
36/36
32/32
2/25
8/35
Myc (Sep1)/Hoechst
C
17XNL
ΔRbpm1
0 mpa
30 mpa
30/30
44/44
3/30
5/48
TER-119/Hoechst

Supplementary Figure 2. Normal ability of genome replication and erythrocyte rupture for the RBPm1-null parasite during male gametogenesis

A. Flow cytometry analysis of genomic DNA content in male gametocytes during gametogenesis. The *DFsc7*;Δ*Rbpm1* is a *DFsc7*-derived RBPm1-null parasite line. Male gametocytes (GFP+) were gated, and genomic DNA content was measured based on the Hoechst 33342 fluorescence intensity. Representative for three independent experiments.

B. IFA detection of the parasitophorous vacuole membrane (PVM) rupture. SEP1 protein is a marker for PVM. Male gametocytes from the *sep1::4Myc* parasite and the derived RBPm1-null parasite *sep1::4Myc*;Δ*Rbpm1* were analyzed. Representative for three independent experiments. Scale bars: 5 μm.

C. IFA detection of the erythrocyte plasma membrane (EM) rupture. TER-119 protein is a marker of mouse EM. Male gametocytes from the 17XNL and Δ*Rbpm1* parasites were stained with anti-TER-119 antibody. Representative for three independent experiments. Scale bars: 5 μm.

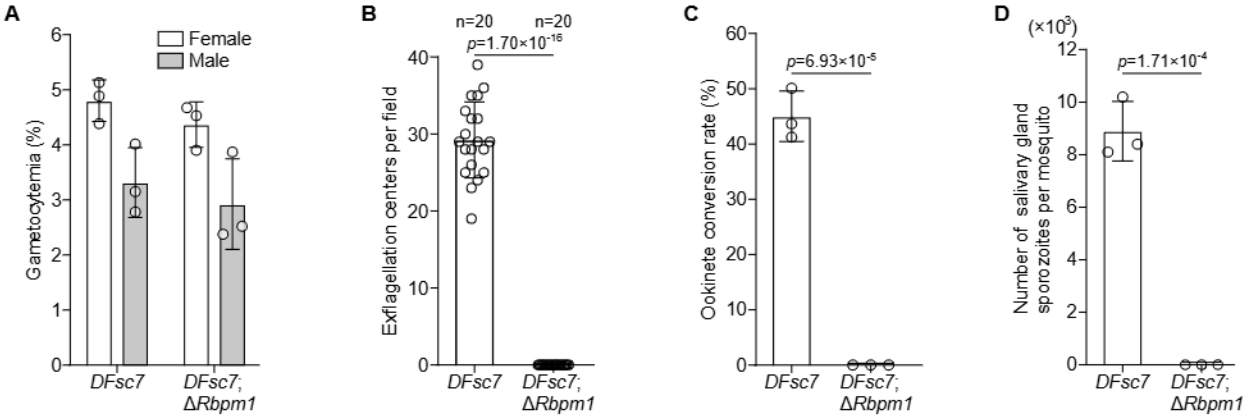
A
Female
Male
Gametocytemia (%)
DFsc7
DFsc7; ΔRbpm1
B
n=20
n=20
p=1.70×10-16
Exflagellation centers per field
C
p=6.93×10-5
Ookinete conversion rate (%)
D
(×10³)
p=1.71×10-4
Number of salivary gland sporozoites per mosquito

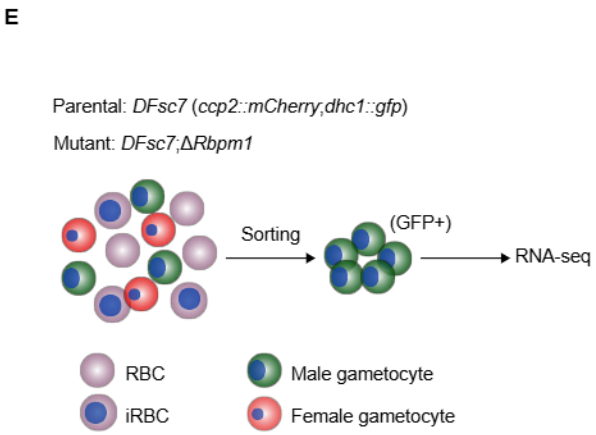
E
Parental: DFsc7 (ccp2::mCherry;dhc1::gfp)
Mutant: DFsc7;ΔRbpm1
Sorting
(GFP+)
RNA-seq
RBC
iRBC
Male gametocyte
Female gametocyte

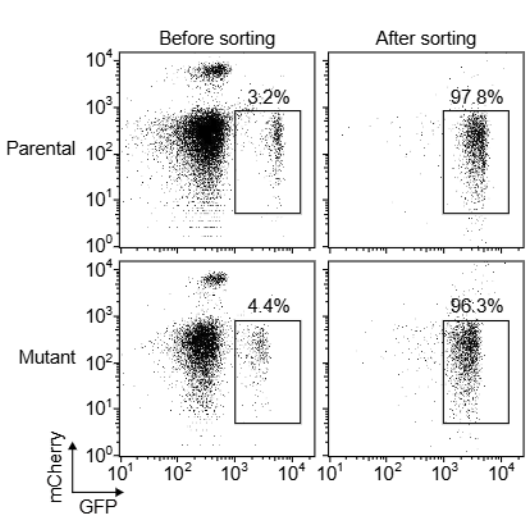
F
Before sorting
After sorting
Parental
Mutant
3.2%
97.8%
4.4%
96.3%
mCherry
GFP

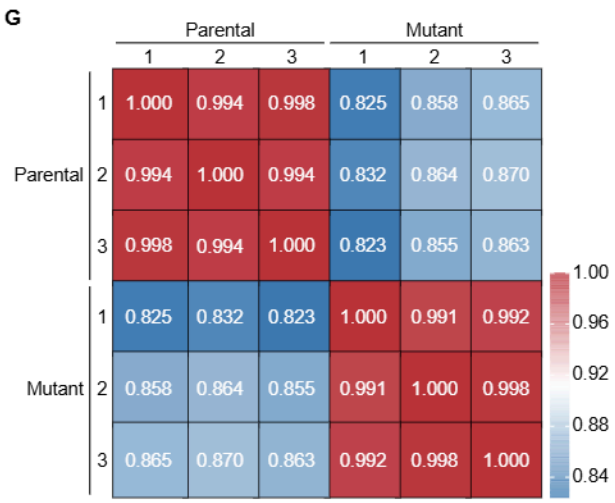
G
Parental
Mutant
1.000 0.994 0.998 0.825 0.858 0.865
0.994 1.000 0.994 0.832 0.864 0.870
0.998 0.994 1.000 0.823 0.855 0.863
0.825 0.832 0.823 1.000 0.991 0.992
0.858 0.864 0.855 0.991 1.000 0.998
0.865 0.870 0.863 0.992 0.998 1.000
1.00
0.96
0.92
0.88
0.84

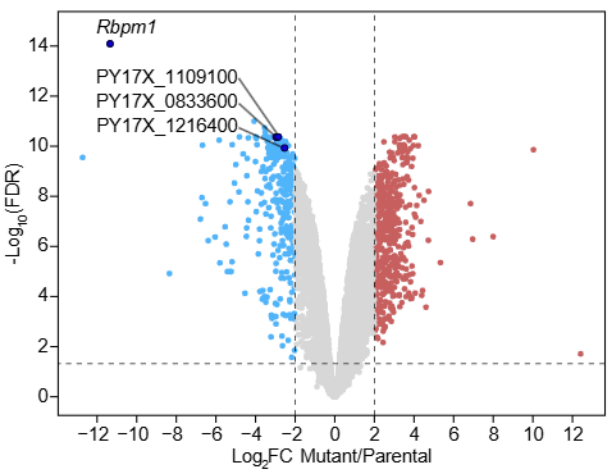
H
Rbpm1
PY17X_1109100
PY17X_0833600
PY17X_1216400
-Log10(FDR)
Log2FC Mutant/Parental

Supplementary Figure 3. Generation, purification and transcriptome analysis of male gametocytes with RBPm1 deficiency

A-D. Phenotype analysis of *DFsc7* (parental) and *DFsc7*;Δ*Rbpm1* (mutant) parasite lines, including gametocyte formation (**A**), male gamete formation (**B**), ookinete formation *in vitro* (**C**), and salivary gland sporozoite in mosquitoes (**D**). Data are means ± SEM of three independent experiments, two-sided *t*-test.

E. Flowchart showing the purification of male gametocytes (green, GFP+) from both *DFsc7* and *DFsc7*;Δ*Rbpm1* parasites for transcriptome analysis via RNA-seq.

F. Flow cytometry detection of male gametocytes (GFP+) before and after sorting, with indicated purity. Representative results from three independent experiments.

G. A heatmap showing the Pearson correlation coefficient between *DFsc7* (parental) and *DFsc7*;Δ*Rbpm1* (mutant) male gametocyte RNA-seq data.

H. A volcano plot showing the differentially expressed genes in male gametocytes between the *DFsc7* (parental) and *DFsc7*;Δ*Rbpm1* (mutant) lines. The threshold for the $\log_2$ fold change ($\log_2$FC) and false discovery rate (FDR) are ±2 and 0.05, respectively. There are 481 genes up-regulated and 295 genes down-regulated in male gametocytes after loss of RBPm1. Three down-regulated genes (PY17X_1109100, PY17X_0833600, and PY17X_1216400), which exhibited intron retention in further study, are highlighted.

A

26 genes with intron retention

Molecular function	Gene ID	Total number of introns in gene	# of the retained intron	Length of the retained intron (bp)	Male transcription (normalized counts)	Female transcription (normalized counts)	Ratio (Male/Female)
Basal body & axoneme assembly	*kinesin8b* (PY17X_0204100)	4	1	239	5148	2	3217
	PF16 (PY17X_0919000)	1	1	276	580	38	15
Axoneme motility	*dhc6* (PY17X_0603800)	33	20	241	842	5	160
	dhc7 (PY17X_0510800)	10	7	235	1070	3	318
	dlc1 (PY17X_1241500)	5	4	193	296	68	4
	dlc2 (PY17X_0302800)	3	1	195	503	19	27
	drc1 (PY17X_0721100)	9	2, 3	179, 150	597	93	6
	dbc (PY17X_1333900)	5	1	772	2059	40	51
Function unknown	*md2* (PY17X_1450400)	1	1	505	1534	53	29
	PY17X_1109100	3	1	353	1662	55	30
	PY17X_0521800	16	1	278	777	38	20
	PY17X_1311800	13	5	248	1342	3	446
	PY17X_1323900	1	1	322	710	103	7
	PY17X_1357300	7	5, 7	212, 143	2644	4	630
	PY17X_1335600	1	1	338	1320	3	417
	PY17X_1452900	13	1	367	1686	6	295
	PY17X_1122300	2	1	240	161	10	15
	PY17X_0523500	5	2, 3	192, 318	348	1	533
	PY17X_0508900	7	5	380	485	10	49
	PY17X_1320300	3	2	183	195	24	8
	PY17X_0833600	2	2	302	526	12	46
	PY17X_1341200	5	1	208	731	1	803
	PY17X_1305400	15	11, 12	261, 330	1583	14	116
	PY17X_0415900	13	13	171	431	2	201
	PY17X_0105800	1	1	193	107	3	33
	PY17X_1216400	10	5	134	712	1	596

B

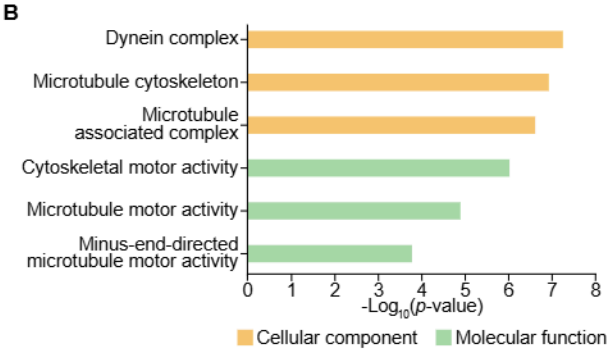

Supplementary Figure 4. Expression and function information of 26 intron-retained genes identified in the RBPm1-null male gametocytes

A. List of 26 genes with intron retention detected in the RBPm1-null male gametocytes. Among them, 22 genes had one retained intron while 4 genes (*drc1*, PY17X_1357300, PY17X_0523500, and PY17X_1305400) possessed two retained introns after loss of RBPm1. Information including the protein function, gene ID, exon-intron structure, retained intron, and gender transcription, is provided. Gender transcription (TMM normalized counts) were from the gametocyte transcriptome data in this study.

B. Gene ontology enrichment analysis of the 26 genes indicates male-specific or preferential biological processes. Hypergeometric test was applied.

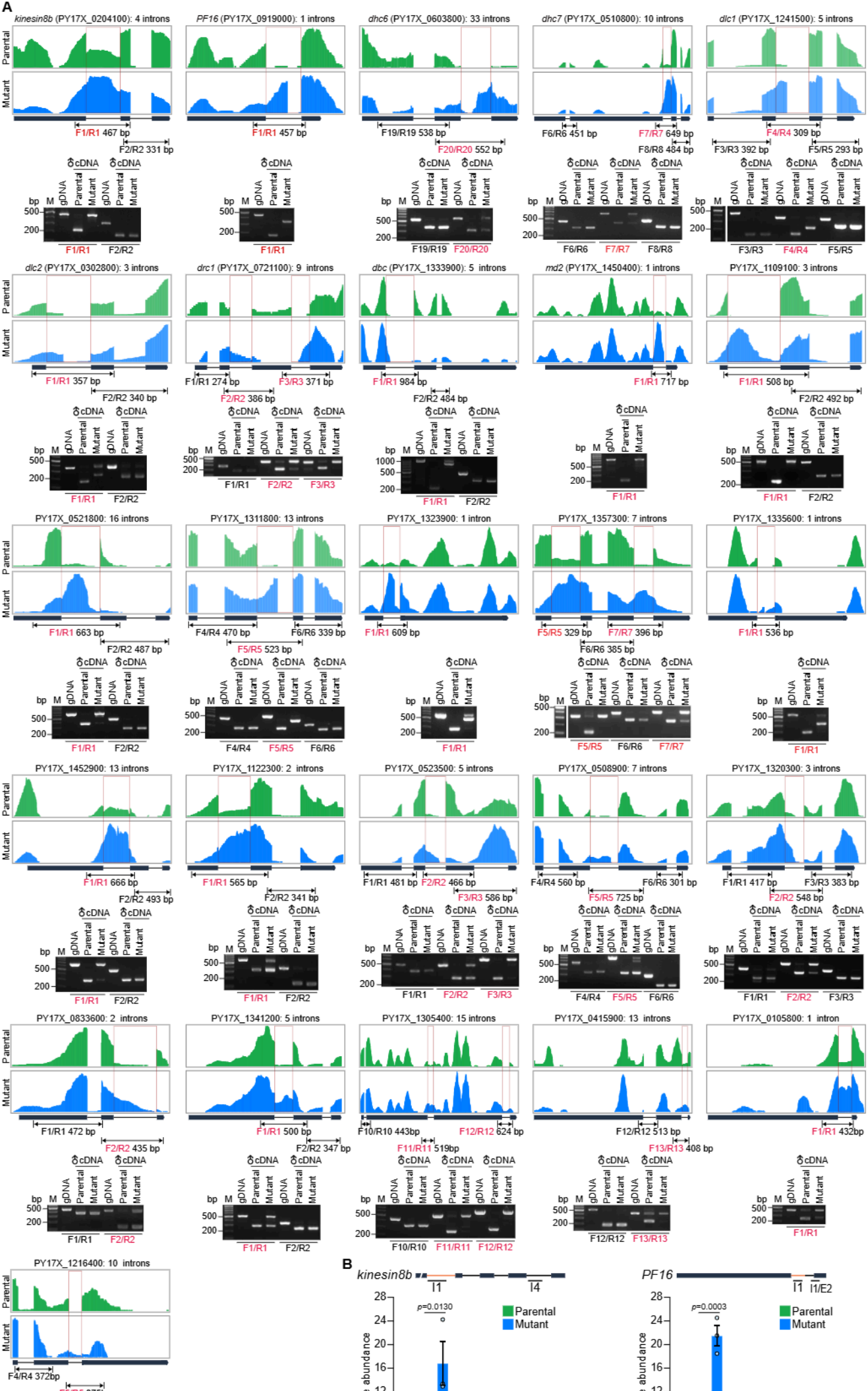
A
kinesin8b (PY17X_0204100): 4 introns
PF16 (PY17X_0919000): 1 introns
dhc6 (PY17X_0603800): 33 introns
dhc7 (PY17X_0510800): 10 introns
dlc1 (PY17X_1241500): 5 introns
dlc2 (PY17X_0302800): 3 introns
drc1 (PY17X_0721100): 9 introns
dbc (PY17X_1333900): 5 introns
md2 (PY17X_1450400): 1 introns
PY17X_1109100: 3 introns
PY17X_0521800: 16 introns
PY17X_1311800: 13 introns
PY17X_1323900: 1 intron
PY17X_1357300: 7 introns
PY17X_1335600: 1 introns
PY17X_1452900: 13 introns
PY17X_1122300: 2 introns
PY17X_0523500: 5 introns
PY17X_0508900: 7 introns
PY17X_1320300: 3 introns
PY17X_0833600: 2 introns
PY17X_1341200: 5 introns
PY17X_1305400: 15 introns
PY17X_0415900: 13 introns
PY17X_0105800: 1 intron
PY17X_1216400: 10 introns
Parental
Mutant
gDNA
cDNA
bp
M
B
kinesin8b
PF16
I1
I4
I1/E2
p=0.0130
p=0.0003
Parental
Mutant
abundance

Supplementary Figure 5. Verification of intron retention for 30 introns at 26 genes in the RBPm1-null male gametocytes

A. RT-PCR confirmation of intron retention in the 26 genes after loss of RBPm1. For each gene, the mapped views of the RNA-seq results (*DFsc7* in green and *DFsc7*;Δ*Rbpm1* in blue, representative for three biological replicates) and the exon-intron structure (black) are shown in the upper panels. Intron retention is highlighted with red boxes. The primers (F or R) designed for detecting the intron via RT-PCR and the expected PCR products are shown. RT-PCR analysis using the genomic DNA (gDNA) from 17XNL parasite, complementary DNA (cDNA) from male gametocytes of parental and mutant parasites showed the intron retention (red) and intron splicing (black).

B. RT-qPCR confirmation of intron retention in the *kinesin8b* and *PF16* genes after loss of RBPm1. The top schematic of gene exon-intron structure shows the positions of the retained intron (orange line) and the RT-qPCR amplicon. RT-qPCR analysis using cDNA from male gametocytes of parental and mutant parasites showed the retention of *kinesin8b* intron1 and *PF16* intron1. Data are means ± SEM from three independent experiments, two-sided *t*-test.

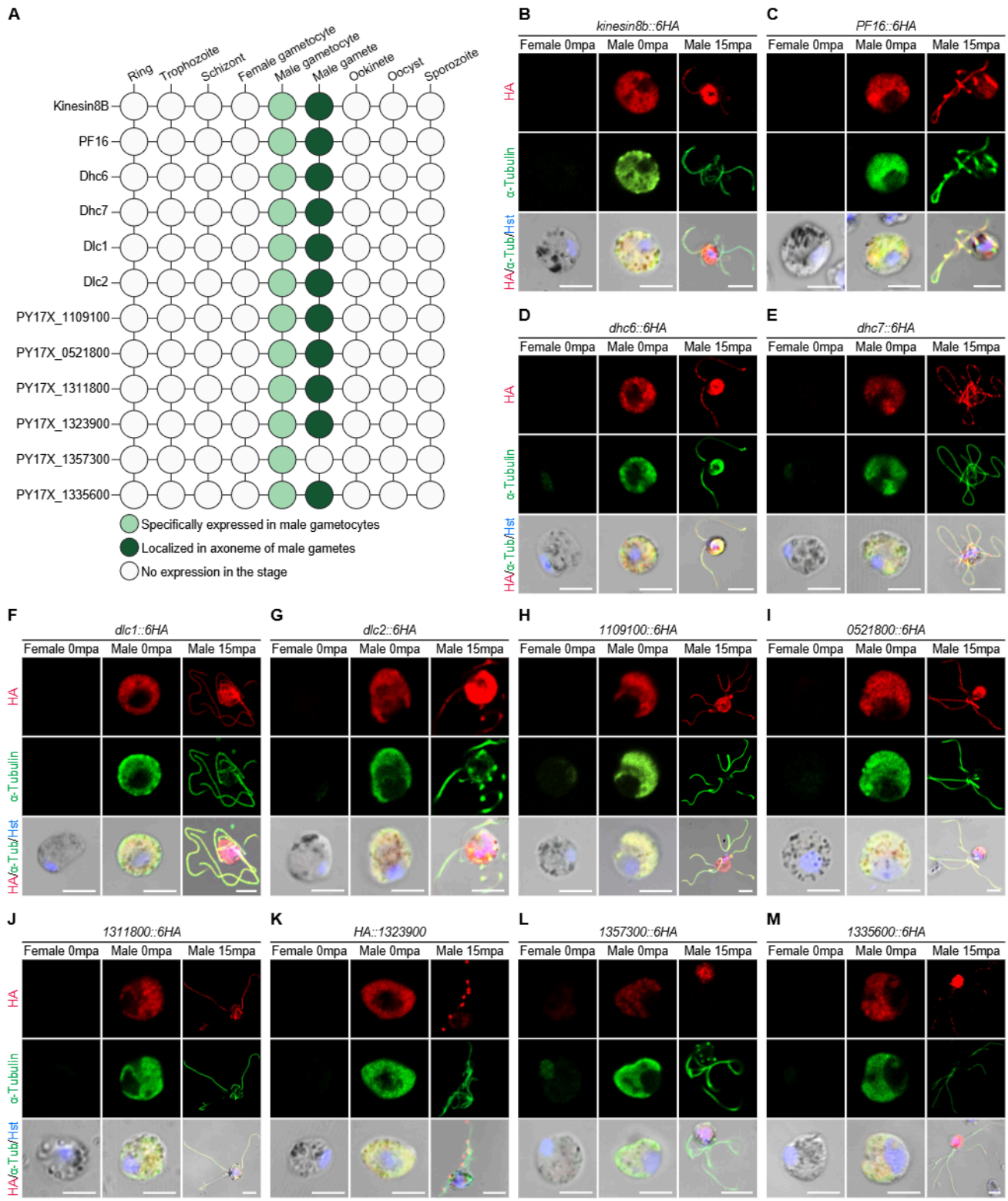
A
Ring
Trophozoite
Schizont
Female gametocyte
Male gametocyte
Male gamete
Ookinete
Oocyst
Sporozoite
Kinesin8B
PF16
Dhc6
Dhc7
Dlc1
Dlc2
PY17X_1109100
PY17X_0521800
PY17X_1311800
PY17X_1323900
PY17X_1357300
PY17X_1335600
Specifically expressed in male gametocytes
Localized in axoneme of male gametes
No expression in the stage
B
kinesin8b::6HA
C
PF16::6HA
D
dhc6::6HA
E
dhc7::6HA
F
dlc1::6HA
G
dlc2::6HA
H
1109100::6HA
I
0521800::6HA
J
1311800::6HA
K
HA::1323900
L
1357300::6HA
M
1335600::6HA
Female 0mpa
Male 0mpa
Male 15mpa
HA
α-Tubulin
HA/α-Tub/Hst

Supplementary Figure 6. RBPm1-regulating genes encode axoneme-associated proteins

A. Summary of protein stage expression and localization of 12 selected intron-retained genes in the *P. yoelii*. These genes include 6 annotated genes (*kinesin8b*, *PF16*, *dhc6*, *dhc7*, *dlc1*, *dlc2*) and 6 unannotated genes (PY17X_1109100, PY17X_0521800, PY17X_1311800, PY17X_1323900, PY17X_1357300, PY17X_1335600). Each gene was endogenously tagged at the N- or C-terminus with a 6HA in the 17XNL, generating the HA-tagged lines for protein expression and localization analysis. Due to the space limit, only the results of protein expression at the gametocytes were shown in **B-M.**

B-M. Protein expression and localization analysis of the 12 intron-retaining genes in gametocytes. IFA of the HA-tagged target protein and α-Tubulin in female gametocytes (0 mpa) and male gametocytes (0 and 15 mpa). Representative results from two independent experiments. Scale bars: 5 μm.

kinesin8b (PY17X_0204100)

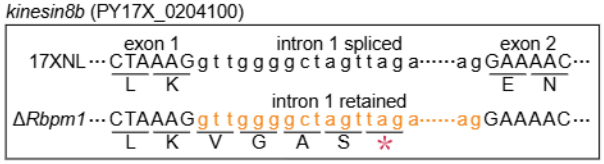

PF16 (PY17X_0919000)

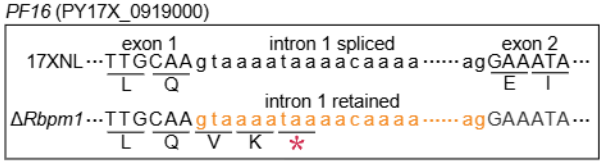

dhc6 (PY17X_0603800)

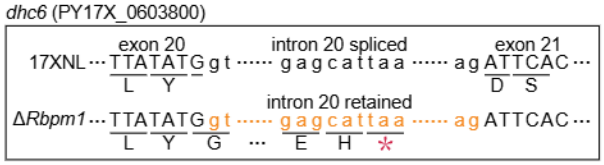

dhc7 (PY17X_0510800)

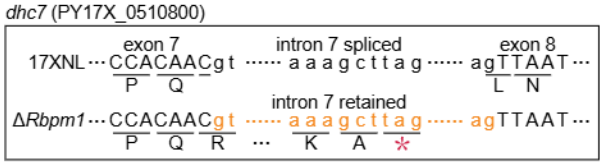

dlc1 (PY17X_1241500)

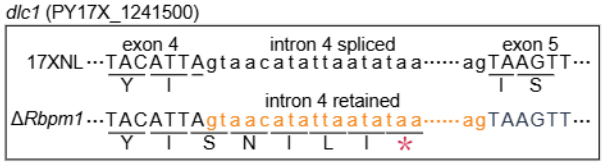

dlc2 (PY17X_0302800)

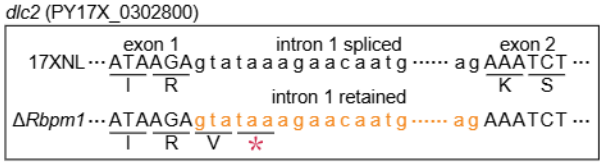

drc1 (PY17X_0721100)

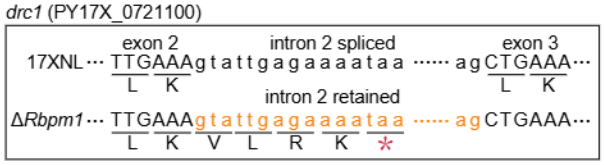

dbc (PY17X_1333900)

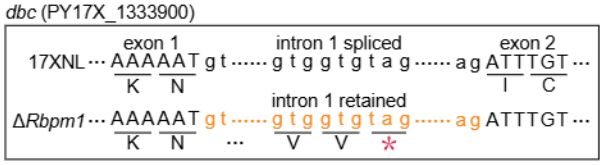

md2 (PY17X_1450400)

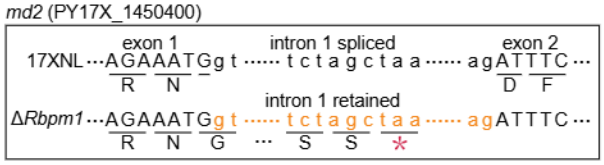

PY17X_1109100

PY17X_0521800

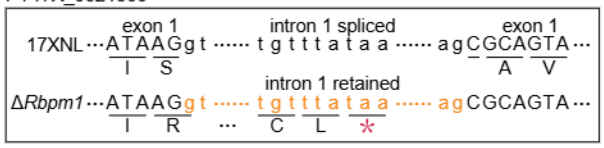

PY17X_1311800

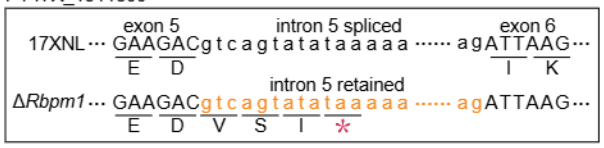

PY17X_1323900

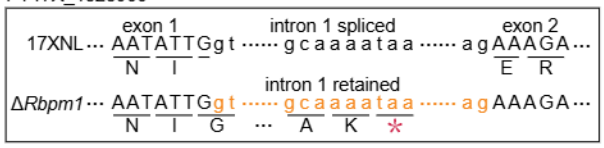

PY17X_1357300

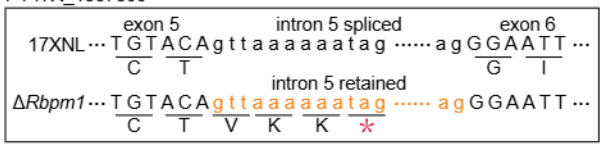

PY17X_1335600

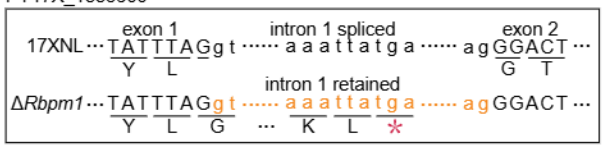

PY17X_1452900

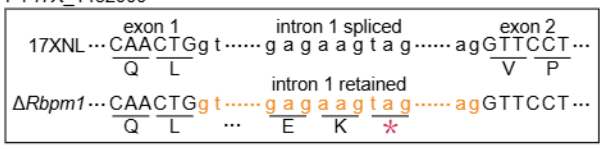

PY17X_1122300

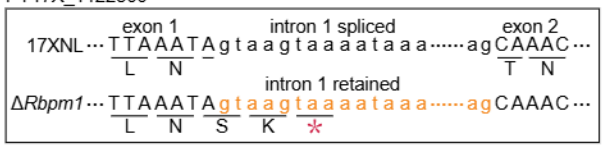

PY17X_0523500

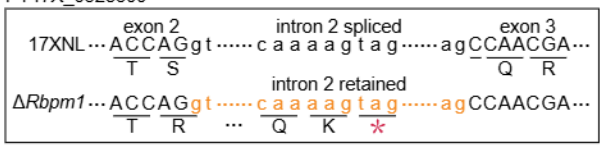

PY17X_0508900

PY17X_1320300

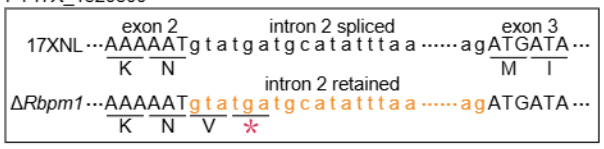

PY17X_0833600

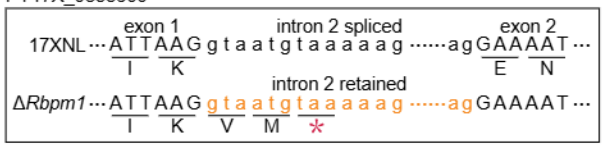

PY17X_1341200

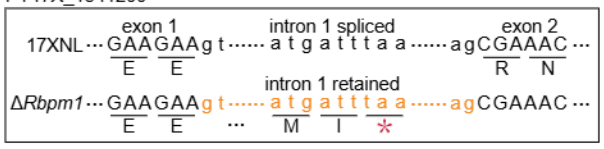

PY17X_1305400

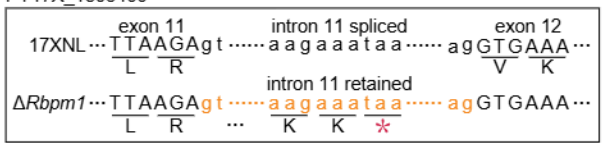

PY17X_0415900

PY17X_0105800

PY17X_1216400

Supplementary Figure 7. Intron retention causes premature stop codons in RBPm1 target transcripts

Amino acid and nucleotide sequence analysis of the retained introns in the 26 genes. For each gene, intron retention (highlighted in orange lowercase letter) creates at least one premature stop codon (red asterisk) at the transcripts in the RBPm1-null parasites.

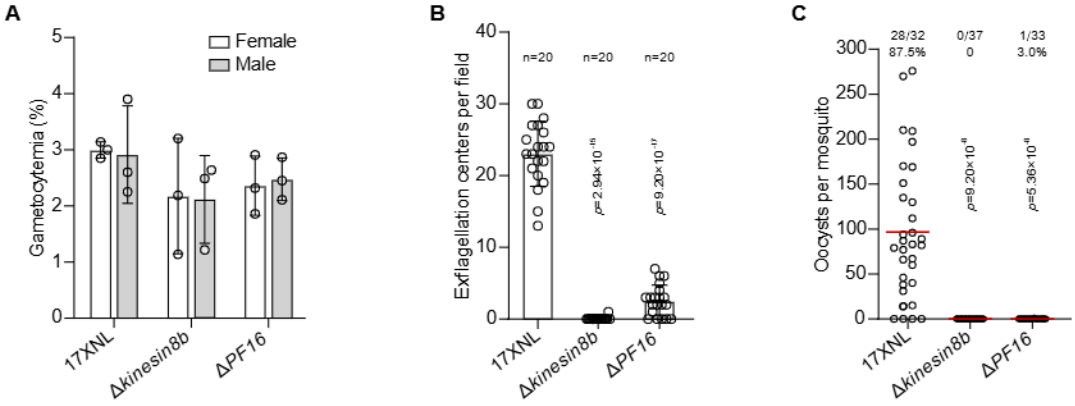

D

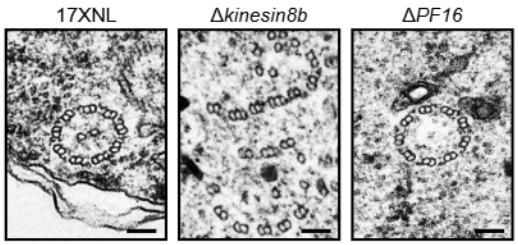

E

	17XNL n=162	Δ*kinesin8b* n=300	Δ*PF16* n=360
"9+2"	93%	0%	19%
"9+1"	1%	0%	10%
"9+0"	1%	0%	52%

Supplementary Figure 8. Depletion of *kinesin8b* or *PF16* phenocopies RBPm1 deficiency

A. Female and male gametocyte formation in mice. Data are means ± SEM from three independent experiments.

B. Exflagellation center (EC) formation of male gametocytes at 10 mpa. Data are means ± SEM from three independent experiments, two-sided *t*-test.

C. Midgut oocyst formation in mosquitoes at 7 days after blood feeding. x/y at the top represents the number of mosquitoes containing oocysts/the number of dissected mosquitoes, and the percentage represents the infection prevalence of mosquitoes. Red lines show the mean value of oocyst numbers, two-sided Mann–Whitney *U* test. Representative results from two independent experiments.

D. Transmission electron microscopy of axoneme architecture in male gametocytes at 8 mpa. Scale bars: 100 nm.

E. Quantification of axoneme formation in the mutant parasites in **D**. n is the total number of the intact and defective axoneme structures observed in each group. Representative for three independent experiments.

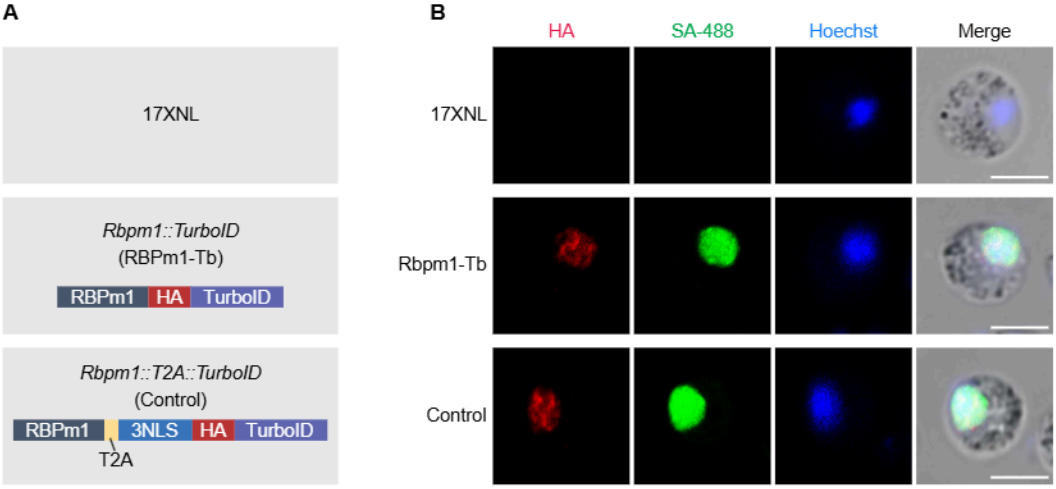

C

E complex			A complex			B complex			C complex		
Components	GeneID	Log_2FC	Components	GeneID	Log_2FC	Components	GeneID	Log_2FC	Components	GeneID	Log_2FC
U1-70K	PY17X_1144300		SNRPA1	PY17X_1147000		DDX23	PY17X_1236700		PRPF19	PY17X_0409200	
U1-A	PY17X_1407100		SNRPB2	PY17X_0839200		CD2BP2	PY17X_0516500		CRNKL1	PY17X_1002800	
U1-C	PY17X_1426800		SF3A1	PY17X_1305300		EFTUD2	PY17X_1205300		CDC5L	PY17X_0518500	
SF1	PY17X_1123900		SF3A2	PY17X_1120200		SNRNP200	PY17X_0524300		ISY1	PY17X_1339900	
U2AF1	PY17X_0930800		SF3A3	PY17X_0828900		TXNL4A	PY17X_1448700		BCAS2	PY17X_1232600	
U2AF2	PY17X_1336700		SF3B1	PY17X_0409500		PRPF8	PY17X_1004500		XAB2	PY17X_1453000	
			SF3B2	PY17X_1329100		PRPF6	PY17X_0939400		PLRG1	PY17X_0403200	
			SF3B3	PY17X_1451900		SNRNP40	PY17X_0708100		SNW1	PY17X_0315900	
			SF3B4	PY17X_1025100		PRPF3	PY17X_1409600		BUD31	PY17X_1240800	
			SF3B5	PY17X_1133600		NHP2L1	PY17X_0926400		CCDC12	PY17X_1319000	
			PHF5A	PY17X_0503800		PRPF4	PY17X_1362600		AQR	PY17X_1371100	
			SF3B14	PY17X_1442300		PRPF31	PY17X_1008100		CWC15	PY17X_0622700	
						PPIH	PY17X_1229000		PPIL1	PY17X_1246700	
						SART1	PY17X_1218000				
						USP39	PY17X_1417200				
						SNRNP27	PY17X_0713000				

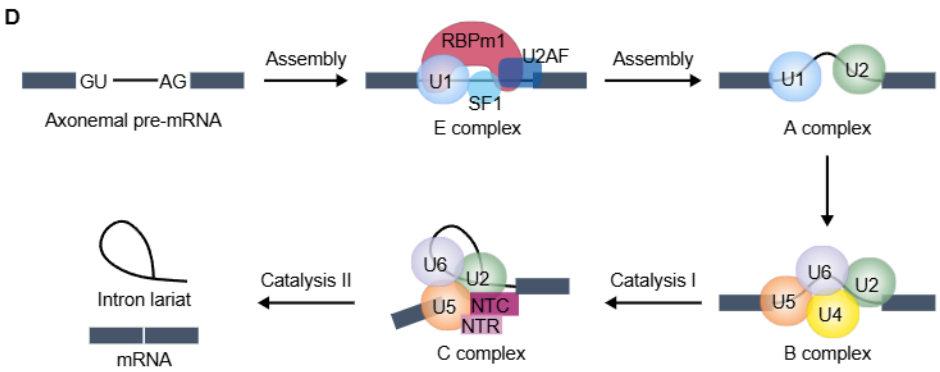

Supplementary Figure 9. RBPm1 interacts with spliceosome E complex

A. A schematic of two modified parasite lines generated for detecting the RBPm1-interacting proteins in gametocytes by TurboID ligase-based proximity labeling. Endogenous RBPm1 was C-terminally tagged with an HA::TurboID motif by CRISPR-Cas9 in 17XNL, generating the *Rbpm1::TurboID* line. A control line *Rbpm1::T2A::TurboID* was generated, in which a "ribosome skip" T2A was inserted between RBPm1 and 3NLS::HA::TurboID for separated nuclear expression of RBPm1 and TurboID.

B. Co-staining of HA-tagged TurboID ligase (red) and biotinylated proteins (SA-488, green) in male gametocytes of the *Rbpm1::TurboID* and *Rbpm1::T2A::TurboID* lines. Gametocytes incubated with 50 μM biotin at 37°C for 20 minutes were co-stained with the fluorescent-conjugated streptavidin (SA-488) and anti-HA antibody. Scale bars: 5 μm. Representative for three independent experiments.

C. Protein interaction analysis between RBPm1 and spliceosome at different stages of assembly based on the data from TurboID-based proximity labeling and mass spectrometry. The upper panels show the spliceosome complexes from early to later stages during assembly, including E, A, B, and C complexes. The lower panels show the enrichment level (log_2FC value) of protein components in different spliceosome complexes.

D. Proposed model showing RBPm1 interaction with the early spliceosome E complex for intron splicing of axonemal genes.

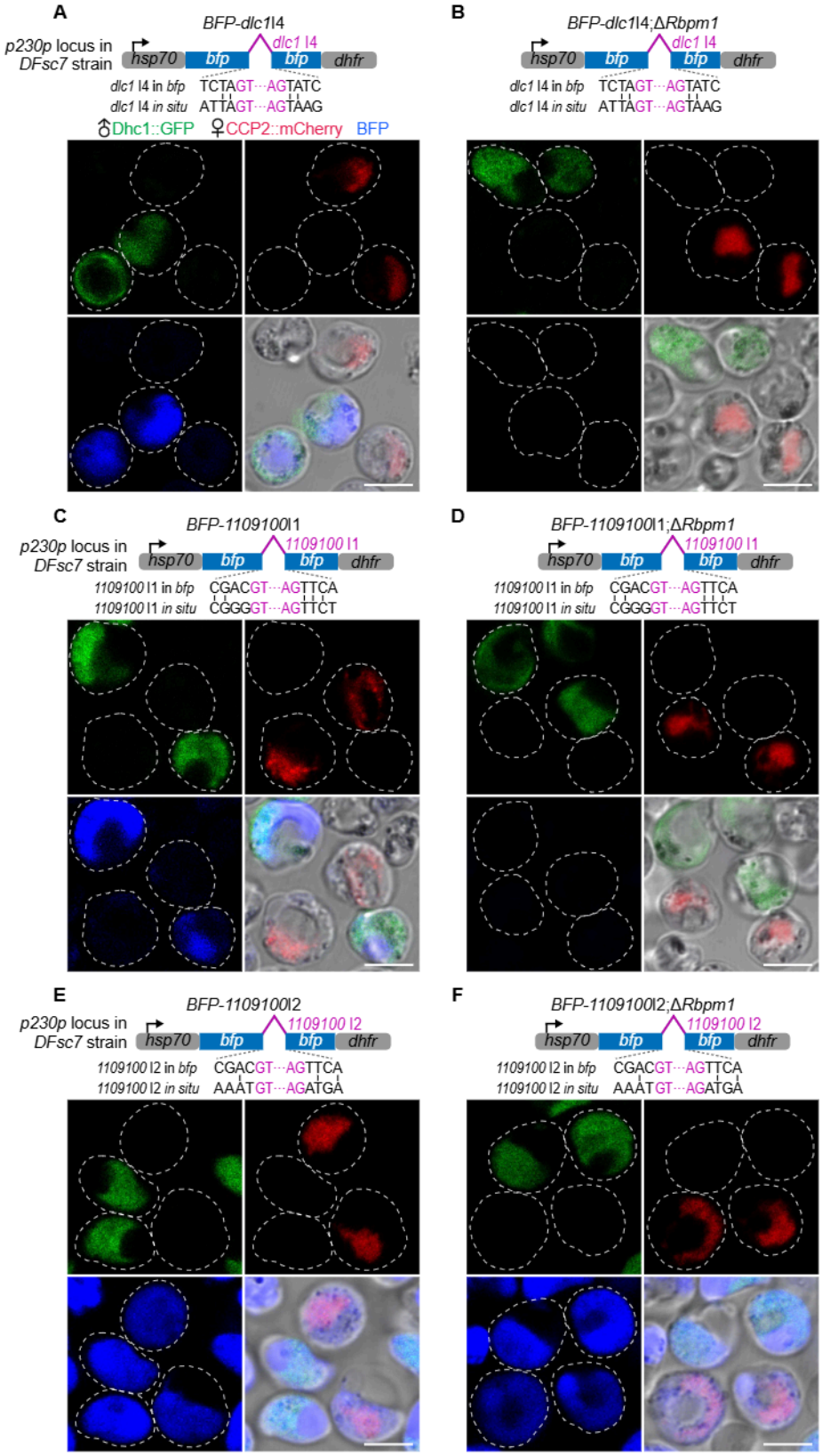
A
BFP-dlc1I4
p230p locus in DFsc7 strain
hsp70
bfp
dlc1 I4
bfp
dhfr
dlc1 I4 in bfp TCTAGT···AGTATC
dlc1 I4 in situ ATTAGT···AGTAAG
Dhc1::GFP
CCP2::mCherry
BFP
B
BFP-dlc1I4;ΔRbpm1
C
BFP-1109100I1
1109100 I1
1109100 I1 in bfp CGACGT···AGTTCA
1109100 I1 in situ CGGGGT···AGTTCT
D
BFP-1109100I1;ΔRbpm1
E
BFP-1109100I2
1109100 I2
1109100 I2 in bfp CGACGT···AGTTCA
1109100 I2 in situ AAATGT···AGATGA
F
BFP-1109100I2;ΔRbpm1

Supplementary Figure 10. RBPm1-dependent splicing of axonemal introns inserted in the reporter gene. Related to Figure 7

A. A transgenic line *BFP-dlc1*I4 with a *dlc1* intron4 (*dlc1*I4, purple line)-inserted *bfp* cassette integrated at the *p230p* locus of the *DFsc7* line. Similar analysis as in **Figure 5B**. *dlc1* intron4 was inserted into the *bfp* gene at the nucleotides 455-456 to mimic the splice site (vertical lines) of *in situ dlc1*I4. BFP expression was detected specifically in male gametocytes of the *BFP-dlc1*I4 parasites. Representative for three independent experiments. Scale bars: 5 μm.

B. A *BFP-dlc1*I4 derived RBPm1 mutant line, *BFP-dlc1*I4;Δ*Rbpm1*, showed no BFP expression in male gametocytes. Representative for three independent experiments. Scale bars: 5 μm.

C. Effect of the *PY17X_1109100* intron1 (*BFP-1109100*I1) insertion on the gametocyte expression of BFP. Similar analysis as in **A**. *PY17X_1109100* intron1 was inserted into the *bfp* gene at the nucleotides 390-391 to mimic the splice site (vertical lines) of *in situ PY17X_1109100* intron1. BFP expression was detected specifically in male gametocytes of the *BFP-1109100*I1 parasites.

D. A *BFP-1109100*I1 derived RBPm1 mutant line, *BFP-1109100*I1;Δ*Rbpm1*, showed no BFP expression in male gametocytes. Similar analysis as in **B**.

E. Effect of the *PY17X_1109100* intron2 (*BFP-1109100*I2) insertion on the gametocyte expression of BFP. Similar analysis as in **A**. *PY17X_1109100* intron2 was inserted into the *bfp* gene at the nucleotides 384-385. BFP expression was detected in both male and female gametocytes of the *BFP-1109100*I2 parasites.

F. A *BFP-1109100*I2 derived RBPm1 mutant line *BFP-1109100*I2;Δ*Rbpm1*, showed BFP expression in both male and female gametocytes. Similar analysis as in **B**.

A

PF16 normalized counts

P. yoelii in this study

Male	Female
580	38

P. berghei [31]

Male	Female
352	53

P. falciparum [30]

Male	Female
72	25

B

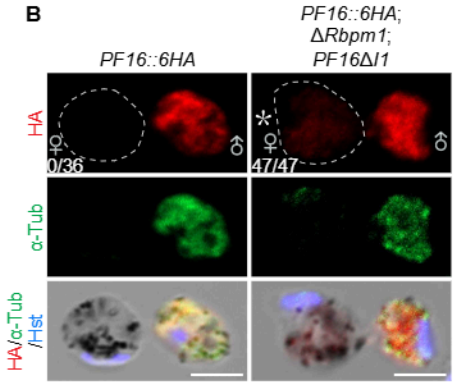

C

dlc1 normalized counts

P. yoelii in this study

Male	Female
296	68

P. berghei [31]

Male	Female
194	63

P. falciparum [30]

Male	Female
96	32

D

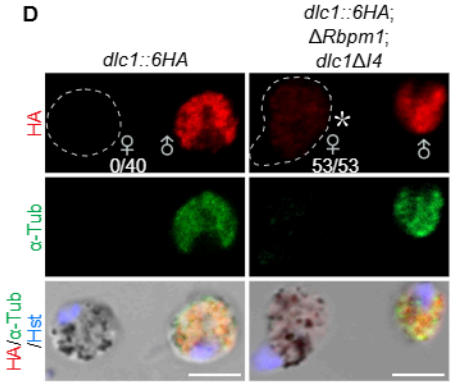

E

1109100 normalized counts

P. yoelii in this study

Male	Female
1662	55

P. berghei [31]

Male	Female
743	67

P. falciparum [30]

Male	Female
561	16

F

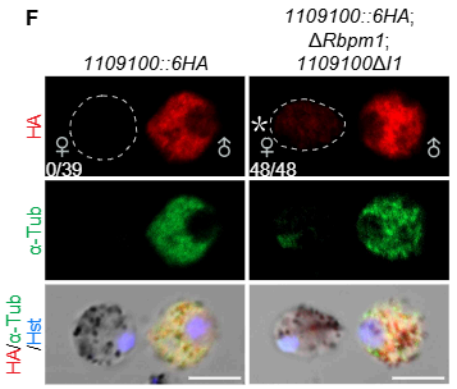

G

kinesin8b normalized counts

P. yoelii in this study

Male	Female
5148	2

P. berghei [31]

Male	Female
333	34

P. falciparum [30]

Male	Female
879	146

H

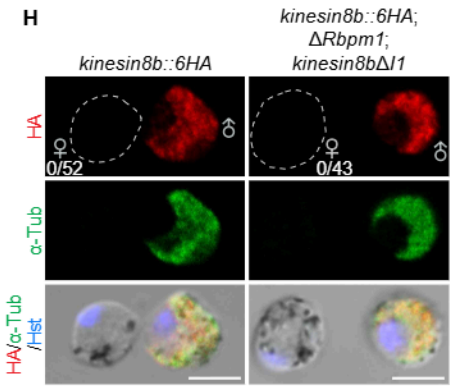

I

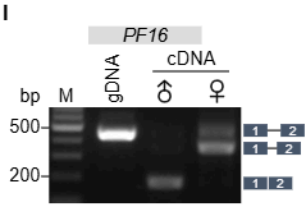

J

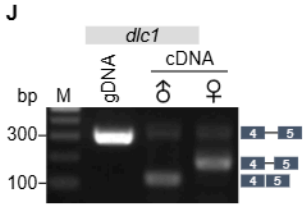

K

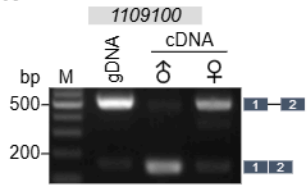

L

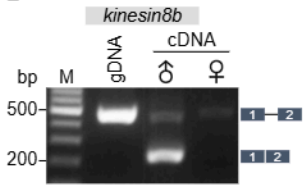

M

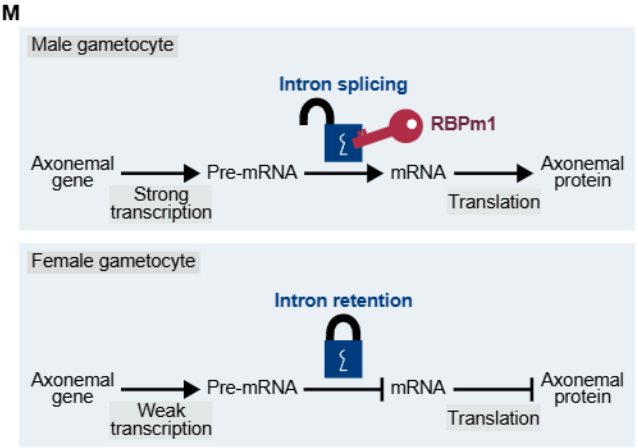

Supplementary Figure 11. Intron retention prevents expression of axonemal proteins in female gametocytes

A. Transcription level of the *PF16* gene in male and female gametocytes. TMM normalized counts are from the gametocyte transcriptomes in this study and the published dataset contributed by Yeoh, L.M. and Lasonder, E.

B. IFA of 6HA-tagged PF16 in female and male gametocytes of the *PF16::6HA* and *PF16::6HA*;Δ*Rbpm1*;*PF16*Δ*I1* (*PF16* intron1-deleted line described in the **Figure 5D**) parasites. In each image, one male and one female gametocytes were shown. The HA-positive female gametocyte was highlighted with an asterisk. x/y represents the number of HA-positive female gametocytes/the total number of female gametocytes tested. Representative for three independent experiments. Scale bars: 5 μm.

C and D. Low-level expression of the Dlc1 protein detected in female gametocytes after deletion of the *dlc1* intron4. Similar illustration as in **A** and **B**. The *dlc1* intron4-deleted line was described in the **Figure 5G**.

E and F. Low-level expression of the PY17X_1109100 protein detected in female gametocytes after deletion of the *PY17X_1109100* intron1. Similar illustration as in **A** and **B**. The *PY17X_1109100* intron1-deleted line was described in the **Figure 5J**.

G and H. Undetectable expression of the Kinesin8B protein in female gametocytes after deletion of the *kinesin8b* Δ*intron1*. Similar illustration as in **A** and **B**. Note that the *kinesin8b* transcripts are almost undetectable in female gametocytes of *P. yoelii*.

I, J, K, and L. RT-PCR confirmation of intron retention at the transcripts of 4 genes (*PF16*, *dlc1*, *PY17X_1109100*, and *kinesin8b*) in female gametocytes. Genomic DNA (gDNA) from 17XNL parasite, complementary DNA (cDNA) from the purified male and female gametocytes of *DFsc7* were analyzed. Exons are indicated by boxes and introns by lines. Representative for three independent experiments.

M. Proposed different roles of RBPm1-target introns in axonemal gene expression at male and female gametocytes respectively. In male gametocytes, RBPm1 (as a key)-directed splicing of axonemal intron (as a lock) allows protein expression of the axonemal genes. In female gametocytes, dual blockage via weak transcription and IR prevents protein expression of the axonemal genes.

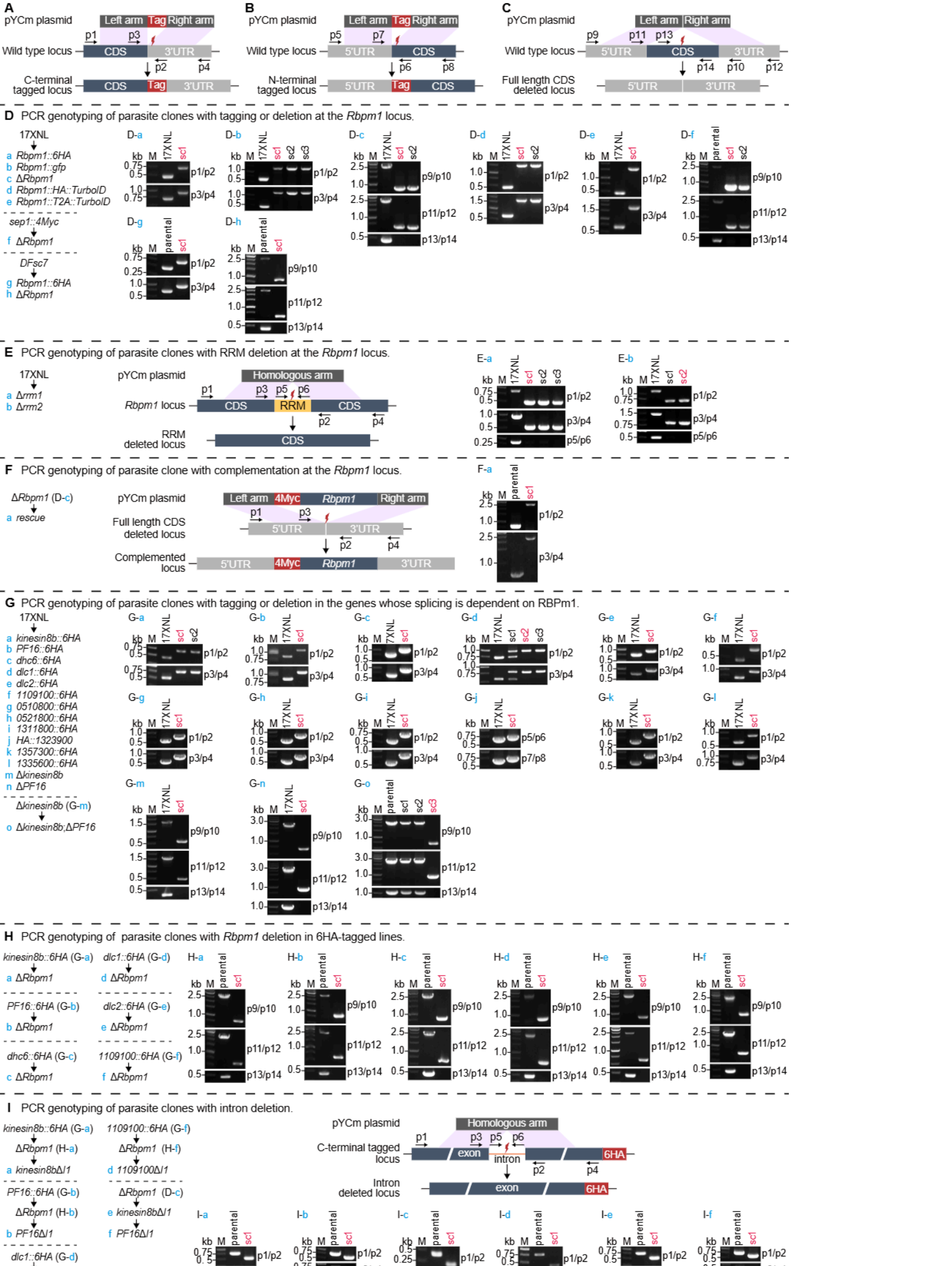
A
pYCm plasmid
Left arm
Tag
Right arm
p1
p3
Wild type locus
CDS
3'UTR
p2
p4
C-terminal tagged locus
B
pYCm plasmid
Left arm
Tag
Right arm
p5
p7
Wild type locus
5'UTR
CDS
p6
p8
N-terminal tagged locus
C
pYCm plasmid
Left arm
Right arm
p9
p11
p13
Wild type locus
5'UTR
CDS
3'UTR
p14
p10
p12
Full length CDS deleted locus
D PCR genotyping of parasite clones with tagging or deletion at the Rbpm1 locus.
17XNL
a Rbpm1::6HA
b Rbpm1::gfp
c ΔRbpm1
d Rbpm1::HA::TurboID
e Rbpm1::T2A::TurboID
sep1::4Myc
f ΔRbpm1
DFsc7
g Rbpm1::6HA
h ΔRbpm1
D-a
D-b
D-c
D-d
D-e
D-f
D-g
D-h
kb
M
17XNL
parental
sc1
sc2
sc3
p1/p2
p3/p4
p9/p10
p11/p12
p13/p14
E PCR genotyping of parasite clones with RRM deletion at the Rbpm1 locus.
17XNL
a Δrrm1
b Δrrm2
pYCm plasmid
Homologous arm
p1
p3
p5
p6
Rbpm1 locus
CDS
RRM
CDS
p2
p4
RRM deleted locus
CDS
E-a
E-b
p5/p6
F PCR genotyping of parasite clone with complementation at the Rbpm1 locus.
ΔRbpm1 (D-c)
a rescue
pYCm plasmid
Left arm
4Myc
Rbpm1
Right arm
p1
p3
Full length CDS deleted locus
5'UTR
3'UTR
p2
p4
Complemented locus
5'UTR
4Myc
Rbpm1
3'UTR
F-a
G PCR genotyping of parasite clones with tagging or deletion in the genes whose splicing is dependent on RBPm1.
17XNL
a kinesin8b::6HA
b PF16::6HA
c dhc6::6HA
d dlc1::6HA
e dlc2::6HA
f 1109100::6HA
g 0510800::6HA
h 0521800::6HA
i 1311800::6HA
j HA::1323900
k 1357300::6HA
l 1335600::6HA
m Δkinesin8b
n ΔPF16
Δkinesin8b (G-m)
o Δkinesin8b;ΔPF16
G-a
G-b
G-c
G-d
G-e
G-f
G-g
G-h
G-i
G-j
G-k
G-l
G-m
G-n
G-o
p5/p6
p7/p8
H PCR genotyping of parasite clones with Rbpm1 deletion in 6HA-tagged lines.
kinesin8b::6HA (G-a)
a ΔRbpm1
PF16::6HA (G-b)
b ΔRbpm1
dhc6::6HA (G-c)
c ΔRbpm1
dlc1::6HA (G-d)
d ΔRbpm1
dlc2::6HA (G-e)
e ΔRbpm1
1109100::6HA (G-f)
f ΔRbpm1
H-a
H-b
H-c
H-d
H-e
H-f
I PCR genotyping of parasite clones with intron deletion.
kinesin8b::6HA (G-a)
ΔRbpm1 (H-a)
a kinesin8bΔI1
PF16::6HA (G-b)
ΔRbpm1 (H-b)
b PF16ΔI1
dlc1::6HA (G-d)
1109100::6HA (G-f)
ΔRbpm1 (H-f)
d 1109100ΔI1
ΔRbpm1 (D-c)
e kinesin8bΔI1
f PF16ΔI1
pYCm plasmid
Homologous arm
p1
p3
p5
p6
C-terminal tagged locus
exon
intron
6HA
p2
p4
Intron deleted locus
exon
6HA
I-a
I-b
I-c
I-d
I-e
I-f

Supplementary Figure 12. Genotyping of genetically modified parasite lines

A-C. Schematic diagrams showing CRISPR/Cas9-mediated gene tagging at C-terminus (**A**), gene tagging at N-terminus (**B**), and gene deletion (**C**) via double cross-over homologous recombination. 'p' represents the primers for PCR, and the red lightning bolt represents the sites for sgRNA recognition.

D-L. Genotyping PCR results showing correct 5' and 3' homologous recombination in the modified parasite lines in this study. For each modification, usually 1-3 parasite single clones (sc) were obtained via limiting dilution. The red-colored sc was selected for further analysis. Oligo sequences used for plasmid construction and primers used for genotyping PCR are listed in Supplementary Table 2.

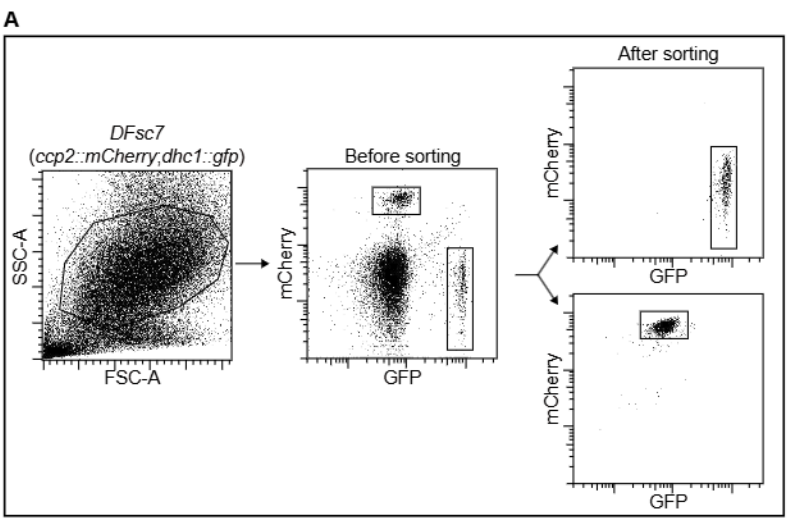
A
DFsc7
(ccp2::mCherry;dhc1::gfp)
SSC-A
FSC-A
Before sorting
mCherry
GFP
After sorting
mCherry
GFP
mCherry
GFP

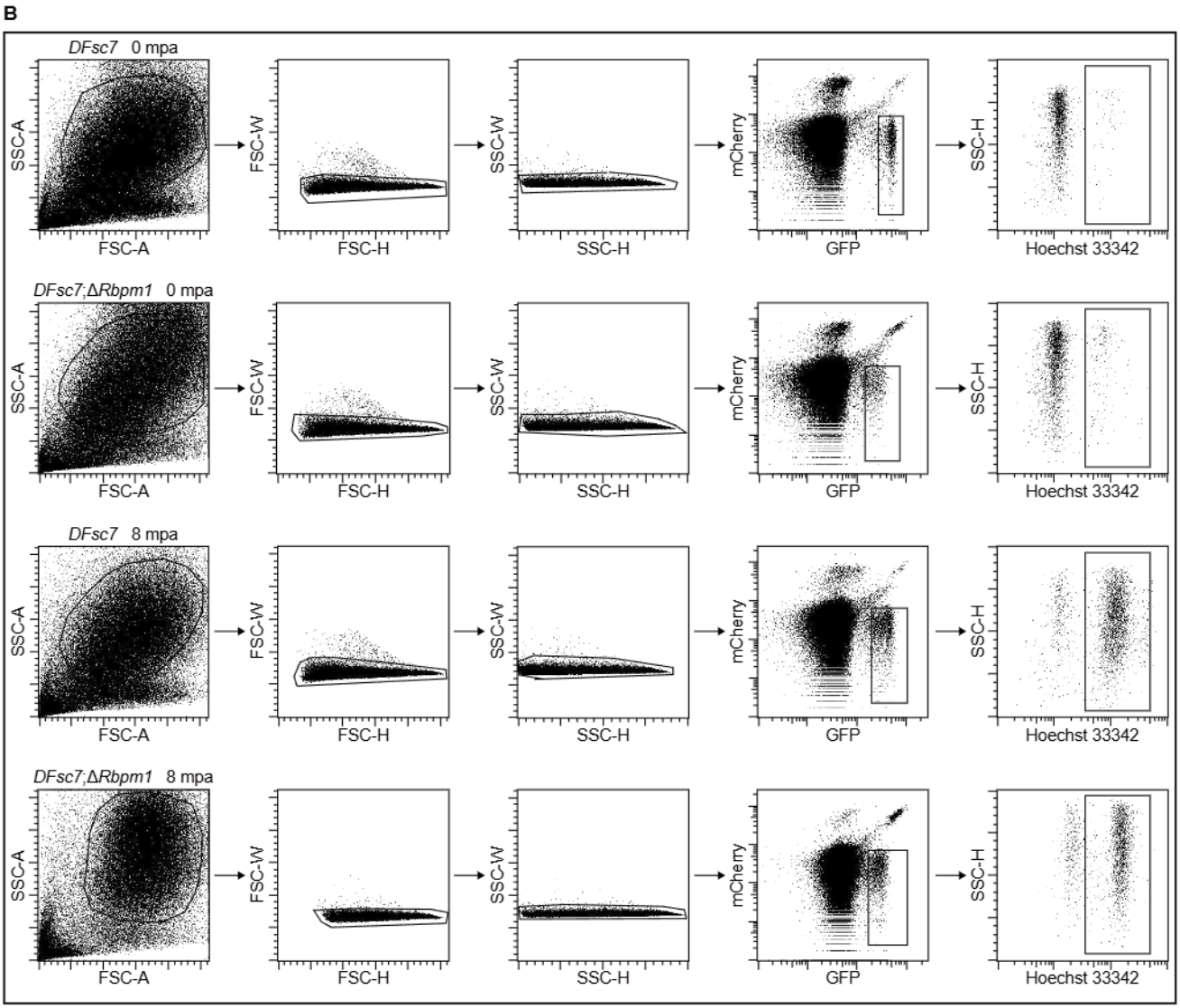
B
DFsc7 0 mpa
DFsc7;ΔRbpm1 0 mpa
DFsc7 8 mpa
DFsc7;ΔRbpm1 8 mpa
SSC-A
FSC-A
FSC-W
FSC-H
SSC-W
SSC-H
mCherry
GFP
SSC-H
Hoechst 33342

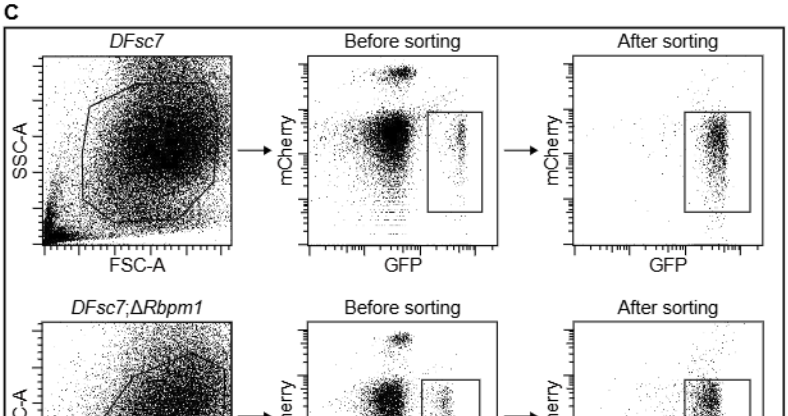
C
DFsc7
DFsc7;ΔRbpm1
Before sorting
After sorting
SSC-A
FSC-A
mCherry
GFP

Supplementary Figure 13. Flow cytometry gating strategies

A. Gating strategy for sorting male and female gametocytes from a *P. yoelii* parasite reporter line *DFsc7* presented in Supplementary Fig. 1A. Forward and side scatter signals were used to distinguish red blood cells from debris, doublets, and white blood cells. Male and female gametocytes were sorted based on GFP fluorescence and mCherry fluorescence. After sorting, gametocyte purity was assessed by re-analysis of a sample fraction.

B. Gating strategy for analyzing DNA content of male gametocytes presented in Supplementary Fig. 2A. Forward and side scatter signals were used to distinguish red blood cells from debris, doublets, and white blood cells. Male gametocytes were identified by GFP fluorescence and analyzed for Hoechst 33342 fluorescence.

C. Gating strategy for sorting male gametocytes from the *DFsc7* and *DFsc7*;Δ*Rbpm1* lines presented in Supplementary Fig. 3F. Forward and side scatter signals were used to distinguish red blood cells from debris, doublets, and white blood cells. Male gametocytes were sorted based on GFP fluorescence. After sorting, male gametocyte purity was assessed by re-analysis of a sample fraction.

Table S1. List of genetically modified parasite strains in this study

Strain	Parental strain	Description	Resource
17XNL	/	*Plasmodium yoelii* 17XNL strain	NIH
Parasites with gene tagging			
DFsc7	17XNL	*DFsc7* expresses mCherry and GFP reporters mutual-exclusively in the female and male gametocytes	Liu et al. 2018
sep1::4Myc	17XNL	*sep1* C-terminally tagged with 4Myc	Jiang et al. 2020
Rbpm1::6HA	17XNL	*Rbpm1* C-terminally tagged with 6HA	Fig S12
Rbpm1::gfp	17XNL	*Rbpm1* C-terminally tagged with GFP	Fig S12
DFsc7;Rbpm1::6HA	*DFsc7*	*Rbpm1* C-terminally tagged with 6HA	Fig S12
Rbpm1::HA::TurboID	17XNL	*Rbpm1* C-terminally tagged with HA-TurboID	Fig S12
Rbpm1::T2A::TurboID	17XNL	*Rbpm1* C-terminally tagged with 3NLS-HA-TurboID	Fig S12
kinesin8b::6HA	17XNL	*kinesin8b* C-terminally tagged with 6HA	Fig S12
PF16::6HA	17XNL	*PF16* C-terminally tagged with 6HA	Fig S12
dhc6::6HA	17XNL	*dhc6* C-terminally tagged with 6HA	Fig S12
dhc7::6HA	17XNL	*0510800* C-terminally tagged with 6HA	Fig S12
dlc1::6HA	17XNL	*dlc1* C-terminally tagged with 6HA	Fig S12
dlc2::6HA	17XNL	*dlc2* C-terminally tagged with 6HA	Fig S12
1109100::6HA	17XNL	*1109100* C-terminally tagged with 6HA	Fig S12
0521800::6HA	17XNL	*0521800* C-terminally tagged with 6HA	Fig S12
1311800::6HA	17XNL	*1311800* C-terminally tagged with 6HA	Fig S12
HA::1323900	17XNL	*1323900* N-terminally tagged with HA	Fig S12
1357300::6HA	17XNL	*1357300* C-terminally tagged with 6HA	Fig S12
1335600::6HA	17XNL	*1335600* C-terminally tagged with 6HA	Fig S12
Rbpm1::6HA;U1-70K::4Myc	*Rbpm1::6HA*	*U1-70K* C-terminally tagged with 4Myc	Fig S12
Rbpm1::6HA;U1-A::4Myc	*Rbpm1::6HA*	*U1-A* C-terminally tagged with 4Myc	Fig S12
Rbpm1::6HA;U1-C::4Myc	*Rbpm1::6HA*	*U1-C* C-terminally tagged with 4Myc	Fig S12
Parasites with gene knockout			
ΔRbpm1	17XNL	Deletion of the whole coding sequences of *Rbpm1*	Fig S12
Δnke4	17XNL	Deletion of the partial coding sequences of *nek4*	Jiang et al. 2020
Δmap2	17XNL	Deletion of the partial coding sequences of *map2*	Jiang et al. 2020
sep1::4Myc;ΔRbpm1	*sep1::4Myc*	Deletion of the whole coding sequences of *Rbpm1*	Fig S12
DFsc7;ΔRbpm1	*DFsc7*	Deletion of the whole coding sequences of *Rbpm1*	Fig S12
Δkinesin8b	17XNL	Deletion of the N-terminal 1184 bp coding sequence of *kinesin8b*	Fig S12
ΔPF16	17XNL	Deletion of the whole coding sequences of *PF16*	Fig S12
Δkinesin8b;ΔPF16	*Δkinesin8b*	Deletion of the whole coding sequences of *PF16*	Fig S12
kinesin8b::6HA;ΔRbpm1	*kinesin8b::6HA*	Deletion of the whole coding sequences of *Rbpm1*	Fig S12
PF16::6HA;ΔRbpm1	*PF16::6HA*	Deletion of the whole coding sequences of *Rbpm1*	Fig S12
dhc6::6HA;ΔRbpm1	*dhc6::6HA*	Deletion of the whole coding sequences of *Rbpm1*	Fig S12
dlc1::6HA;ΔRbpm1	*dlc1::6HA*	Deletion of the whole coding sequences of *Rbpm1*	Fig S12
dlc2::6HA;ΔRbpm1	*dlc2::6HA*	Deletion of the whole coding sequences of *Rbpm1*	Fig S12
1109100::6HA;ΔRbpm1	*1109100::6HA*	Deletion of the whole coding sequences of *Rbpm1*	Fig S12
Δgep1	17XNL	Deletion of the whole coding sequences of *gep1*	Jiang et al. 2020
Parasites with RRM deletion at the *Rbpm1* locus			
Δrrm1	17XNL	Deletion of the 565-981 bp coding sequence of *Rbpm1*	Fig S12
Δrrm2	17XNL	Deletion of the 1018-1519 bp coding sequence of *Rbpm1*	Fig S12
Parasites with gene compelementation			
rescue	*ΔRbpm1*	*In situ* complementation of *Rbpm1* N-terminally tagged with 4Myc	Fig S12
Parasites with intron deletion			
kinesin8b::6HA;ΔRbpm1;kinesin8b ΔI1	*kinesin8b::6HA;ΔRbpm1*	Deletion of *Kinesin8b* intron 1	Fig S12
PF16::6HA;ΔRbpm1;PF16 ΔI1	*PF16::6HA;ΔRbpm1*	Deletion of *PF16* intron 1	Fig S12
dlc1::6HA;ΔRbpm1;dlc1 ΔI4	*dlc1::6HA;ΔRbpm1*	Deletion of *dlc1* intron4	Fig S12
1109100::6HA;ΔRbpm1;1109100 ΔI1	*1109100::6HA;ΔRbpm1*	Deletion of *1109100* intron 1	Fig S12
ΔRbpm1;kinesin8b ΔI1	*ΔRbpm1*	Deletion of *kinesin8b* intron 1	Fig S12
ΔRbpm1;kinesin8b ΔI1;PF16 ΔI1	*ΔRbpm1;kinesin8b ΔI1*	Deletion of *PF16* intron 1	Fig S12
Parasites with modification at the *p230p* locus			
BFP	*DFsc7*	Coding region of *p230p* gene was replaced with the *BFP* expression cassette	Fig S12
BFP-Kin8b I1	*DFsc7*	Coding region of *p230p* gene was replaced with the *BFP-Kin8b* I1 expression cassette	Fig S12
BFP-Kin8b I1;*ΔRbpm1*	*DFsc7;ΔRbpm1*	Coding region of *p230p* gene was replaced with the *BFP-Kin8b* I1 expression cassette	Fig S12
BFP-Kin8b I2	*DFsc7*	Coding region of *p230p* gene was replaced with the *BFP-Kin8b* I2 expression cassette	Fig S12
BFP-Kin8b I2;*ΔRbpm1*	*DFsc7;ΔRbpm1*	Coding region of *p230p* gene was replaced with the *BFP-Kin8b* I2 expression cassette	Fig S12
BFP-PF16 I1	*DFsc7*	Coding region of *p230p* gene was replaced with the *BFP-PF16* I1 expression cassette	Fig S12
BFP-PF16 I1;*ΔRbpm1*	*DFsc7;ΔRbpm1*	Coding region of *p230p* gene was replaced with the *BFP-PF16* I1 expression cassette	Fig S12
BFP-dlc1 I4	*DFsc7*	Coding region of *p230p* gene was replaced with the *BFP-dlc1* I4 expression cassette	Fig S12
BFP-dlc1 I4;*ΔRbpm1*	*DFsc7;ΔRbpm1*	Coding region of *p230p* gene was replaced with the *BFP-dlc1* I4 expression cassette	Fig S12
BFP-1109100 I1	*DFsc7*	Coding region of *p230p* gene was replaced with the *BFP-1109100* I1 expression cassette	Fig S12
BFP-1109100 I1;*ΔRbpm1*	*DFsc7;ΔRbpm1*	Coding region of *p230p* gene was replaced with the *BFP-1109100* I1 expression cassette	Fig S12
BFP-1109100 I2	*DFsc7*	Coding region of *p230p* gene was replaced with the *BFP-1109100* I2 expression cassette	Fig S12
BFP-1109100 I2;*ΔRbpm1*	*DFsc7;ΔRbpm1*	Coding region of *p230p* gene was replaced with the *BFP-1109100* I2 expression cassette	Fig S12
Parasites with axonemal intron inserted at the *gep1* locus			
gep1-Kin8b I1	17XNL	Insertion of *Kinesin8b* intron 1 into exon 3 of *gep1*	Fig S12
gep1-PF16 I1	17XNL	Insertion of *PF16* intron 1 into exon 1 of *gep1*	Fig S12
nt: not tested			

Table S2. Oligonucleotides and primers used in this study

Oligo sequences for constructing gene tagging plasmids

Gene name	Gene ID	Tag	Left homologous arm		Right homologous arm		Target site of sgRNA	
			Forward primer	Reverse primer	Forward primer	Reverse primer	Forward oligo	Reverse oligo
Rbpm1	PY17X_0716700	C-terminal 6HA	CCCAAGCTTGCCGAACCTAAGAAGCCAAA	CATGCCATGGATTGTTATAATCCGGTTGTTGC	CCGCTCGAGTTTATGTCATTTTTTGAGGT	CCGGAATTCGTTCCAATGAAGACAAACAA	TATTGTAAGGGAAAGGACCCATAAA	AAACTTTATGGGTCCTTTCCCTTAC
Rbpm1	PY17X_0716700	C-terminal GFP	CCCAAGCTTGCCGAACCTAAGAAGCCAAA	CATGCCATGGATTGTTATAATCCGGTTGTTGC	CCGCTCGAGTTTATGTCATTTTTTGAGGT	CCGGAATTCGTTCCAATGAAGACAAACAA	TATTGTAAGGGAAAGGACCCATAAA	AAACTTTATGGGTCCTTTCCCTTAC
Rbpm1	PY17X_0716700	C-terminal HA-TurboID	CCCAAGCTTGCCGAACCTAAGAAGCCAAA	CATGCCATGGATTGTTATAATCCGGTTGTTGC	CCGCTCGAGTTTATGTCATTTTTTGAGGT	CCGGAATTCGTTCCAATGAAGACAAACAA	TATTGTAAGGGAAAGGACCCATAAA	AAACTTTATGGGTCCTTTCCCTTAC
Rbpm1	PY17X_0716700	C-terminal 3NLS-HA-TurboID	CCCAAGCTTGCCGAACCTAAGAAGCCAAA	CATGCCATGGATTGTTATAATCCGGTTGTTGC	CCGCTCGAGTTTATGTCATTTTTTGAGGT	CCGGAATTCGTTCCAATGAAGACAAACAA	TATTGTAAGGGAAAGGACCCATAAA	AAACTTTATGGGTCCTTTCCCTTAC
kinesin8b	PY17X_0204100	C-terminal 6HA	CCCAAGCTTGATGACCAAATGAAGAGCTT	CATGCCATGGAGTTTTATTTTTGTTGATGCTAG	CCGCTCGAGAAATGTTTGAACTTTACCATTC	GGGCTTAAGGAAAAAGGCAATGATGCCAT	TATTGTGCGTCAGTTAATTTATGA	AAACTCATAAATTAACTGACGCAC
PF16	PY17X_0919000	C-terminal 6HA	CCCAAGCTTACATCCTGTATTTCTAAAATC	CATGCCATGGTTCTTCGGTATTTTCAACTTC	CCGCTCGAGAACAAGGAAATAACAAGT	GGGCTTAAGCTCGCAATTCCTCCTTTTGC	TATTGTGTGTACATACTTCATGTG	AAACCACATGAAGTATGTACACAC
dhc6	PY17X_0603800	C-terminal 6HA	CCCAAGCTTGTGTGTGCAAACGCAAATAT	CATGCCATGGATTATATATAAATAAAATAG	CCGCTCGAGAAAAAATACGATATACAAAT	CCGGAATTCACGATTATATTATACCAGTA	TATTGGAAGTAGAAATGCCGTTGT	AAACACAACGGCATTTCTACTTCC
dhc7	PY17X_0510800	C-terminal 6HA	CGGGGTACCTGATGATAATGAATTTATTT	CATGCCATGGTAGTAGCATATGAACTTTAA	CCGCTCGAGTTTTTCGTTTTATTTTTTAA	CCCCTTAAGCATCACATTCTTTCATTTTA	TATTGTGGAGACTAGGATCTGAAGG	AAACCCTTCAGATCCTAGTCTCCAC
dic1	PY17X_1241500	C-terminal 6HA	CCCAAGCTTCTCGAAAATGCTTCCTCTCAA	CATGCCATGGAAGATGAGCTACGGATCCATC	CCGCTCGAGATTGAAAAGGCAACATGCTCA	CCGGAATTCCAAAATTATAGGAAATTGCAA	TATTGTTACTGAAAAGTACGTTATA	AAACTATAACGTACTTTTCATGTAAC
dic2	PY17X_0302800	C-terminal 6HA	CGGGGTACCCCTTATCATAATCAGAAATAA	CATGCCATGGACACTTATATACAACAATTG	CCGCTCGAGAATATGATAATTAAATGTGG	GGGCTTAAGGGGGTGAAAATAATTTGG	TATTGCTATATGATGTATGCTATTA	AAACTATAGCATACATCATATAGC
1109100	PY17X_1109100	C-terminal 6HA	CCCAAGCTTGTACCACAAACAATGGTGGA	CGGGGTACCGGATTGTCGTCATTATTGTAAGTGGAA	CCGCTCGAGGGGGTCCATATAAGATGGAA	CCGGAATTCTGGGTTTAACCTTGTACACC	TATTGTTGCTGCTTGGCTTGTTGCT	AAACAGCAACAAGCCAAGCAGCAAC
0521800	PY17X_0521800	C-terminal 6HA	CGGGGTACCCAATAAATAGTGGAAACAAA	CATGCCATGGCAGTTTATCCCCTAATAAAT	CCGCTCGAGATATTGATAATAATCTC	CCCCTTAAGGGGAAACAATATATACGAAT	TATTGTGAAGTCTATATGACCAAGT	AAACACTTGGTCATATAGACTTCAC
1311800	PY17X_1311800	C-terminal 6HA	CGGGGTACCCCCCGAGGACCAATCTTTTG	CATGCCATGGTTGTCCAGTTAAATAATACA	CCGCTCGAGAAAAAAAGAGAAATAAAGAA	CCCCTTAAGGTGTGCCTAAAAGTATGTTC	TATTAATCAGAGGATGAAGTTGCA	AAACTGCAACTTCATCCTCTGATT
1323900	PY17X_1323900	N-terminal HA	CCCAAGCTTGGCATTACTGTCGAAGGACT	CATGCCATGGATTAATTACAAGGAAAGGTA	CCGCTCGAGATGGAACAAAAAAAAAATAG	CCCCTTAAGACCTGTTTATCAAAATGCGA	TATTGTAAATATGAAGGGAGGAGGA	AAACTCCTCCTCCCTTCATATTTAC
1357300	PY17X_1357300	C-terminal 6HA	CGGGGTACCACCCCGATCTTAATACAAC	CATGCCATGGATCTATTTCAAATAATTT	CCGCTCGAGCATACAAATAAATTAAAAAG	CCCCTTAAGTATGCCAGCTTGTATGCCAG	TATTGCATATGCACATTATCAAAAG	AAACCTTTTGATAATGTGCATATGC
1335600	PY17X_1335600	C-terminal 6HA	CCCAAGCTTCGAAATAAATGGAGATAAA	CATGCCATGGCTTTTTTTTATATTTGTCTTTAAAAG	CCGCTCGAGAATTTTTATAATGAACTTAGC	CCGGAATTCTAATGATCTGTTAATTGC	TATTGCCCTTTATGGCTACCTATTA	AAACTAATAGGTAGCCATAAAGGGC
U1-70K	PY17X_1144300	C-terminal 4Myc	CCCAAGCTTGGAAAAGGTCCTTCTAGGGG	CATGCCATGGTTCATACCCTTCATTATGATC	CCGCTCGAGAAGTTTTTCGTAAAAATATCATAAT	CCGGAATTCGTAACTTGCTTAAAATGACA	TATTGATGTCCATATTCCCTATTT	AAACTCTCTGCCTCTATCTCTGTC
U1-A	PY17X_1407100	C-terminal 4Myc	CCCAAGCTTCAGGATTTGTTGAAGCCAGA	CATGCCATGGTCGTTTCGCATATGATATTTTAAC	CCGCTCGAGCCTTTTTTTTTTTTTTGGAATTATT	CCGGAATTAAGGCATATCTGTGTCGTTTGTA	TATTGTATGTCCATATTCCCTATTT	AAACAAATAGGGAATATGGACATAC
U1-C	PY17X_1426800	C-terminal 4Myc	CCCAAGCTTCACATAGTTCACCAGTAGGT	CATGCCATGGCTCATTATTTTTATTTACAAAATTTGC	CCGCTCGAGCCCAATTAAGGGAAGTATAT	GGGCTTAAGGAGTATATACACGTTCGAAA	TATTAGAGCAGGCTATGTTCCCCC	AAACGGGGGAACATAGCCTGCTCT

Diagnositc PCR primers for C-terminal tagging

Gene name	Gene ID	Tag	P1	P2	P3	P4		
Rbpm1	PY17X_0716700	C-terminal 6HA	GGATAAAATGGTTGAAGTTAG	GGTTAAAAGCTAAAAAGGCC	TGAAAATATGCAACAACCGG	TGATTCTACCTGTACACCAG		
Rbpm1	PY17X_0716700	C-terminal GFP	GGATAAAATGGTTGAAGTTAG	GGTTAAAAGCTAAAAAGGCC	TGAAAATATGCAACAACCGG	TGATTCTACCTGTACACCAG		
Rbpm1	PY17X_0716700	C-terminal HA-TurboID	GGATAAAATGGTTGAAGTTAG	GGTTAAAAGCTAAAAAGGCC	TGAAAATATGCAACAACCGG	TGATTCTACCTGTACACCAG		
Rbpm1	PY17X_0716700	C-terminal 3NLS-HA-TurboID	GGATAAAATGGTTGAAGTTAG	GGTTAAAAGCTAAAAAGGCC	TGAAAATATGCAACAACCGG	TGATTCTACCTGTACACCAG		
Rbpm1	PY17X_0716700	C-terminal 6HA	GGATAAAATGGTTGAAGTTAG	GGTTAAAAGCTAAAAAGGCC	TGAAAATATGCAACAACCGG	TGATTCTACCTGTACACCAG		
kinesin8b	PY17X_0204100	C-terminal 6HA	TTAATAAACAAACTAGTTGC	GAATGGTAAAGTTCAAACATT	CGCACCAAAGATCTCAAACC	CCCACTTAGATATTTCGAAA		
PF16	PY17X_0919000	C-terminal 6HA	CTAATGAGTCATCTGATGAT	TATAGTAAGAAATAGCAGAC	CACACCTGGATATTCTGAAA	CCTTGAAGTAATCTTATCAC		
dhc6	PY17X_0603800	C-terminal 6HA	CGTTAAGATATGCAACTGTC	TACAAAAATAGCAAACGGTT	CAAATCTGAAAAACATAAATCC	GTCTCGAACAAATTTAAATG		
dhc7	PY17X_0510800	C-terminal 6HA	GACGATGAATCAAATTCGAA	ACAGGTTAAAAAATTAAACG	GCCATGCATCCATAGCAAA	GTTTTGAATTTCTTCTAACTC		
dic1	PY17X_1241500	C-terminal 6HA	GGTCCAACATAATTTGTGAAG	GAAAATTTAGAAAACATATGT	AGATGGATCCGTAGCTCATC	GACCTCTTACTATGTGTAAC		
dic2	PY17X_0302800	C-terminal 6HA	GGCATAAGTTGAATAAGCATTCA	CATATGAGTGTTTTCATCCC	GCATTATTTTGTAGGAGGAGT	ATCATTCCCTATATTTCCTGAATT		
1109100	PY17X_1109100	C-terminal 6HA	TCTACAAAAGAGGAAGCTTC	TTCCATCTTATATGGACCCC	GACACTTACAATAATGACGA	CCGAAGCACAATTAGCAATC		
0521800	PY17X_0521800	C-terminal 6HA	CAAGGTAATAATATGTACATG	AACTTCCATGATATTTTGAG	ATTTATTAGGGGATAAACTG	TGTGTATATTGACAACATCC		
1311800	PY17X_1311800	C-terminal 6HA	ATAGGAAAAACTGGATTTCC	TCCCTTTGTTTTTTTCGTTG	CAGAGGATGAAGTTGCATGG	GGCGTAAGCCAAAGAATGAAC		
1357300	PY17X_1357300	C-terminal 6HA	AAAACTGCAGGAGAAAATGC	CGGGGGAAGGGGTATATTTG	CAACTTCCGATAATTCAATAG	ACAATATGCCACGTGCACAA		
1335600	PY17X_1335600	C-terminal 6HA	CTGATGATATTTTTGAAACC	TAGGAAATATGAATTAGGAG	AAAATCGAGAGATGCAAAAC	ATGATTATGGGGATATAGTC		
U1-70K	PY17X_1144300	C-terminal 4Myc	TACCTAGAAGATTAGGAGGG	TATCATTTGGAATATCAAAGG	GCCAGGAAAATGGAGAATAT	CCCTATATATGTGGTTATATC		
U1-A	PY17X_1407100	C-terminal 4Myc	GAAAATGTTAATACTGAAGC	CTACATATATTGTGCGTTTT	AGTTAAAAATATCATATGCG	TAACGGATGGTTAGATAAGA		
U1-C	PY17X_1426800	C-terminal 4Myc	GTGAATATTGCGATATATATC	ATAACTTAAACATTTCATGTG	CAAATGAATAAAGAAAATGC	CGGAATAACTGCTCATTTAT		

Diagnositc PCR primers for N-terminal tagging

Gene name	Gene ID	Tag	P5	P6	P7	P8		
1323900	PY17X_1323900	N-terminal HA	GGGGGGAATGATGGAAAAAA	ACTAAATGAAGGCGACTCAC	GTTCTTTTACCTTTCCTTGT	GGAAAGGTTTTGTGTAGCTA		
kinesin8b	PY17X_0204100	N-terminal 6HA	GTTTACTCTCTTGTCCACAT	GATCCTGCACATTTTTAAGA	GTGGATCTACTTGATATACT	CATCATAATATTGAGTTTTA		
PF16	PY17X_0919000	N-terminal 6HA	GCAAAAATGTAGACAATAATCC	CGACCTATTATAATCGTCAA	AAAAAATTTCACAAAAAAGG	GGTATGATACCTTTATCAAC		

Oligo sequences for constructing gene knockout plasmids

Gene name	Gene ID	Gene size (bp) / deleted gene size (bp)	Left homologous arm		Right homologous arm		Target site of sgRNA	
			Forward primer	Reverse primer	Forward primer	Reverse primer	Forward oligo	Reverse oligo
Rbpm1	PY17X_0716700	1904/1904	CGGGGTACCGCATACACGAGGAAATACTA	CATGCCATGGTTTGTGTATTTTATTTTTCGTCG	CCGCTCGAGTTTATGTCATTTTTGAGGT	CCGGAATTCGTTCCAATGAAGACAAACAA	TATTGTAGGGGGGTTAAGCTACTAT	AAACATAGTAGCTTAACCCCCCTAC
kinesin8b	PY17X_0204100	5137/1184	CGGGGTACCCCGGTTGTGCATTTATTATTT	CATGCCATGGATTTGATCTTACTATATT	CCGCTCGAGACAGAACAACTTAATGGACAG	CCGGAATTCCTTTCTCTTCATTCATTTCCTTG	TATTGTTACCCTCAGTATACAAAAT	AAACATTTTGTATACTGAGGGTAAC
PF16	PY17X_0919000	1809/1809	CCCAAGCTTACGGTTTCTAAAGTAATAATATCAC	CATGCCATGGTTTTTTTTTTTTATTAACAGTCA	CCGCTCGAGAACAAGGAAATAACAAGT	GGGCTTAAGCTCGCAATTCCTCCTTTTGC	TATTAGTGCATGTGTTTGGACTGT	AAACACAGTCCAAACACATGCACT

Diagnostic PCR primers for gene knockout

Gene name	Gene ID	P9	P10	P11	P12	P13	P14	
Rbpm1	PY17X_0716700	AAGCGAAATAAATGAAACGG	GGTTAAAAGCTAAAAAGGCC	CGACGAAAAATAAAATACACAAA	CGTAATTTCAAAAATGAAGA	GCGGACACTCTAAGTACTGG	GGTTACAAAGGCAAACCCTC	
kinesin8b	PY17X_0204100	GTTTACTCTCTTGTCCACAT	CTGTCCATTAAGTTGTTCTG	CTATATATGTGGATCTACTTG	TATGATATTTTTGGCGTCTC	CGATGCAAACTATAACATCT	GATTCTGTATGTTGAGGGGT	
PF16	PY17X_0919000	CAGATTATTGTCATATCATC	AAAGCACAATAATGTATTGG	CCTCCCCACTTTTAGTACTG	CGACATGACTTGTACAGGTG	GCAACAGTAATACTAGCGAA	AAGCTTCAAGATCCGTAACT	

Oligo sequences for constructing RRM deletion plasmids

Strain	Homologous arm		Mutation primers		Target site of sgRNA	
	Forward primer	Reverse primer	Forward primer	Reverse primer	Forward oligo	Reverse oligo
Δrrm1	CCGCTCGAGCGAGAACGAAGTTTATCTAA	GGGCTTAAGGGACATATACACTATATCTCCT	GTAACTCAAAAAATATAAATGAACCATTTGAGGAACACAATACG	ATCTGAGGGTGTCGTATTGTGTTCCTCAAATGGTTCATTTATAT	TATTATTAGAAAAATAAAAATTGT	AAACACAATTTTTATTTTTCTAATC
Δrrm2	CCGCTCGAGCATTGGAGGAATTCCACAAA	GGGCTTAAGTGTTATAATCCGGTTGTTGC	CGACACCCTCAGATATTCAAAGAAAAGCCGAACCTAAG	TTGGCTTCTTAGGTTCGGCTTTTCTTTGAATATCTGAG	TATTGTAAGGGAAAGGACCCATAAA	AAACTTTATGGGTCCTTTCCCTTAC

Diagnostic PCR primers for RRM deletion

Strain	P1	P2	P3	P4	P5	P6		
Δrrm1	CAACAATTGTGAAAACAGAG	AGGGTGTCGTATTGTGTTCC	CTTCAACAGGAATTATTGAA	CTCCTCATTCCACTATTATT	TTTCATTGGAGGAATTCCAC	ATTTATATGAGATGACATGG		
Δrrm2	GTTGGCAACATATCTGAACT	ATGAGCCAATACATACACAC	ATTGAATGGGAAACGAGTGG	GTTCCAATGAAGACAAACAA	GGGGGTTAAGCTACTATTGG	CTAACTTCAACCATTTTATC		

Oligo sequences for constructing gene *in situ* complementation plasmids

Gene name	Gene ID	Tag	Left homologous arm		Right homologous arm		Target site of sgRNA	
			Forward primer	Reverse primer	Forward primer	Reverse primer	Forward oligo	Reverse oligo
Rbpm1	PY17X_0716700	N-terminal 4Myc	CGGGGTACCGCATACACGAGGAAATACTA	CATGCCATGGTTTGTGTATTTTATTTTTCGTCG	CCGCTCGAGTTTATGTCATTTTTGAGGT	CCGGAATTCGTTCCAATGAAGACAAACAA	TATTGCGGACGCTAATCGTAGCTA	AAACTAGCTACGATTAGCGTCCGC

Diagnostic PCR primers for *in situ* complementation gene

Strain	P1	P2	P3	P4				
rescue	AAGCGAAATAAATGAAACGG	GGTTAAAAGCTAAAAAGGCC	CGACGAAAAATAAAATACACAAA	CGTAATTTCAAAAATGAAGA				

Oligo sequences for constructing intron deletion plasmids

Strain	Homologous arm		Mutation primers		Target site of sgRNA	
	Forward primer	Reverse primer	Forward primer	Reverse primer	Forward oligo	Reverse oligo
kinesin8b Δi1	CATGCCATGGTGATAAAGAAAAAACACACG	CCGCTCGAGCATGTTTAGGTAGATAATGT	ACTCAACTAAAGGAAAACATAACAGATAAAGACAAT	TGTTATGTTTTCCTTTAGTTGAGTGTATTTGCGTTT	TATTGTGACGCTTGACTAACGATG	AAACCATCGTTAGTCAAGCGTCAC
PF16 Δi1	CGGGGTACCCCAGCTATATTATGTCTTGG	CCGCTCGAGTTCTTCGGTATTTTTCAACTTCATCA	TCAGGGTGCTTAAAATATTTGCAAGTAATTTTTATC	AAATACAATGGGGATAAAAATTACTTGCAAATATTT	TATTGTGTGTACATACTTCATGTG	AAACCACATGAAGTATGTACACAC
dic1 Δi4	CGGGGTACCGGCCATACTATTTATAAACA	CCGCTCGAGATGCTCTATAAAATACAGC	TCAAATACATTATAAGTTGCTACATTTTAAAGAATT	TGTAGCAACTTATAATGTATTTGAGAGGAAGCATTT	TATTGCATTCTTCACAAATTATGT	AAACACATAATTTGTGAAGAATGC

1109100Δi1	CGGGGTACCGTACGTACATGTAGGACAAA	CCGGAATTCGTGGGAAAAAATAAGTATTAC	GTTGAGCGCGGGTTCTAAGCCCTTAGAAATATGGAA	AAGGGCTTAGAACCCGCGCTCAACAAGAGTGACAAT	TATTGGAAAATGAGAACAAAAAAA	AAACTTTTTTTGTTCTCATTTTCC		
Diagnostic PCR primers for intron deletion								
Strain	**P1**	**P2**	**P3**	**P4**	**P5**	**P6**		
kinesin8b Δi1	CTGAAATAGAATGCTTAAAAGAAC	GCATTGTCTTTATCTGTTATGTT	AATTTGGGTTCTATAACCCCC	CGCTCATTTAAAACCTGTTTAC	GGGGCTAGTTAGATCGTACC	CGGATAATGAACCATCGATTC		
PF16Δi1	GTACGTGCAGGTGCTTTACC	CCTCACATGAAGTATGTACA	CATTTATTAAATCAGGGTGC	GCACAATAATGTATTGGAAA	CCTAGTTGTAATTTCTCAAA	ACGATTTGGTTATATATAAT		
dic1 Δi4	GCACACGTAATCAAATTTAA	TCTTTAAAATGTAGCAACTTA	GCTTCCTCTCAAATACATTA	CCATCTGATACTTTCAATGC	TTCAAAAAGTAGAAGTATGC	CTGAAAAGTACGTTATAAGG		
1109100Δi1	CATATGCAAATAATATTTGCAC	TATTTCTAAGGGCTTAGAAC	ATTGTCACTCTTGTTGAGCG	TATTCATCTAAGCAGAAAAAT	CGGTAGCAGTATATGTAGTT	CTGATTATAAAAGGAAAGAC		
Oligo sequences for constructing *bfp* reproter assay plasmids								
Expression element	**Forward primer**	**Reverse primer**	**Reporter gene**	**Forward primer**	**Reverse primer**	**Expression element**	**Forward primer**	**Reverse primer**
The 5'-UTR of *hsp70*	CGGGGTACCGTAAAGAGGATGATGTATGT	CATGCCATGGCTTTTTTTTTTTTTAATTGCAA	*bfp*	CATGCCATGGGGATGGTGAGCAAGGGCGAGGAGCT	CCGCTCGAGTTACTTGTACAGCTCGTCCATGC	The 3'-UTR of *dhfr*	CCGCTCGAGTGTTCATTTTTCTTATTTAT	CCGGAATTCCCTGAAGAAGAACAGTCCGA
Reporter gene	**Upstream *bfp* sequence**		**Intron**		**Downstream *bfp* sequence**		**Overlap PCR**	
	Forward primer	**Reverse primer**	**Forward primer**	**Reverse primer**	**Forward primer**	**Reverse primer**	**Forward primer**	**Reverse primer**
bfp-Kin8bI1	CATGCCATGGGGATGGTGAGCAAGGGCGAGGA	TAGCCCCAACCTTGAAGTCGACGCCCTTCA	CGACTTCAAGGTTGGGGCTAGTTAGATCGT	TGCCGTCCTCCTACAAATAAACAAAATAAC	TTATTTGTAGGAGGACGGCAACATCCTGGG	CCGCTCGAGTTACTTGTACAGCTCGTCCATGC	CATGCCATGGGGATGGTGAGCAAGGGCGAGGA	CCGCTCGAGTTACTTGTACAGCTCGTCCATGC
bfp-Kin8bI2	CATGCCATGGGGATGGTGAGCAAGGGCGAGGA	CTGAATATACTTGTGGCCGTTTACGTCGCC	ACGGCCACAAGTATATTCAGTTCTTTCCAT	CACGCTGAACCTGTTTACATATATTAAAAA	ATGTAAACAGGTTCAGCGTGAGGGGCGAGG	CCGCTCGAGTTACTTGTACAGCTCGTCCATGC	CATGCCATGGGGATGGTGAGCAAGGGCGAGGA	CCGCTCGAGTTACTTGTACAGCTCGTCCATGC
bfp-PF16I1	CATGCCATGGGGATGGTGAGCAAGGGCGAGGA	TTTATTTTACTTGAAGTTCACCTTGATGCC	TGAACTTCAAGTAAAATAAAACAAAACAAA	GTGGCGGATCCTAAATAAAAGAGAAAAGCC	TTTTATTTAGGATCCGCCACAACGTGGAGG	CCGCTCGAGTTACTTGTACAGCTCGTCCATGC	CATGCCATGGGGATGGTGAGCAAGGGCGAGGA	CCGCTCGAGTTACTTGTACAGCTCGTCCATGC
bfp-dic1I4	CATGCCATGGGGATGGTGAGCAAGGGCGAGGA	AATATGTTACTAGATGTTGTGGCTGTTGAA	ACAACATCTAGTAACATATTAATATAATTT	GGCCATGATACTGAAAAGTACGTTATAAGG	TACTTTTCAGTATCATGGCCGTCAACGCAGA	CCGCTCGAGTTACTTGTACAGCTCGTCCATGC	CATGCCATGGGGATGGTGAGCAAGGGCGAGGA	CCGCTCGAGTTACTTGTACAGCTCGTCCATGC
bfp-1109100I1	CATGCCATGGGGATGGTGAGCAAGGGCGAGGA	ATTAAATTACGTCGACGCCCTTCAGCTCGA	GGGCGTCGACGTAATTTAATATTATAATAA	CCTCCTTGAACTGATTATAAAAGGAAAAGAC	TTATAATCAGTTCAAGGAGGACGGCAACAT	CCGCTCGAGTTACTTGTACAGCTCGTCCATGC	CATGCCATGGGGATGGTGAGCAAGGGCGAGGA	CCGCTCGAGTTACTTGTACAGCTCGTCCATGC
bfp-1109100I2	CATGCCATGGGGATGGTGAGCAAGGGCGAGGA	TAAGTATTACGTCGACGCCCTTCAGCTCGA	GGGCGTCGACGTAATACTTATTTTTTCCCA	CCTCCTTGAACTAAGCAGAAAAATTTTAAA	TTCTGCTTAGTTCAAGGAGGACGGCAACAT	CCGCTCGAGTTACTTGTACAGCTCGTCCATGC	CATGCCATGGGGATGGTGAGCAAGGGCGAGGA	CCGCTCGAGTTACTTGTACAGCTCGTCCATGC
Diagnostic PCR primers for expression cassette integrated into the *p230p* locus								
P1	**P2**	**P3**	**P4**	**P5**	**P6**			
GGAAAAGTATGATAACGATG	GACGGACACATACATCATCC	TCGGACTGTTCTTCTTCAGG	AGATGATATCGCTATATATC	GATGCATCTATAACTCCAGA	TGCTGAGTCAGTGGTGTTCC			
Oligo sequences for constructing plasmids with axonemal intron insertion into *gep1*								
Strain	**Upstream *gep1* sequence**		**Intron**		**Downstream *gep1* sequence**		**Overlap PCR**	
	Forward primer	**Reverse primer**	**Forward primer**	**Reverse primer**	**Forward primer**	**Reverse primer**	**Forward primer**	**Reverse primer**
gep1-Kin8bI1	CGGGGTACCGTCAAATCATGAAGTTTGGA	TAGCCCCAACCTTTTTGATGCTGATATAAG	CATCAAAAAGGTTGGGGCTAGTTAGATCGT	TACATCTATCCTACAAATAAACAAAATAAC	TTATTTGTAGGATAGATGTATTATTTTTGT	CATGCCATGGCTTTGAGGAGAGAGTGTGGG	CGGGGTACCGTCAAATCATGAAGTTTGGA	CATGCCATGGCTTTGAGGAGAGAGTGTGGG
gep1-PF16I1	CGGGGTACCATGTGTTGAAATAAAAGATG	TTTATTTTACTTGCAATAAAAATGGAGCCG	TTTATTGCAAGTAAAATAAAACAAAACAAA	CATTAATCTCCTAAAATAAAAGAGAAAAGCC	TTTTATTTAGGAGATTAATGGAGGAAGATT	GGGCTTAAGGTAGACTTACCAACTTCATT	CGGGGTACCATGTGTTGAAATAAAAGATG	CATGCCATGGCTTTGAGGAGAGAGTGTGGG
Strain	**Target site of sgRNA**							
	Forward oligo	**Reverse oligo**						
gep1-Kin8bI1	TATTGTATTGATTCCGAGTCTGAAA	AAACTTTCAGACTCGGAATCAATAC						
gep1-PF16I1	TATTGTTATTGCAAGAGATTAATGG	AAACCCATTAATCTCTTGCAATAAC						
Diagnostic PCR primers for axonemal intron inserted into *gep1*								
Strain	**P1**	**P2**	**P3**	**P4**				
gep1-Kin8I1	TATTGAGCTACTGTCAGCAG	ACAAAAATAATACATCTATC	GCTTATATCAGCATCAAAAAG	CTCATTTTTCGGCTTATCAC				
gep1-PF16I1	GTGATGTACGAAAAATTCGA	GGCAAGTGTTTATAGAATTG	CGGCTCCATTTTTATTGCAA	GAAAGCAATGATGTCTCATCC				
Primers for RT-PCR								
Primer name	**Primer sequence**	**Primer name**	**Primer sequence**		**Primer name**	**Primer sequence**	**Primer name**	**Primer sequence**
kinesin8b F1	CAAAGTTAATCTTCAAGAGT	*kinesin8b* R1	AGTTCATCTTGCAATCCTTC		PY17X_1357300 F6	GGAATTTGCAGAAAGTACCC	PY17X_1357300 R6	CGATTTTTTTTCCGATTTTT
kinesin8b F2	GAAAACATAACAGATAAAGA	*kinesin8b* R2	CTCCTCAAGCATCTTAATAT		PY17X_1357300 F7	GGAGAAGCCACTCAACTTAT	PY17X_1357300 R7	GTATCATTAAACATGGAATC
PF16 F1	CATTTATTAAATCAGGGTGC	*PF16* R1	TCGGTATTTTCAACTTCATC		PY17X_1335600 F1	CAATGAAGAAGGAAATTCCG	PY17X_1335600 R1	GAACTATCCGAGCAACTCTC
dhc6 F19	CAAGAAAATGATGCATTAAA	*dhc6* R19	GTAGCGTTGATTTTCCACTA		PY17X_1452900 F1	CAGCCTGAATATAAACCTAA	PY17X_1452900 R1	ATATGCTGTTTAAACTCCAC
dhc6 F20	TTTCTACAACAAGAGAGAAT	*dhc6* R20	GGAGTCATATAATTGATCTT		PY17X_1452900 F2	GTGGAGTTTAAACAGCATAT	PY17X_1452900 R2	ATCAGCAAAACTTATGTGGG
dhc7 F6	GAGGCAATTATGATGACGTG	*dhc7* R6	CTTCAAAACATGATTTAACA		PY17X_1122300 F1	GCCTTTTTAGCTATTTTTGTG	PY17X_1122300 R1	GTAGAATCCGAAGTAATTCG
dhc7 F7	CCTACTAATCTTATAACATT	*dhc7* R7	TTTGTATCTCAATAAGCTTC		PY17X_1122300 F2	CGAATTACTTCGGATTCTAC	PY17X_1122300 R2	TTCCATTTATGATAATCGTC
dhc7 F8	ATCTGATCCAAGAATACAAC	*dhc7* R8	GCTCACGAATATTAGTTCCC		PY17X_0523500 F1	TAACACCATATAACAATAAC	PY17X_0523500 R1	ATAATGTGAAAAGATCTTCC
dic1 F3	ACGTTTTAAAGAACAAAATG	*dic1* R3	TAATGTATTTGAGAGGAAGC		PY17X_0523500 F2	CACCACATCTATCTTACCAG	PY17X_0523500 R2	GGGATCCAGAATTGCAAGGT
dic1 F4	TGGTCCAACATAATTTGTGAAG	*dic1* R4	TGAATAGAAGTCTCTGCATTCG		PY17X_0523500 F3	GACAATATTCCAGACACTAA	PY17X_0523500 R3	AATTTGTGGAAATGTCCAGA
dic1 F5	GCTACATTTTAAAGAATTCG	*dic1* R5	GCACAATATATATGAGCATG		PY17X_0508900 F4	CAAATTCCGATTTTTACGAT	PY17X_0508900 R4	CCTTCTTTTTACTCATTAAT
dic2 F1	ATGAGTTCCGAAAATTTTTC	*dic2* R1	TTCAACTTGTATAGCATTTG		PY17X_0508900 F5	AGACAGAGGACTTAATTCAG	PY17X_0508900 R5	GTGTGTCATCAATTAGTTGT
dic2 F2	AAATCTAATATTCCTTATCA	*dic2* R2	CTTTGCTGAGATGTTAAACG		PY17X_0508900 F6	GCTTTCTTATGATGTTAACA	PY17X_0508900 R6	CGCATTTGCTTTCTTCGCTC
drc1 F1	ATGCTACAAAACAATCTTAA	*drc1* R1	TTTCAAATTTCTTAACAGAC		PY17X_1320300 F1	GGGAAGATAACATTGAGGAG	PY17X_1320300 R1	TATGTACTAGTTTTTTCTGC
drc1 F2	GTCCAACCACTTTAAGATGG	*drc1* R2	CTATTAACACATTTACACTGC		PY17X_1320300 F2	CTCATGAAAATTTGGAAGAG	PY17X_1320300 R2	CTCGTCATGTGATTGCTTAA
drc1 F3	ATTTTGAAGATGATCAAGAG	*drc1* R3	CGTTTTATCATTTTCTTCCT		PY17X_1320300 F3	AAAATATTAAAATTGAAAGC	PY17X_1320300 R3	CATTCATGAGTTTCTTTTGA
dbc F1	CGCAGCGGATAATATCCAAC	*dbc* R1	TTTCAAAATTTACTTCCTCC		PY17X_0833600 F1	CAGATGGAGTATTAATGGCA	PY17X_0833600 R1	TTTAAAGGGTCGGGGTTCTG
dbc F2	GAGTTATCAAAAACACTGGAT	*dbc* R2	CGTACTTTAATTTACGTATCC		PY17X_0833600 F2	CAGAACCCCGACCCTTTAAA	PY17X_0833600 R2	TATTTAATGCCTCAATTTTC
md2 F1	CTAGCTAGAGCTATGCGTAA	*md2* R1	TCAATAGGAACTTGTGAATC		PY17X_1341200 F1	GCAGTAATGACAATAGAAGT	PY17X_1341200 R1	GGATGTCGAGTTTTTATCCT
PY17X_1109100 F1	TTGTCACTCTTGTTGAGCGC	PY17X_1109100 R1	GCTGTGTATATGTACGAGTC		PY17X_1341200 F2	AGGATAAAAACTCGACATCC	PY17X_1341200 R2	TACAAATGATACTTTTTGCG
PY17X_1109100 F2	GGGTGTGTTAGAAAAGTTTT	PY17X_1109100 R2	TTCGAAAAGTTCTTCGACAC		PY17X_1305400 F10	GAGATTTGTACGAATGTCGA	PY17X_1305400 R10	CCTGACTCCATATTATATCT
PY17X_0521800 F1	CGAAACTGATGTTAAAAATA	PY17X_0521800 R1	CTCGTCAGAATTAAAGTATT		PY17X_1305400 F12	CACAAAGAAGGCAATCATGT	PY17X_1305400 R12	GTCATTGATAAGTTGATCTG
PY17X_0521800 F2	CGCAGTAAATATAGAGTTAG	PY17X_0521800 R2	TATAAAAACTTCTTCGTCAG		PY17X_1305400 F13	GATTCTGAGGAATTTGATCA	PY17X_1305400 R13	CATCATTTAGTTCTTTGCAA
PY17X_1311800 F4	ATAGTGTTTTATCCTAAATC	PY17X_1311800 R4	GTCTTCTATTTCTCCACTCT		PY17X_0415900 F12	CGTTGAAAATGTTTCCTCAA	PY17X_0415900 R12	TCTTATGCATTTTTATCTCC
PY17X_1311800 F5	GATATTACCCATAAGGTGTG	PY17X_1311800 R5	CGTAGCTAAATATCATGTAG		PY17X_0415900 F13	GCCACATTTTTACGAAAATG	PY17X_0415900 R13	AGTATGTCTCTGGCCCTTAT
PY17X_1311800 F6	ATTAAGATTGTATTCCTTCC	PY17X_1311800 R6	ATATCTATATTCATAGACCC		PY17X_0105800 F1	GCTACCTGTCTTATTTTATC	PY17X_0105800 R1	ACGTCCTCAAACTTGAGCTC
PY17X_1323900 F1	GTATTTGCTCGACAAAAATG	PY17X_1323900 R1	GTCTTTCCAGTTTTATACAC		PY17X_1216400 F4	GAGAGGAAACATAAATTTGTC	PY17X_1216400 R4	CTTTTCTAACTCATAAGTTTG
PY17X_1357300 F5	AATATAAGCATCTATCACAG	PY17X_1357300 R5	GGATCGTTTTATGTATCCAA		PY17X_1216400 F5	CGCAGACATTAAAAAGAGGG	PY17X_1216400 R5	ATCGTTTCCTTCTGTTTCAG
Primers for RT-qPCR								
Location	**Gene ID**	**Forward primer**	**Reverse primer**		**Location**	**Gene ID**	**Forward primer**	**Reverse primer**
GAPDH	PY17X_1330200	GAGCAGGTAGATCAGCTTTGT	ACTCTAAAGGCAACACCAGTTA		*1216400*	PY17X_1216400	CAACCCTGAAGAGATACCTCAAAA	CCCGTTATCTTCTTCATCAGCA
α-tubulin 2	PY17X_0524100	ATGTTGGTCAAGCAGGTATCC	CAACTTGATCACTGGGCATTTG		*kinesin8b* I1	PY17X_0204100	GGCTAGTTAGATCGTACCACTTC	TGGCGCTTGACTAACGATAT
β-tubulin	PY17X_1210100	CGGAGAAGGTATGGACGAAATG	CTTCAGCAGTGGCATCTTGATA		*kinesin8b* I4	PY17X_0204100	AAGCAAGGAAAATGCAACGC	GAGAGTTAAACAATGAGCAG
Rbpm1	PY17X_0716700	CGCACAAGATCACGAGACAA	CATCCACTCGTTTCCCATTCA		*PF16* I1	PY17X_0919000	ATTCCTAGTTGTAATTTCTC	CCAATGTGTAAATATTGCAT
1109100	PY17X_1109100	TTGTCACTCTTGTTGAGCGC	GCTGTGTATATGTACGAGTC		*PF16* I1/E2	PY17X_0919000	GTGTGTACATACTTCATGTG	CGAATTTCGTGGAATCTTCAC
0833600	PY17X_0833600	CATGGGTGTGGAAAAAGTCC	GGGATTTCCGTTTCATGACT					
Primers for RIP-qPCR								
Location	**Gene ID**	**Forward primer**	**Reverse primer**		**Location**	**Gene ID**	**Forward primer**	**Reverse primer**
kinesin8b I1	PY17X_0204100	GGCTAGTTAGATCGTACCACTTC	TGGCGCTTGACTAACGATAT		*dic1* I4	PY17X_1241500	TTCAAAAAGTAGAAGTATGC	GTGATAGTTGTGCAAATAATAC
kinesin8b I4	PY17X_0204100	AAGCAAGGAAAATGCAACGC	GAGAGTTAAACAATGAGCAG		*dic1* I3	PY17X_1241500	GTGCATATCCTACACGGTTG	GGTGATACACACATTACTAT
PF16 E1	PY17X_0919000	GCTAGCTAATATTGTTGCTGAAGA	GATTGCACACAATGCGTTAATAC		*dic2* I1	PY17X_0302800	GAAACAATAATAAGCGAAATCG	TCACATACATACTTTTTTAAC
PF16 I1	PY17X_0919000	GAATAATTTAACCATCTTTTTCAC	CCCTACGATTTGGTTATATATA		*dic2* I3	PY17X_0302800	GTTAGAGCATGCTTTATAGA	TGAAGTAAAATTGTGACACC
dhc6 I20	PY17X_0603800	CAATCCTAATAGGCACCCCC	TATATTTGTCTGTATGAACG		PY17X_1109100 I1	PY17X_1109100	CGGTAGCAGTATATGTAGTT	CTAGTTCAATGTTTTCTACA
dhc6 E22	PY17X_0603800	CCTCCTATAGACGAATCTAA	CTCTTTCTGCTTGTGATATAC		PY17X_1109100 I2	PY17X_1109100	CCCACTTTTTTCAATTCCCC	CAGGTATATTTATGCGTATAC
Primers for obtaining *in vitro* transcription templates								

Probe	Gene ID	Forward primer	Reverse primer		Probe	Gene ID	Forward primer	Reverse primer
kinesin8b I4 probe	PY17X_0204100	TAATACGACTCACTATAGGGAGACTAAAATGGAAAACCAGTTAC	TAAGGTGAATGGTAAAGTTC		*bfp*	/	TAATACGACTCACTATAGGGAGAATGGTGAGCAAGGGCGAGGA	CTTGTACAGCTCGTCCATGC
kinesin8b I1 probe	PY17X_0204100	TAATACGACTCACTATAGGGAGAATGAAAAATTATTTATAGAC	TAAGTTCATCTTGCAATCCT		*bfp-Kin8b* I1	/	TAATACGACTCACTATAGGGAGAATGGTGAGCAAGGGCGAGGA	CTTGTACAGCTCGTCCATGC
PF1ô E1 probe	PY17X_0919000	TAATACGACTCACTATAGGGAGAAGATAAAGTTCCTATAGTTC	AAAATTTGATTAAATTTGGT		*bfp-PF1ô* I1	/	TAATACGACTCACTATAGGGAGAATGGTGAGCAAGGGCGAGGA	CTTGTACAGCTCGTCCATGC
PF1ô I1 probe	PY17X_0919000	TAATACGACTCACTATAGGGAGACTAAAATCACCTTTAAAACT	TCAGAATATCCAGGTGTGTA					
Note: The blue sequences are designed for the restriction enzyme digestion. The red sequences are T7 promoter sequence.								